UNIVERSITY OF CALIFORNIA, SAN DIEGO

Improved Techniques for Passive Optical Networks

A dissertation submitted in partial satisfaction of the requirement

for the degree Doctor of Philosophy in

Electrical Engineering (Photonics)

By

Douglas Ryan Tourtillott Jorgesen

Committee in charge:

Professor Sadik Esener, Chair
Professor Andrew Kummel
Professor Ramamohan Paturi
Professor Stojan Radic
Professor Paul Yu

2010

The Dissertation of Douglas Ryan Tourtillott Jorgesen is approved, and it is acceptable in quality and form for publication on microfilm and electronically:

Chair

University of California, San Diego
2010

TABLE OF CONTENTS

LIST OF TABLES

LIST OF FIGURES

LIST OF ABBREVIATIONS

ACF ----------Autocorrelation Function
AWG ----------Arrayed Waveguide Grating
ASE ----------Amplified Spontaneous Emission
BER ----------Bit Error Rate
CIB ----------Consecutive Identical Bits
CLS----------Centralized Light Source
CO----------Central Office
CS----------Current Source
CWDM ----------Coarse Wavelength Division Multiplexing
DCA----------Digital Communication Analyzer
Demux ----------Demultiplexer
DFB ----------Distributed Feedback Laser
DSP----------Digital Signal Processing
EDFA ----------Erbium Doped Fiber Amplifier
ER ----------Extinction Ratio
FEC ----------Forward Error Correction
FPLA----------Fabry-Perot Laser Amplifier
FTTP----------Fiber to the Premises
FWHM ----------Full Width at Half Maximum
FWM----------Four Wave Mixing
HDTV----------High Definition Television
HFC----------High Frequency Cutoff
IM-DD----------Intensity Modulated Direction Detection
I/O----------Input-Output
ISI ----------Inter-symbol Interference
LFC ----------Low Frequency Cutoff
LPF----------Lowpass Filter
MD----------Modulation Depth
MZM----------Mach-Zehnder Modulator
NRZ ----------Non-return to Zero
OBPF ----------Optical Bandpass Filter
OEO----------Optical-Electrical-Optical
OFC----------Optical Fiber Communications Conference
OFDM ----------Orthogonal Frequency Division Multiplexing
OIP ----------Optical Information Processing
ONU----------Optical Network Unit
OSA ----------Optical Spectrum Analyzer
OSNR----------Optical Signal to Noise Ratio
$OSNR_{ASE}$ ----------Optical Signal to Noise Ratio due to ASE
$OSNR_{RB}$ ----------Optical Signal to Noise Ratio due to RB
OSP----------Optical Signal Processing
PBS----------Polarization Beam Splitter

PDF----------Probability Density Function
PM----------Phase Modulator
POLC----------Polarization Controller
PON----------Passive Optical Network
PRBS----------Pseudo-random Bit Sequence
PSD----------Power Spectral Density
QSM----------Quadrature Subcarrier Modulation
RB ----------Rayleigh Backscattering
RB_1 ----------Type 1 Rayleigh Backscattering
RB_2 ----------Type 2 Rayleigh Backscattering
RSOA ----------Reflective Semiconductor Optical Amplifier
RZ ----------Return to Zero
SBS ----------Stimulated Brillouin Scattering
SCM ----------Subcarrier Modulated
SMF ----------Single Mode Fiber
S/N, SNR ----------Signal to Noise Ratio
SOA ----------Semiconductor Optical Amplifier
TC ----------Transfer characteristic, Temperature controller
TDM ----------Time Division Multiplexing
VCEAM ----------Vertical Cavity Electro-Absorption Modulator
VCSEL ----------Vertical Cavity Surface Emitting Laser
VCSOA----------Vertical Cavity Semiconductor Optical Amplifier
VOA----------Variable Optical Attenuator
WDM----------Wavelength Division Multiplexing
XGM----------Cross Gain Modulation

ACKNOWLEDGEMENTS

My graduate career is the result of a small handful of people. The first is Prof. Sadik Esener, my advisor and endless supporter. As a member of the Esener research group you are provided with as much freedom as you would like, and then some. I wouldn't have it any other way.

The majority of the work in this thesis, and certainly the best work, is the direct result of the advising and mentoring I received from Dr. Christopher Marki. I only know whatever he taught me about lab techniques, how to perform good science, what makes meaningful engineering work, how to solve difficult problems, how to write papers, and how to meet women. The experiments in chapter 2 and at the end of chapter 3 were performed at his family company, Marki Microwave, which makes extremely high quality microwave components including splitters, filters, amplifiers, diplexers, triplexers, doublers, and of course mixers. It was only through the free use of this high quality equipment that I was able to demonstrate the Quadrature Subcarrier Modulation technique in Chapter 3 that is the most important achievement of my time as a graduate student.

I would finally like to thank my parents, who have supported me without question for as long as I can remember. From an early stage I absorbed their abilities in math and interest in science. They encouraged me to take on challenges at each step, and were forever supportive and appreciative of my accomplishments without ever telling me what to do. When I had the option of the hard, expensive school or the cheap, easy school they encouraged me to take the harder path. It was my father's

advice when I asked what I should major in, to “try engineering, that seems like a good thing to do”, that has inspired me to devote my life to applied science. My mother was never critical and always encouraged me to remain in school as long as I possibly could. She always encouraged me to delay growing up and learn as much as possible while I’m young. Their tireless faith in me, regardless of whether I know what I’m doing or not, has bred the solid confidence that I value more with each passing year.

Section 2.1 is, in part, a reprint of “Improved High Pass Filtering for Passive Optical Networks”, published in *Photonics Technology Letters*, 2010 by D. Jorgesen, C. F. Marki, and S. Esener. Section 2.2 is, in part, a reprint of “Analysis of High Pass Filtering of Rayleigh Noise Limited Central Light Source Passive Optical Networks”, submitted to the *Journal of Lightwave Technology*, 2010 by D. Jorgesen, C.F. Marki, and S. Esener.

Section 3.3 is, in part, a reprint of “Bidirectional Quadrature Subcarrier Modulation for Central Light Source PONs”, to be submitted to *Photonics Technology Letters*, 2010 by D. Jorgesen, C.F. Marki, and S. Esener.

Section 4.3 is, in part, a reprint of the material in "Observation of counterclockwise, clockwise and butterfly bistability in 1550 nm VCSOAs," from Optics Express, 2007 by C. F. Marki, D. R. Jorgesen, H. Zhang, P. Wen, and S. C. Esener and "Low power optical bistability in 1550 nm VCSOAs," presented at CLEO, Baltimore, MD, 2007 by D. R. Jorgesen, C. F. Marki, H. Zhang, P. Wen, and S. Esener. The dissertation author and C. F. Marki contributed equally to the first authorship of these publications.

VITA

2000	Graduate, International Baccalaureate School
2004	Bachelor of Science, Electrical Engineering, University of Illinois at Urbana-Champaign, (Honors)
2004-2010	Research Assistant, Electrical and Computer Engineering, University of California, San Diego
2005	Graduate Research Intern, Intel Corporation, Santa Clara
2007	Masters of Science, Electrical and Computer Engineering (Photonics), University of California, San Diego
2008	Technical Consultant, Ziva Corporation, San Diego
2009	Graduate Research Intern, Sun Microsystems, San Diego
2010	Doctor of Philosophy, Electrical and Computer Engineering (Photonics), University of California, San Diego
2010-current	Technical Consultant, L-3 Photonics, Carlsbad, CA

PUBLICATIONS

N.A. Riza and D. Jorgesen, "Minimally Invasive Optical Beam Profiler", Optics Express, vol. 12, no. 9, pp. 1892-1901, 2004.

D.Q. Song, D. Jorgesen, M. Gross,and S. Esener, "Integration of Precisely Aligned Lenslet Arrays with Waveguide Arrays", Optical Engineering, vol. 46, no. 6, pp. 065401/1-4, 2007.

C.F. Marki, D.R. Jorgesen, H-J Zhang, P-Y Wen, and S.C. Esener"Observation of counterclockwise, clockwise, and butterfly bistability in 1550 nm VCSOAs" Optics Express, vol. 15, no.8, pp. 4953-4959, 2007.

D.R. Jorgesen, C.F. Marki, H-J Zhang, P-Y Wen, and S. Esener, "Low Power Optical Bistability in 1550 nm VCSOAs", Proc. Conf. Lasers and Electro-Optics, pp. 2776-2777, 2007.

C.F. Marki, S. Moro, D.R. Jorgesen, P. Wen, and S.C. Esener,"Cascadable Optical Inversion using 1550 nm VCSEL", Electronics Letters, vol. 44, no. 4, pp. 292-293, 2008.

S.F. Tsai, M. Gross, D.R. Jorgesen, and S.C. Esener, "Spectrally Sliced Coarse WDM-PON for Remote Monitoring Systems", accepted for publication in Optical Engineering, April 2010.

V. Gauss, A. Hurtado, D. Jorgesen, M.J. Adams, and S. Esener, "Static and Dynamic Analysis of an All-Optical Inverter based on a Vertical Cavity Semiconductor Optical Amplifier (VCSOA)", submitted to Optics Communications, 2010.

D. Jorgesen, C.F. Marki, and S. Esener, "Improved High Pass Filtering for Passive Optical Networks", IEEE Photonics Technology Letters, vol. 22, no. 15, pp. 1144-1146, 2010.

D. Jorgesen, C.F. Marki, and S. Esener, "Analysis of High Pass Filtering of Rayleigh Noise Limited Central Light Source Passive Optical Networks", submitted to IEEE Journal of Lightwave Technology, May 2010.

D. Jorgesen, C.F. Marki, and S. Esener, "Bidirectional Quadrature Subcarrier Modulation for Central Light Source Passive Optical Networks",submitted to IEEE Photonics Technology Letters, August 2010

.

ABSTRACT OF THE DISSERTATION

Improved Techniques for Passive Optical Networks

by

Douglas Ryan Tourtillott Jorgesen

Doctor of Philosophy in Electrical Engineering (Photonics)

University of California, San Diego, 2010

Professor Sadik Esener, Chair

The work in this thesis introduces a variety of techniques that can be used to improve the performance of previous state of the art passive optical networks (PONs). These networks will be of increasing importance as increasing bandwidth demand drives the penetration of optical fiber into access networks. PONs require novel design techniques due to their bidirectional nature and tight cost requirements. In this thesis improvements are proposed in three categories: filtering of bidirectional noise; novel modulation techniques; and use of non-traditional low cost devices (specifically vertical cavity surface emitting lasers (VCSELs)).

High pass filtering (HPF) is shown to reduce the impact of bidirectional Rayleigh noise, which is dominant in PONs. It is demonstrated that under certain circumstances Rayleigh noise immunity is improved by up to 10 dB with proper selection of an HPF. A model to predict the effects of baseline wander caused by HPF is developed and experimentally validated. This model is combined with an

existing Rayleigh noise model, which is experimentally validated. This model is extended to predict the performance of a bidirectional on-off keyed (OOK) PON and experimentally verified.

Three methods are investigated to improve the ONU modulator. First it is shown that transmitter pre-distortion can provide a doubling of the non-equalized datarate of a low modulation bandwidth ONU modulator. Next a four level intensity modulation format is demonstrated. It is shown that while this method is possible, it provides no improvement over OOK modulation. A novel method for modulating the orthogonal phases of an intensity modulated microwave subcarrier, similar to quadrature amplitude modulation (QAM), is demonstrated. Significant performance improvement is realized with this scheme.

Finally the use of a VCSEL in PONs is evaluated. It is predicted that using a VCSEL as central office (CO) laser will offer minor benefits and some moderate challenges. Use of a vertical cavity semiconductor optical amplifier (VCSOA) as an ONU modulator is prevented by a dispersive nonlinearity. This nonlinearity leads to bistability. First demonstration of butterfly bistability in a 1550 nm VCSOA and record low power bistability are demonstrated.

1. Introduction

In the past 40 years the dramatic increase in available computing power has been much noted and celebrated [1]. Less commonly noted is the even more extraordinary explosion in achievable bandwidths over long distances. While transistor cost has been reduced in half and computations per unit time have been doubling roughly every 18-24 months, the cost of transmitting a bit a given distance has been reduced by half and the number of bits transmitted per unit time has been doubling every 9 months [2]. Unlike semiconductor technology this increase in capacity has been driven not by planned and incremental improvements to every node in the technology chain, but by revolutionary breakthroughs such as the arrayed waveguide grating, the erbium doped fiber amplifier, and more recently the use of planar lightwave circuits to detect and decode polarization multiplexed quadrature modulated optical signals [3]. Indeed, the optical fiber communication system itself was a disruptive innovation to the previous electrical communication infrastructure that it has replaced.

This dramatic and unprecedented increase in capacity has not been uniformly distributed. The increase has always been demonstrated first in research labs, then replicated in the long haul links that make up the backbone of international communication networks. With WDM technology, commercial long haul links easily carry in excess of tens of gigabits per second (Gb/s). The distribution network, however, has not kept pace with this greatly expanded internet backbone. The recent

advent of high definition video, particularly user generated high definition video, has created a strong and growing demand for bidirectional “last mile” bandwidth improvements [4]. The term last mile generally refers to the connection from the end user to the first link in the network. This link is typically under 50 km, and frequently under 10 km for urban areas, and has traditionally been served by electrical communication. This is in contrast to typical long haul backbone links that operate across hundred to thousands of km and have been optical for several decades.

1.1 Passive Optical Networks

High bandwidth, high flexibility, and low cost are the major motivating factors behind the passive optical network (PON). The term “passive optical network” is used to describe a broad class of optical networks whose common characteristic is the absence any kind of electrical repeater or other electrical circuit between the broader network connection (the central office (CO) under the IEEE terminology or optical line terminal (OLT) under the ITU terminology) and the end user (usually called the optical network unit (ONU), though sometimes referred to as the optical network terminal (ONT)). First proposed in the mid 1980s [5], it is different from traditional point to point optical networks in that each CO serves many ONUs, making it a point to multipoint network while a traditional network is point to point [6]. This means that the high bandwidth-length product optical network can be used to serve several customers, reducing the per customer cost.

1.1.1 Time Division Multiplexed PONs

Currently deployed PONs broadcast data downstream and use time division multiplexing (TDM) to separate upstream data. The structure of a TDM PON is shown in Fig. 1.1. In this scheme the downstream data is addressed to a specific ONU, encrypted, and broadcast to all ONUs on the network (typically 32 or 64 depending on the split ratio at the passive node). Each ONU decodes only the data addressed to it and ignores the other data. For upsteam data a separate wavelength is used in combination with coarse wavelength division multiplexing (CWDM) filters. Time slots on this wavelength are allocated by the CO to each ONU to prevent collisions. The TDM PON has the significant advantage that the optical transmitter and receiver cost, in addition to the installed fiber cost, can be split among several subscribers. It is limited in that increased bandwidth demands can only be met by increasing the line rate of the transmitters. This is only economical to a certain point.

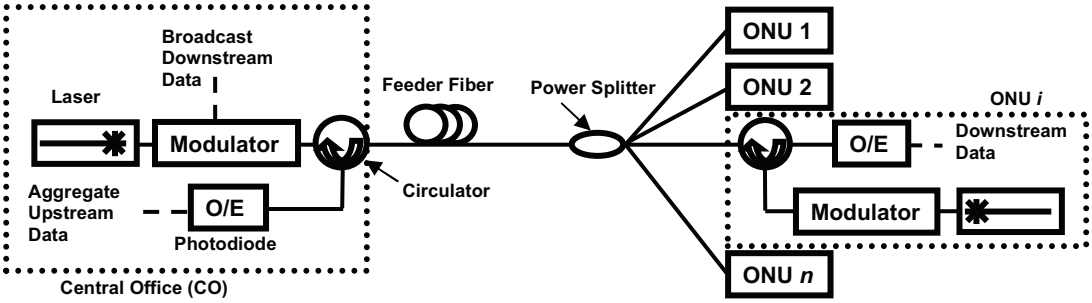

Fig. 1.1. TDM-PON schematic diagram. A single CO serves the aggregate data needs of *n* ONUs on the same fiber.

1.1.2 Wavelength Division Multiplexed PONs

A promising alternative topology is the wavelength division multiplexed (WDM) PON, which will be the main topic of this thesis. WDM networks refer to systems where multiple channels are communicated across a single optical fiber using different wavelengths. This is possible because the high ratio of datarate to carrier

frequency inherent in optical communications systems (Gigabits of data on a 193 THz carrier) is low enough that many data channels will fit within the low loss window of a single optical fiber without significant crosstalk. WDM technology was initially researched in the late 1970s and was deployed in commercial networks by the early 1980s [7]. This technology has been one of the main forces in increasing network bandwidth, as the ITU transmission grid recognizes 72 DWDM channels at a spacing of 100 GHz in the low loss C band [8]. This provides over 1 Tb/s of bandwidth if each channel is populated even with a conservative 20 Gb/s data stream.

For PONs the evolution from a purely TDM to a WDM network offers a number of advantages. The topology of a WDM-PON network is shown in Fig. 1.2. By adding arrayed waveguide gratings (AWG) on each end of the feeder fiber a physical point to point connection can be created between multiple ONUs and the CO over a single feeder fiber. Since each wavelength of light travels directly from the CO to the ONU or the CO to the ONU all the benefits of a point to point network are realized, including high bandwidth, modulation format independence, and security/privacy. Since the whole bandwidth of each channel is allocated directly to each ONU the components can operate at the link bandwidth, instead of requiring a linerate equal to the aggregate link bandwidth [9] (i.e. for a 1 Gb/s link in a 1x16 link each modulator and receiver would need to operate at a minimum of 16 Gb/s). Additionally the implementation of a WDM PON does not necessarily disrupt currently operating PON links, allowing a smooth, evolutionary upgrade path where more channels can be populated as the bandwidth requirements of the network increase [6].

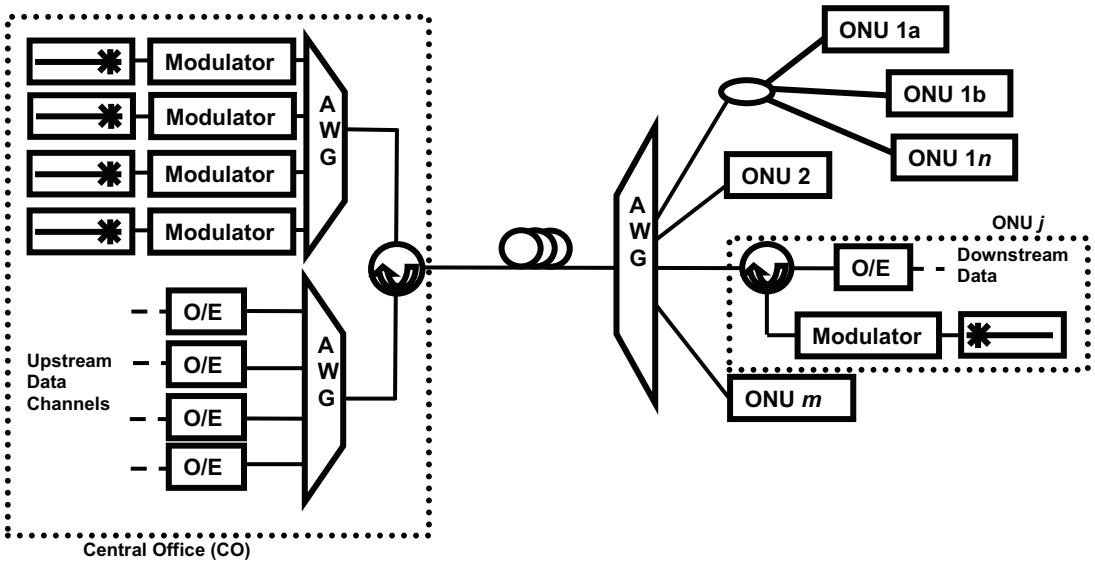

Fig. 1.2. WDM-PON schematic diagram. Note that a single channel can serve an entire TDM-PON with sufficient link budget.

While the advantages of a WDM-PON are significant, it creates distinct challenges as well. A TDM-PON typically uses one wavelength for downstream transmission (1490 nm) and another wavelength for upstream transmission (1310 nm), requiring the use of only two different wavelength lasers without tight wavelength control. For a WDM-PON each ONU needs to have a laser of a specific wavelength, which means that either an expensive tunable laser needs to be employed or the wavelength of each individual ONU has to be tracked and managed. This maintenance must be performed at both the CO and ONU sides and continuously updated to match the temperature sensitive wavelength channels of the AWG. Since the ONUs are located at remote sites the cost of modifying them would then be considerable, and an inventory of transmitters at every possible wavelength would need to be maintained. Additionally, each of the ONU lasers would need to be temperature controlled to maintain wavelength stability.

1.1.3 Central Light Source WDM-PONs

One solution proposed to this problem is to generate light at the CO and distribute a specific allocated wavelength to each ONU, which then modulates this seed light, amplifies it if necessary, and re-transmits it back to the CO. This method was first proposed in 1994 [10] and is called the central light source (CLS) PON. As with the improvement to WDM-PON it offers several advantages at an increased cost. The idea of a CLS-WDM-PON (simply CLS-PON throughout this thesis) is illustrated schematically in Fig. 1.3. The primary advantage is that a wavelength specific source is no longer necessary at the ONU, which can be replaced with a wavelength insensitive modulator. This also means that no temperature control is necessary at the ONU, and the only tuning necessary is at the CO to align the source laser with the AWG wavelengths.

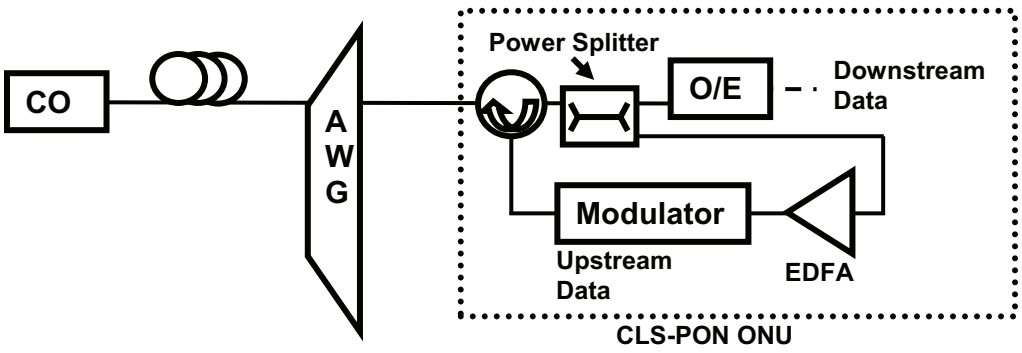

Fig. 1.3. CLS-WDM-PON schematic diagram.

This topology presents novel challenges, however. It is these challenges, and methods to overcome them, that will be the subject of this thesis. Each variation from the standard, unidirectional, point to point optical link brings a new set of challenges to be overcome. Because of the bidirectional nature and stringent cost requirements of this type of network, standard design methodologies are insufficient. In the chapters that follow I shall identify the unique requirements of this scheme, methods

to meet these requirements, and through theoretical analysis and experimentation evaluate the degree to which these requirements are met by the proposed methods.

1.2 Technical Challenges for CLS-PONs

There are three major technical aspects of CLS-PON design that must be addressed and are significantly different from traditional link design. Three of these are addressed in the following chapters: noise sources in bidirectional networks, selection of an appropriate modulation system for bidirectional optical communication, and hardware selection for the CO and ONU transmitters. To properly design a PON attention must also be paid to the design and selection of other hardware including receivers, splitters, circulators, and particularly AWGs. However, since these components are common to almost all optical networks and its treatment delves into details of component design it will be considered outside of the scope of this thesis.

1.2.1 Noise Sources in Bidirectional Links

Typical optical links are dominated by a small number of noise sources. Typically one noise source dominates the performance of an optical link, and this noise source will determine the error rate. For long haul links it is typically fiber dispersion or, if the dispersion is managed, amplified spontaneous emission (ASE) from the fiber amplifiers employed. If the signal power is low enough the thermal noise in the electronics will dominate, and if everything else is clean the shot noise of the receiver will eventually come into play [11]. For a bidirectional network three new sources of noise come into play, all reflections of the light launched downstream back to the receivers [12-13].

The first type of noise is Fresnel reflections from discontinuities, dust, scratches, and other imperfections at the junctions between fibers in the network. These discontinuities cause discrete reflections of the signal that return to the receiver with a phase delay from the launched signal. The spectrum of this noise is identical to the signal spectrum since it is identical to the signal. The second type of noise is intrinsic to the fiber regardless of the care with which fibers are connected together. It arises from the amorphous nature of the silica in optical fibers, which causes index of refraction variations on a scale shorter than the wavelength of the light. This noise is referred to as Rayleigh backscattering noise, or simply Rayleigh noise. The last type of noise to come into play occurs when the energy from the light inside the fiber causes the dipoles of the fiber to align and create a grating. This grating creates a standing wave that reinforces itself as more light is incident upon it, causing a feedback process. The backreflection from this grating is referred to as stimulated Brillouin scattering (SBS).

Each of these types of noise has distinct properties. Since SBS involves interaction with the dipoles of the glass it is associated with a phase shift of 10 GHz to either side of the carrier. The longer wavelength (lower frequency) shift is favored since it emits energy instead of requiring it. SBS is a highly nonlinear process which is largely undetectable until roughly -2 dBm of unmodulated light at 1550 nm is launched into a fiber, as shown in Fig. 1.4. With more power than this, however, it rapidly becomes the dominant noise source. When 8 dBm of CW light is launched into the fiber almost half of it is reflected as SBS. Since this is such a dominant noise

source the link must either be designed with launched powers below this threshold or some kind of frequency dithering must be employed to increase the SBS threshold.

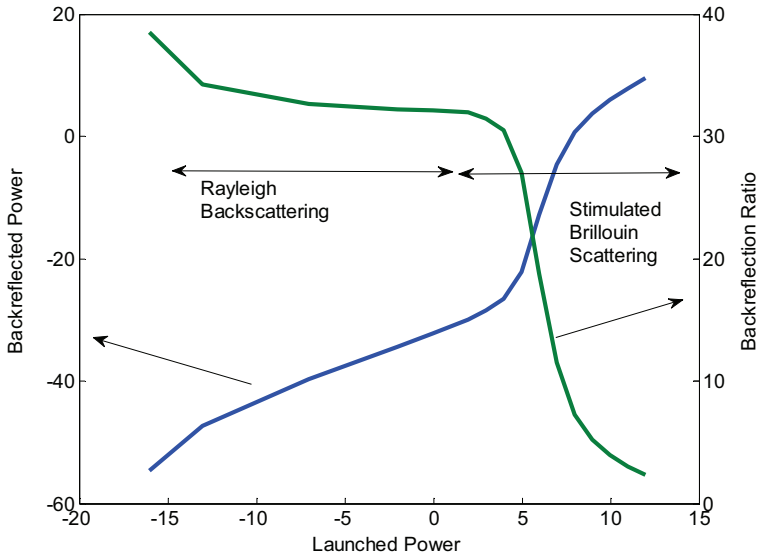

Fig. 1.4. Backreflection from fiber as a function of input power. The Onset of stimulated Brillouin scattering begins around 0 dBm.

In contrast Rayleigh scattering is a very linear process. It is a simple reflection with no meaningful interaction with the medium. As such the spectrum of the backreflected light is identical to that of initially launched light. As a result of the backscattering process it is partially polarized with a degree of polarization (DOP) of 1/3, meaning that 2/3 of the backreflected light is in the launched polarization while 1/3 is in the orthogonal polarization [12]. Further since the backreflected light is attenuated by travel down the fiber (primarily by Rayleigh backreflection) it rapidly converges to a fixed backreflection value, which is roughly 32 dB of the launched light level for a 1550 nm light in standard single mode fiber (S-SMF).

The ITU standards for PONs, G983.3 and G984.2, require that optical return loss (ORL) from connectors and fibers be fixed at 32 dB [15]. This means that

backreflections must be kept below the Rayleigh backscattering loss. Since PONs are generally short distance links with minimal amplification in them, ASE and dispersion will be minimal. Assuming the link is also designed with low enough launch powers to prevent SBS, Rayleigh backscattering has been identified as the primary noise source in CLS-PONs [16]. The mitigation of Rayleigh noise as a limiting factor will be considered of the highest priority throughout this thesis.

1.2.2 Modulation Methods for Bidirectional Systems

Various schemes have been investigated to improve the performance of the CLS-PON, particularly for the case where data is transmitted bidirectionally. The simplest of these is to use equalization to improve the modulation bandwidth of the components in the link [17,18]. This will be the subject of the first section of chapter 3. Another technique to increase the datarate above the modulation bandwidth of the RSOA is to use multilevel modulation, which is the subject of the second section of chapter 3. This technique has been used to increase the datarate of a VCSEL based network [19], but there has been limited research into this area otherwise.

In contrast to these lightly researched areas, significant effort has been expended to determine the optimal combination of modulation formats for downstream and upstream transmission when re-using the downstream light. This is a novel problem in communications; new theoretical techniques and transmission schemes are useful to analyze the problem. Many techniques have been investigated with some common characteristics. Upstream transmission is exclusively amplitude modulated since the ONU modulator must be low cost. Downstream transmission is designed to minimize the noise on the upstream signal.

The techniques employed in this pursuit can be broadly categorized into either baseband or subcarrier techniques. Among baseband techniques demonstrated are differential phase shift keying (DPSK) downstream with OOK upstream [19]; DPSK downstream and duobinary upstream [20]; FSK downstream and OOK upstream [21]; inverse return-to-zero (IRZ) downstream and NRZ upstream [22]; Manchester coded downstream and NRZ upstream [23]; polarization shift keying (PolSK) downstream and NRZ upstream [24]; RZ amplitude shift keying (ASK) downstream and DPSK upstream [25]; PolSK in both the down and upstream directions [26]; dark IRZ downstream and DPSK upstream [27]; DPSK both up and downstream [28]; and the trivial case of NRZ intensity modulation both up and downstream [29], to which our experiments will be compared.

The second class of techniques that have been employed for bidirectional data transmission in a PON are those that intensity modulate a microwave subcarrier onto the upstream signal, downstream signal, or both [30]. This microwave signal is then phase and intensity modulated. Benefits of this scheme include improved noise tolerance and elimination of residual downstream data in the upstream signal. Among the schemes that fall into this category are downstream OOK and upstream orthogonal frequency division multiplexing (OFDM) [31]; OFDM downstream and OOK upstream [32]; continuous wave (CW) downstream and spectral amplitude coded optical code-division multiple access (SAC-OCDMA) upstream [33]; DPSK downstream and carrier suppressed subcarrier modulation (OCS-SCM) upstream [34]; CW downstream and OFDM upstream [35]; CW downstream and OCS-SCM upstream [36]; SCM downstream and OOK upstream [37]; and OFDM quadrature

amplitude modulation (OFDM-QAM) downstream and NRZ upstream [38]. Research in these areas has focused on the physical architecture necessary to realize these implementations. For example, a variety of schemes use optical filtering techniques at the ONU to eliminate the downstream data and leave a CW carrier to be remodulated for upstream transmission. Another scheme worth noting here is the subcarrier multiple access technique [39], whereby each ONU is assigned a subcarrier and downstream data is broadcast to all ONU on a network. One technique that has not been studied, the use of orthogonal phases on the same subcarrier for downstream and upstream transmission, will be the subject of the last section of chapter 3.

1.2.3 Device Selection for Passive Optical Networks

Early on it was recognized that a low cost multiwavelength source at the CO was a key enabling technology for CLS-PONs [9]. Nonetheless, with some notable exceptions [40-41] research since this time has focused primarily on investigating link topologies with some kind of narrow linewidth single wavelength laser, such as a DFB, as the CO source light. This thesis largely follows this model as it is instructive to investigate various aspects of the link on their own. The most notable deviation from this standard model is the spectrally sliced ASE source as the downstream source [42], which has attracted significant attention since it is a low cost source that requires no temperature stabilization on either the ONU or CO side. One option that has received no notable attention is to use the vertical cavity surface emitting laser (VCSEL) as a downstream transmitter. While upstream transmission for a standard WDM or TDM PON has been demonstrated with a VCSEL [43], no one has yet demonstrated a VCSEL as a downstream CO transmitter.

On the ONU modulator side the main devices investigated are the RSOA [17-18]; a combined SOA-EAM [44]; the injection locked Fabry-Perot (FP) laser [40]; injection locked distributed feedback lasers (DFB) [45]; the injection locked VCSEL [46]; and of course MZMs [27]. One technology that hasn't been investigated previously, the vertical cavity semiconductor optical amplifier (VCSOA), is investigated as an upstream transmitter in chapter 4.

1.3 Optical Logic and Bistability

The final topic addressed by this thesis arises by chance out of previous investigations. This is the topic of optical logic; that is the use of optical signals to process other optical data at high speeds. It is necessary to perform logic operations on optical signals for routing, encryption, and buffering purposes. Currently logic operations are performed exclusively by converting the optical signals to electrical signals, performing the logic operations, and converting the signal back into optical format. Optical logic and memory are difficult to realize because photons inherently do not interact with each other and thus have to interact through a medium. Since light is typically only absorbed or scattered without affecting the medium the logic process must occur through some type of nonlinearity.

Many nonlinearities have been investigated for the purposes of performing optical logic and memory functions. These include four wave mixing (FWM) [47]; cross phase modulation (XPM) based on free carrier absorption [48]; and cross gain modulation (XGM) [49]. XPM based on carrier absorption in an SOA based MZM is of particular interest as it has shown extremely high speed operation [50] and as it uses a similar mechanism to that shown in VCSOAs [51]. This nonlinearity has been

shown capable of producing a memory system [52] as well. Other optical memory techniques include the use of a fiber storage loop [53] and slow light in a photonic crystal, microring resonator, or some other type of optical cavity [54]. Another method for performing optical logic and memory functions is through optical bistability [55]. Optical bistability in a VCSOA will be explored in depth at the end of chapter 4.

1.4 Thesis Outline and Contributions

The contributed work for this thesis comprises the three following chapters. Each chapter addresses a different aspect of passive optical network system design broadly, as defined in the background information above. Chapter 2 begins with an experimental investigation into the circumstances under which Rayleigh backscattering noise can be blocked using low-cost high pass filters at the CO receiver. It is shown that significant improvements of up to 10 dB are possible using this technique to block the reflected CW component of any intensity modulated signal. Next a model for Rayleigh noise is recounted from previous work. A novel model for calculating the effect of baseline wander on the BER of a Gaussian noise limited signal by performing a bitwise error performance calculation is presented and experimentally validated. The model suggests that significant vertical eye closure from baseline wander begins to appear at .001 times the datarate for random data and .01 times the datarate for 8B/10B encoded data.

This model is combined with the original CLS-PON model for Rayleigh noise and used to predict the BER of a CLS-PON in only upstream transmission mode. The results are shown to agree well with theory, particularly as regards the optimal choice

of gain and the relative impact of both filtering and improper gain selection. The model is then used to predict link performance against both extinction ratio and source linewidth; results show that while upstream ER has a significant effect on maximum link reach, the use of 8B/10B encoding on the upstream data signal allows for very broad CO source lasers to be used.

Next the model is expanded again to include the effects of bidirectional transmission. Formulas are derived for the noise on the downstream signal in the presence of Rayleigh noise from the upstream signal; noise on the upstream signal is also calculated with the assumption that mark levels are constantly at the lower level. The model predicts that for a bidirectional NRZ-OOK signal the optimal downstream extinction ratio for a 13 dB upstream ER will be slightly above 3 dB, or alternatively that the downstream modulation depth will be below .5 for an upstream MD near 0. A bidirectional link is built that confirms this prediction as well as the qualitative link performance as a function of ER.

Chapter 3 begins with an exploration of equalization for the purposes of increasing the datarate transmitted by the low modulation bandwidth RSOA ONU modulator. It is shown experimentally that open eyes are possible at up to 5 Gb/s using transmitter predistortion, twice the datarate possible using an unequalized signal. BERs below the forward error correction (FEC) limit of 10^{-3} are shown possible over 20 km of fiber. Next the possibility of four level intensity modulation instead of OOK is examined experimentally in the same system. It is shown that open eyes are possible at up to 8 Gb/s, although the high signal to noise ratios (SNR) required for four level modulation make it inferior to binary modulation.

In the last section of Chapter 3 a novel bidirectional transmission system is proposed using a single subcarrier frequency. Under this scheme the downstream data is mixed with a subcarrier that is intensity modulated onto the CW light. At the ONU the upstream data is mixed onto the same frequency subcarrier, but with a 90° phase shift from the downstream carrier. This allows the CO receiver to filter out both the downstream data and half of the noise by downconverting with an appropriately phased carrier. An analysis of noise susceptibility is performed, and verified experimentally. It is shown that the novel scheme has a noise immunity that is 9 dB better than a linear OOK modulating ONU, and 4 dB better than a gain saturated RSOA OOK modulating ONU. Further experiments show that the scheme performs comparably to OOK modulation in an RSOA based ONU 20 km link. In a 50 km link using MZMs and EDFAs the novel subcarrier multiplexed (SCM) scheme shows error free operation across a wide range of MDs, while OOK has a minimum BER of 10^{-5} at the optimal MD.

Chapter 4 examines the potential use of VCSELs in CLS-PONs. It begins with a theoretical examination of VCSELs as CO source lasers. Because of the larger linewidth of the VCSELs it is shown that they would have a benefit in SBS susceptibility, but a moderate baseline wander penalty due to baseline wander with high pass filtering. Next VCSOAs are experimentally investigated as ONU modulators. It is shown that they are unsuitable due to modulation instabilities even at low bitrates. In the next section these instabilities are shown to be due to a dispersive nonlinearity referred to as optical bistability. For the first time all three forms of this reflective nonlinearity are demonstrated in a 1550 nm VCSOA,

including clockwise, counterclockwise, and butterfly. A counterclockwise bistability is shown with input powers as low as 2 μW. This is the lowest switching power demonstrated to date in a 1550 nm device.

Chapter 5 summarizes the contributions of this thesis and outlines future technical directions for the work.

Finally, the Appendix provides an overview of line coding methods, including 8B/10B and 64B/66B, that are relevant to the high pass filtering discussion in Chapter 2.

1.5 References

[1] Robert W. Keyes, "The Impact of Moore's Law", *IEEE Solid-State Circuits*, September 2006.

[2] Gail Robinson, "Architects of the Internet: David Bishop", *EE Times,* Sept. 26, 2000.

[3] D. van den Borne, V.A.J.M. Sleiffer, M.S. Alfiad, S.L. Jensen, and T. Wuth, "POLMUX-QPSK Modulation and Coherent Detection: the Challenge of Long-Haul 100G Transmission", *Proc. European Conference on Optical Communications*, paper 3.4.1, 2009.

[4] A. Donoghue, "AT&T: Internet to Hit Full Capacity by 2010", *CNET news*, April 18, 2008, http://news.cnet.com/2100-1034_3-6237715.html, retrieved July 2010.

[5] J.R. Stern, J.W. Ballance, D.W. Faulkner, S. Hornung, D.B. Payne, and K. Oakley, "Passive Optical Local Networks for Telephony Applications and Beyond", *Electronics Lett.*, vol. 23, no. 24, pp. 1255-1257, 1987.

[6] M.P. McGarry, M. Reisslein, and M. Maier, "WDM Ethernet Passive Optical Networks", *IEEE Optical Communications*, pp. S18-S25, Feb. 2006.

[7] H. Ishio, J. Minowa, and K. Nosu, "Review and Status of Wavelength-Division-Multiplexing Technology and Its Application", *J. Light. Tech.*, vol. LT-2, no. 4, pp. 448-463, 1984.

[8] Fiberdyne Labs Inc.., "Dense Wave Division Multiplexing (DWDM) ITU Grid C-Band, 100 GHz Spacing", retrieved from http://www.fiberdyne.com/products/itu-grid.html, July 2010.

[9] R.D. Feldman, E.E. Harstead, S. Jiang, T.H. Wood, M. Zirngibl, "An Evaluation of Architectures Incorporating Wavelength Division Multiplexing for Broad-Band Fiber Access", *J. Light. Tech.*, vol. 16, no. 9, pp. 1546-1559, 1998.

[10] N.J. Frigo, P.P. Iannone, P.D. Magill, T.E. Darcie, M.M. Downs, B.N. Desai, U. Koren, T.L. Koch, C. Dragone, H.M. Presby, and G.E. Bodeep, "A Wavelength-Division Multiplexed Passive Optical Network with Cost-Shared Components", *IEEE Phot. Tech. Lett.*, vol. 6, no. 11, pp. 1365-1367, 1994.

[11] G.P. Agrawal and N.K. Dutta, Semiconductor Lasers, *Klewer Academic*, 1993.

[12] J. Bromage, P.J. Winzer, and R.-J. Essiambre, "Multiple Path Interference and Its Impact on System Design" in *Raman Amplifiers for Telecommunications 2*, M.N. Islam, Ed. New York: Springer-Verlag, ch. 15, 2004.

[13] T.H. Wood, R.A. Linke, B.L. Kasper, and E.C. Carr, "Observation of coherent Rayleigh noise in single-source bidirectional optical fiber systems", *IEEE J. Light. Tech.*, vol. 6, pp. 346-352, 1988.

[14] A. Djupsjobacka, G. Jacobsen, B. Tromborg, "Dynamic Stimulated Brillouin Scattering Analysis", *IEEE J. Light. Tech.*, vol. 18, no. 3, pp. 416-424, 2000.

[15] M.-C. Michel, "ORL Measurements in Field Applications", *Application Note 140*, Exfo Communications, available at http://documents.exfo.com/appnotes/anote140-ang.pdf, retrieved July 2010.

[16] M. Fujiwara, J.-i. Kani, H. Suzuki, and K. Iwatsuki, "Impact of Backreflection on Upstream Transmission in WDM Single-Fiber Loopback Access Networks", *IEEE J. Light. Tech.*, vol. 24, pp. 4568-4583, 2006.

[17] I. Papagiannakis, M. Omella, D. Klondis, A. Birbas, J. Kikidis, I. Tomkos, and J. Prat, "Investigation of 10-Gb/s RSOA-Based Upstream Transmission in WDM-PONs Utilizing Optical Filtering and Electronic Equalization", *IEEE Phot. Tech. Lett.*, vol. 20, 24, pp. 2168-2170, 2008.

[18] M. Omella, I. Papagiannakis, B. Schrenk, D. Klonidis, J.A. Lázaro, A.N. Birbas, J. Kikidis, J. Prat, and I. Tomkos, "10 Gb/s Full-Duplex Bidirectional Transmission with RSOA-based ONU Using Detuned Optical Filtering and Decision Feedback Equalization", *Opt. Express*, vol. 17, 7, pp. 5008-5013, 2009.

[19] W. Hung, C.-K. Chan, and F. Tong, "An Optical Network Unit for WDM Access Networks with Downstream DPSK and Upstream Remodulated OOK Data Using Injection Locked FP Laser", *IEEE Phot.Tech. Lett.*, vol. 15, no. 10, pp. 1476-1478, 2003.

[20] G.-K. Chang, A. Chowdhury, Zhensheng Jia, H.-C. Chien, M.-F. Huang, Juanjun Yu, and G. Ellinas, "Key Technologies of WDM-PON for Future Converged Optical Broadband Access Networks", *IEEE J. Opt. Commun. Netw.*, vol. 1, no. 4, pp. C35-C49, 2009.

[21] Minhao Li, Wei Hong, Xinliang Zhang, Wei Li, and Dexiu Huang, "Investigation of a High-Speed Optical FSK Scheme for WDM-PON Applications with Centralized Lightwave Source", *Optics Comm.*, vol. 283, no. 7, pp. 1251-1260, 2010.

[22] SangJo Park and Bong Kyu Kim, "Performance Analysis for Optimizing Threshold Level Control of a Receiver in Asynchronous 2.5 Gbps/1.2 Gbps Optical Subscriber Network with Inverse Return to Zero (RZ) Coded Downstream and NRZ Upstream Re-Modulation", *J. Opt. Soc. Korea*, vol. 13, no. 3, pp. 361-366, 2009.

[23] B.K. Kim, H. Park, S. Park, K. Kim, "Optical Access Network Scheme with Downstream Manchester Coding and Upstream NRZ Remodulation", *Elec. Lett.*, vol. 42, no. 8, pp. 484-485, 2006.

[24] R. Wang, S. Fu, P.P. Shum, and C. Lin, "10 Gbit/s WDM-PON Using Downstream PolSK Coded by Polarisation Modulator and Upstream Intensity Re-modulation", *Elec. Lett.*, vol. 46, no. 6, pp. 428-429, 2010.

[25] Bo Huang, Yaoxiong Liang, Yi Qin, and Nan Chi, "A Novel Coding Method with Remodulation Format Used in a WDM-PON to Enhance Extinction Ratio",*Microwave and Opt. Tech. Lett.*, vol. 51, no. 12, pp. 2994-2997, 2009.

[26] C.W. Chow and C.H. Yeh, "Signal Remodulation Without Power Sacrifice for Carrier Distributed Hybrid WDM-TDM PONs using PolSK", *Opt. Comm.*, vol. 282, no. 7, pp. 1294-1297, 2009;

[27] L. Xu and H.K. Tsang, "WDM-PON Using Differential-Phase-Shift-Keying Remodulation of Dark Return-to-Zero Downstream Channel for Upstream", *IEEE Phot. Tech. Lett.*, vol. 20, no. 9, pp. 833-835, 2008.

[28] C.W. Chow, "Wavelength Remodulation Using DPSK Down-and-Upstream With High Extinction Ratio for 10-Gb/s DWDM-Passive Optical Networks", *Phot. Tech. Lett.*, vol. 20, no. 1, pp. 12-14, 2008.

[29] L.Y. Chan, C.K. Chan, D.T.K. Tong, F. Tong, and L.K. Chen, "Upstream Traffic Transmitter Using Injection-Locked Fabry-Perot Laser Diode as Modulator for WDM Access Networks", *Elec. Lett.*, vol. 38, no. 1, pp. 43-45, 2002.

[30] Zhaowen Xu, Yang Jing Wen, Wen-De Zhong, Tee Hiang Cheng, M. Attygalle, Ziaofei Cheng, Yong-Kee Yeo, Tixin Wang, and Chao Lu, "Characteristics of Subcarrier Modulation and Its Application in WDM-PONs", *IEEE J.. Light. Tech.*vol. 27, no. 12, pp. 2069-2076, 2009.

[31] Chien-Hung Yeh, Chi-Wai Chow, and Chih-Hung Hsu, "40-Gb/s Time-Division-Multiplexed Passive Optical Networks Using Downstream OOK and Upstream OFDM Modulations",*IEEE Phot. Tech. Lett*, vol. 22, no. 2, pp. 118-120, 2010.

[32] Jianjun Yu, Ming-Fang Huang, Dayou Qian, Lin Chen, and Gee-Kung Chang, "Centralized Lightwave WDM-PON Employing 16-QAM Intensity Modulated OFDM Downstream and OOK Modulated Upstream Signals", *IEEE Phot. Tech. Lett*, vol. 20, no. 18, pp. 1545-1547, 2008.

[33] Z. A. El-Sahn, B. J. Shastri, Ming Zeng, N. Kheder, D.V. Plant, L.A. Rusch, "Experimental Demonstration of a SAC-OCDMA PON with Burst-Mode Reception: Local Versus Centralized Sources", *IEEE J. Light. Tech.*, vol. 26, no. 10, pp.1192 -1213, 2008.

[34] A. Chowdhury, Hung-Chang Chien, Ming-Fang Huang, Jianjun Yu, and Gee-Kung Chang, "Rayleigh Backscattering Noise-Eliminated 115-km Long-Reach Bidirectional Centralized WDM-PON with 10-Gb/s DPSK Downstream and Remodulated 2.5-Gb/s OCS-SCM Upstream Signal",*IEEE Phot. Tech Lett.*, vol. 20, no. 24, pp. 2081-2083, 2008.

[35] C.W. Chow, C.H. Yeh, C.H. Wang, F.Y. Shih, and S. Chi, "Rayleigh Backscattering Performance of OFDM-QAM in Carrier Distributed

Passive Optical Networks", *IEEE Phot Tech. Lett.*, vol. 20, no. 22, 2008.

[36] C.W. Chow, G. Talli, A.D. Ellis, and P.D. Townsend, "Rayleigh Noise Mitigation in DWDM LR-PONs Using Carrier Suppressed Subcarrier-Amplitude Modulated Phase Shift Keying", *Opt. Exp.*, vol. 16, no. 3, pp. 1860-1866, 2008.

[37] Ming Tang, Songnian Fu, and Perry Ping Shum, "Seamless Generation and Provisioning of Broadcasting and Independent Services in WDM-PON Access Networks", *Opt. Exp.*, vol. 17, no. 12, pp. 9630-9636, 2009.

[38] C.W. Chow, C.H. Yeh, C.H. Wang, F.Y. Shih, and S. Chi, "Signal Remodulation of OFDM-QAM for Long Reach Carrier Distributed Passive Optical Networks", *IEEE Phot. Tech. Lett.*, vol. 21, no. 11, pp. 715-717, 2009;

[39] L. Giorgi, F. Cavaliere, P. Ghiggino, F. Ponzini, A. Bianchi, and A. D'Errico, "Characterization of a High Capacity Multi-User Optical Access Network Using 1 Gb/s 16 QAM Subcarrier Multiplexing", *IEEE J. Light. Tech.*, vol. 27, no. 9, pp. 1203-1211, 2009.

[40] Q.T. Nguyen, P. Besnard, L. Bramerie, A. Shen, C. Kazmierski, P. Chanclou, Guang-Hua Duan, and J.-C. Simon, "Bidirectional 2.5-Gb/s WDM-PON Using FP-LDs Wavelength-Locked by a Multiple-Wavelength Seeding Source Based on a Mode-Locked Laser", *IEEE Phot. Tech. Lett.*, vol. 22, no. 11, pp. 733-735, 2010.

[41] Su Hwan Oh, Jang-Uk Shin, Yoon-Jung Park, Sung-Bock Kim, Sahnggi Park, Hee-Kyung Sung, Yong-Soon Baek, and Kwang-Ryong Oh, "Multiwavelength Lasers for WDM-PON Optical Line Terminal Source by Silica Planar Lightwave Circuit Hybrid Integration", *IEEE Phot. Tech. Lett*., vol. 19, no. 17, pp. 1622-1624, 2007.

[42] Z. A. El-Sahn, W. Matholouthi, H. Fathallah, S. LaRochelle, and L.A. Rusch, "Dense SS-WDM Over Legacy PONs: Smooth Upgrade of Existing FTTH Networks", *J. Light. Tech.*, vol. 28, no. 10, pp. 1485-1495, 2010.

[43] C.W. Chow, L. Xu, C.H. Yeh, H.K. Tsang, W. Hofmann, and M.C. Amann, "40-Gb/s Upstream Transmitters Using Directly Modulated 1.55-μm VCSEL Array for High-Split-Ratio PONs", *IEEE Phot. Tech. Lett.*, vol. 22, no. 5, pp. 347-349, 2010.

[44] G. Talli and P.D. Townsend, "Hybrid DWDM-TDM Long-Reach PON for Next-Generation Optical Access", *IEEE J. Light. Tech.*, vol. 24, no. 7, pp. 2827-2834, 2006.

[45] W.S. Tsai, H.-H. Lu, S.-J. Tzeng, S.-H. Chen, and T.-S. Chien, "A Bidirectional Hybrid DWDM-PON Employing Optical Injection Locking Technique and Data Comparators", *Opt. Comm.*, vol. 263, no. 2, pp. 201-206, 2006.

[46] Elaine Wong, Xiaoxue Zhao, C.J. Chang-Hasnain, W. Hofmann, and M.C. Amann, "Optically Injection-Locked 1.55 μm VCSELs as Upstream Transmitters in WDM-PONs", *IEEE Phot. Tech. Lett.*, vol. 18, no. 21, pp 2371-2373, 2006.

[47] Songnian Fu, Wen De Zhong, P. Shum, and Chinlon Lin, "Simultaneous Implementation of Photonic Logic OR and AND Gates for CSRZ-OOK Signals", *IEEE Phot. Tech. Lett.*, vol. 22, no. 13, pp. 960-962, 2010.

[48] R. Kumar, Liu Liu, G. Roelkens, E.-J. Geluk, T. de Vries, F. Karouta, P. Regreny, D. Van Thourhout, R. Baets, and G. Morthier, "10 GHz All-Optical Gate Based on a III-V/SOI Microdisk", *IEEE Phot. Tech. Lett.*, vol. 22, no. 13, pp. 981-983, 2010.

[49] Jianji Dong, Xinliang Zhang, and Dexiu Huang, "A Proposal for Two-Input Arbitrary Boolean Logic Gates Using Single Semiconductor Optical Amplifier by Picosecond Pulse Injection", *Opt. Exp.*, vol. 17, no. 10, pp. 7725-7730, 2009.

[50] S. Nakamura, Y. Ueno, and K. Tajima, "168-Gb/s All-Optical Wavelength Conversion with a Symmetric-Mach-Zender-Type Switch", *IEEE Phot. Tech. Lett.*, vol. 13, no. 10, pp. 1091-1093, 2001.

[51] Haijiang Zhang, Pengyue Wen, and S. Esener, "Cascadable All-Optical Inverter Based on a Nonlinear Vertical-Cavity Semiconductor Optical Amplifier", *Opt. Lett.*,vol. 32, no. 13, pp. 1884-1886, 2007.

[52] Deqiang Song, V. Gauss, Haijiang Zhang, M. Gross, Penyue Wen, and S. Esener, "All-Optical Flip-Flop Based on Vertical Cavity Semiconductor Optical Amplifiers", *Opt. Lett.*, vol. 32, no. 20, pp. 2969-2971, 2007.

[53] A.J. Poustie, K.J. Blow, and R.J. Manning, "Storage Threshold and Amplitude Restoration in an All-Optical Regenerative Memory", *Opt. Comm.*, vol. 146, no. 1, pp. 262-267, 1998.

[54] A. Melloni, A. Canciamilla, C. Ferrari, *et al*, "Tunable Delay Lines in Silicon Photonics: Coupled Resonators and Photonic Crystals, a Comparison", *IEEE Phot. Journ.*, vol. 2, no. 2, pp. 181-194, 2010.

[55] M.J. Adams, H.J. Westlake, M.J. Omahony, and I.D. Henning, "A Comparison of Active and Passive Optical Bistability in Semiconductors"*, IEEE J. Quant. Elec.*, vol. 21, no. 9, pp. 1498-1504, 1985.

2. Low Frequency Noise Filtering in a CLS-PON

The design of a central light source passive optical network (CLS-PON) differs significantly from traditional optical link design due to the extreme cost pressure and presence of bidirectional noise. In remotely seeded links the received signal is subject to in-band optical noise as the result reflections from interfaces (Fresnel reflections) and the fiber itself (Rayleigh backscattering) [1,2]. One technique previously proposed for reducing the impact of these in-band noise sources is to high pass filter the received signal [3-5]. In this chapter the possibilities and limits of this technique for cheaply improving the performance of a CLS-PON are explored experimentally and theoretically.

It is first confirmed through experimentation that HPF is capable of significantly reducing the power penalty induced by different types of Rayleigh noise, in certain situations by up to 10 dB. The model from [4] is experimentally verified using a complete CLS-PON link testbed. A model to calculate the effect of baseline wander (BLW) due to HPF is developed and experimentally verified. Finally the incorporation of this model into that developed for Rayleigh noise allows the calculation of link performance as a function of source linewidth. It is shown that through the use of proper HPF and line coding a significantly broader, and cheaper, CO laser can be used as a source.

2.1 Experimental Verification of High Pass Filtering of Rayleigh Noise

Current central light source (CLS) PONs suffer from two types of Rayleigh backscattering. As shown in Fig. 1, type I occurs when the seed light reflects from the feeder fiber creating noise with the same bandwidth as the laser linewidth. Type II occurs when upstream data is reflected back to the optical network unit (ONU), combined with seed light, amplified, and transmitted to the central office (CO) along with the desired signal [2]. Another type of Rayleigh noise will sometimes be present if the lightsource in the CLS-PON is time multiplexed between upstream and downstream transmission, such that sometimes a CW and sometimes a modulated signal is sent downstream. This will be referred to as Coherent Rayleigh after [4]. The PON will be subject to different levels of each of these types of Rayleigh noise depending on the modulation format, source linewidth, and gain of the ONU.

Previous work on this noise has focused on evaluating the impact [1,2,5], reducing the penalty through link engineering [6], reducing it through different modulation formats [7], and reducing it through filtering [3-5]. The potential for system improvement through high pass filtering (HPF) has been demonstrated before [3-5] due to the elimination of signal-Rayleigh beat noise concentrated in low frequencies. The concentration of noise near DC, and thus the effectiveness of HPF, depends on factors such as the type of Rayleigh (I or II) and extinction ratio (ER). In intensity modulated signals beating between Rayleigh noise and the signal creates noise with greater density (mW/Hz) at low frequencies if the spectra of the noise and

signal have strong DC components, as in Fig. 1. The spectrum for Type I is a single tone, and for Type II it has a strong carrier component in intensity modulated signals, and thus will generate noise at low frequencies. The linewidth of the laser causes noise spreading to frequencies above DC, and thus a higher DC blocking capacitor cutoff than is generally used for receiver DC blocking is preferable.

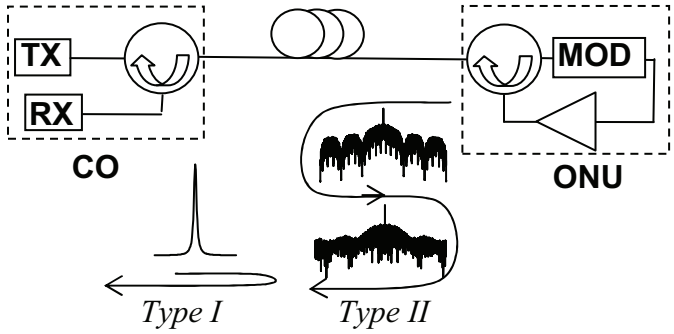

Fig. 2.1. Rayleigh injection experimental setup

2.1.1 Experimental Procedure

2.1.1.1 High Pass Filter Design

Optical receivers are generally AC coupled to the decision circuit by blocking capacitors. In order to implement optimal filtering, therefore, the existing blocking capacitor simply has to be replaced with a lower value (higher cutoff frequency) capacitor. For this experiment the HPFs were created using simple blocking capacitors on microstrip transmission lines. The microstrip and capacitor geometry were designed to minimize the induced penalty. In particular the group delay must be flat (linear phase) across the entire bandwidth of the signal in order to prevent delay of the rising and falling edges and eye closure. Incidentally, in previous work [3]

HPFs were used with worse group delay and filtering characteristics, as shown in Fig. 2, leading to higher penalty and less sensitivity improvement.

First order RC filters were constructed using microstrip transmission lines of 0.75 mm width on a 0.25 mm substrate (ε=2.2) with 0.25 mm x 0.5 mm capacitors. Capacitance values were chosen according to [3]

$$f_{LFC} = \frac{1}{2\pi(R_s + R_L)C} \tag{2.1}$$

where f_{LFC} is the filter 3-dB cutoff frequency, R_s and R_L are the source and load impedances (usually 50 Ω), and C is the capacitor value.

Measured prototype values were 1.55, 3.05, 11, 15, and 21 MHz. Newly constructed filters demonstrated small group delay variation and minimal insertion loss to 20 GHz compared to previously constructed filters.

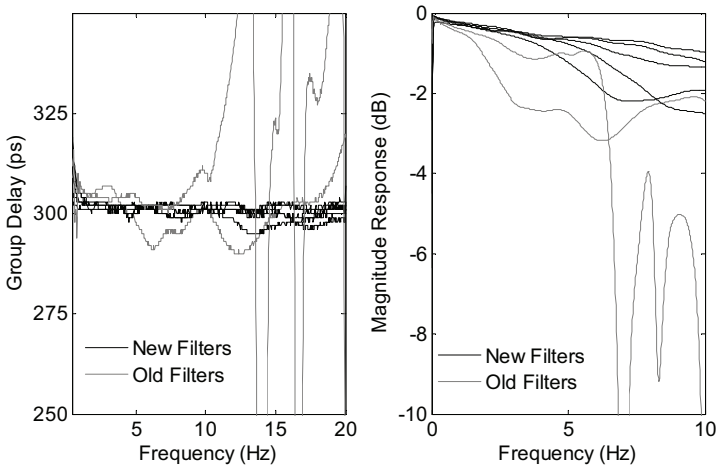

Fig. 2.2. Measured Group Delay and Magnitude Response of HPF used in this experiment (black lines) compared to those used in [3] (gray lines)

The filters were tested in an actual link to ensure that the penalty for using them was small. Fig. 2.3 shows that the penalty due to the insertion of the HPF is extremely small, not measurable even.

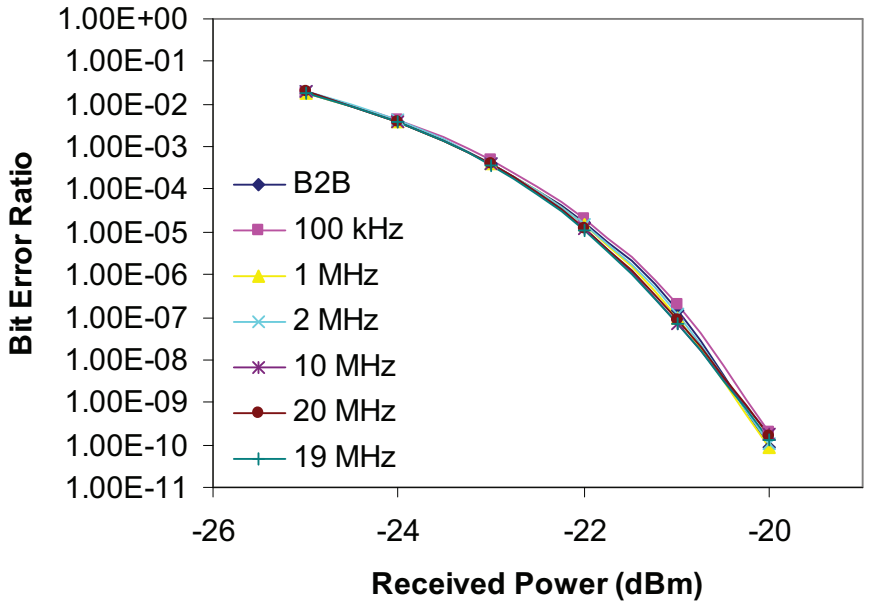

Fig. 2.3. Receiver sensitivity using various DC blocks from this experiment

2.1.1.2 Type I and Coherent Rayleigh Evaluation

A testbed for variable noise and signal injection was constructed to study the effectiveness of HPF on elimination of Type I Rayleigh-signal and Coherent Rayleigh-signal beat noise in upstream data transmission. This setup, shown in Fig. 3, is similar to that employed in [1]. A laser with a 3 MHz linewidth is split into two paths. In the upper path the signal is modulated with a 10 Gb/s Non-Return to Zero (NRZ) on-off keyed (OOK) signal using a Mach-Zender interferometer modulator (MZI). The modulated light is amplified with an EDFA and filtered with an optical band pass filter (OBPF) with a 3 dB bandwidth of 0.5 nm to remove the excess ASE.

Throughout the experiments the OSNR due to ASE from the amplifier was kept above 30 dB to maintain a low penalty due to ASE.

In the lower arm the laser is launched into 50 km of standard single mode fiber (SSMF) terminated with a 20 dB attenuator. Approximately -34 dBm of Rayleigh noise is collected with a circulator and coupled with the signal path through a 90/10 combiner. Polarization controllers are used to ensure that the signal and noise are copolarized. Finally the signal is converted to a single ended electrical signal with an 8 GHz PIN photodiode and the electrical signal is filtered and detected with an error detector.

For each data point a fixed Rayleigh noise level was injected and the signal power level was increased until a bit error ratio (BER) of 10^{-9} was achieved. The measured penalty is the difference between this power level and the power necessary for the same BER with no Rayleigh noise (the sensitivity of the receiver). The ratio between the received signal and Rayleigh noise is the Rayleigh optical signal to noise ratio (ROSNR). The extinction ratio of the modulator was either 13 dB to 6 dB. The bit pattern was varied between 2^{31}-1 and 2^{7}-1 bits to simulate channels with variable low frequency content, as would be present in a line coded signal. For coherent modulated Rayleigh the modulator was placed before the initial splitter to create Rayleigh noise with a spectrum identical to the source, then the signal recombined normally.

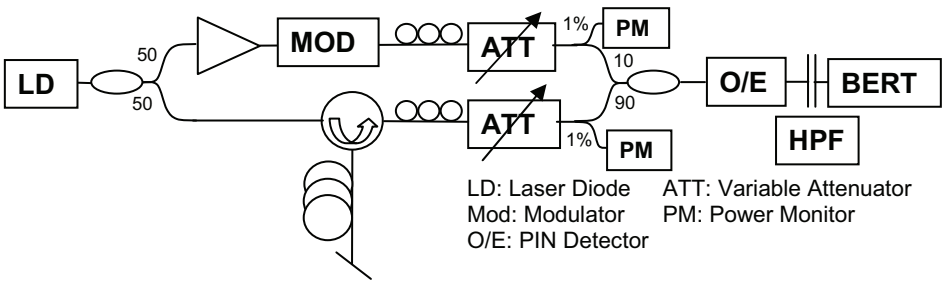

Fig. 2.4. Rayleigh Type I experimental setup

2.1.1.3 Type II Rayleigh Evaluation

A testbed similar to that in [2] was constructed to evaluate the effectiveness of HPF on type II Rayleigh (Fig. 2.4), again using a 10 Gb/s NRZ-OOK signal. In this setup some light is split off from the output of a modulator and looped back to the input of the gain-modulation stage. Note that the ROSNR must be measured as the ratio of noise and CW light *before* the modulator. As mentioned in [1] this causes a shift in the ROSNR baseline between 0 and 3 dB depending on the ER of the signal. Note that the penalty due to type II Rayleigh is also highly dependent on the gain, in this case set to 22.5 dB to nearly match the losses due to the splitters. The relationship between the impact of type II Rayleigh and gain will be further explored later in this chapter.

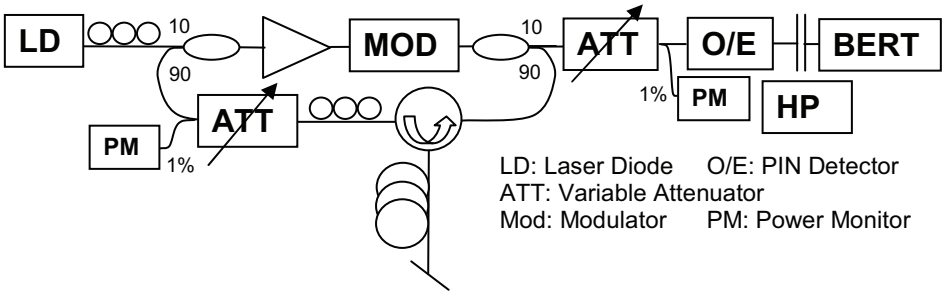

Fig. 2.5. Rayleigh Type II experimental setup

2.1.2. High Pass Filtering Experimental Results

2.1.2.1. Rayleigh I Noise Reduction

The effect of HPF with various cutoff frequencies on signal-Type I Rayleigh noise with various ERs and data patterns are shown in Fig. 2.5. For the 2^7-1 PRBS pattern with a 6 dB ER, as the level of Rayleigh increases the penalty increases dramatically for the low cutoff frequency case. For higher cutoff frequencies the Rayleigh is effectively filtered, resulting in an ROSNR improvement at 1 dB of more than 10 dB.

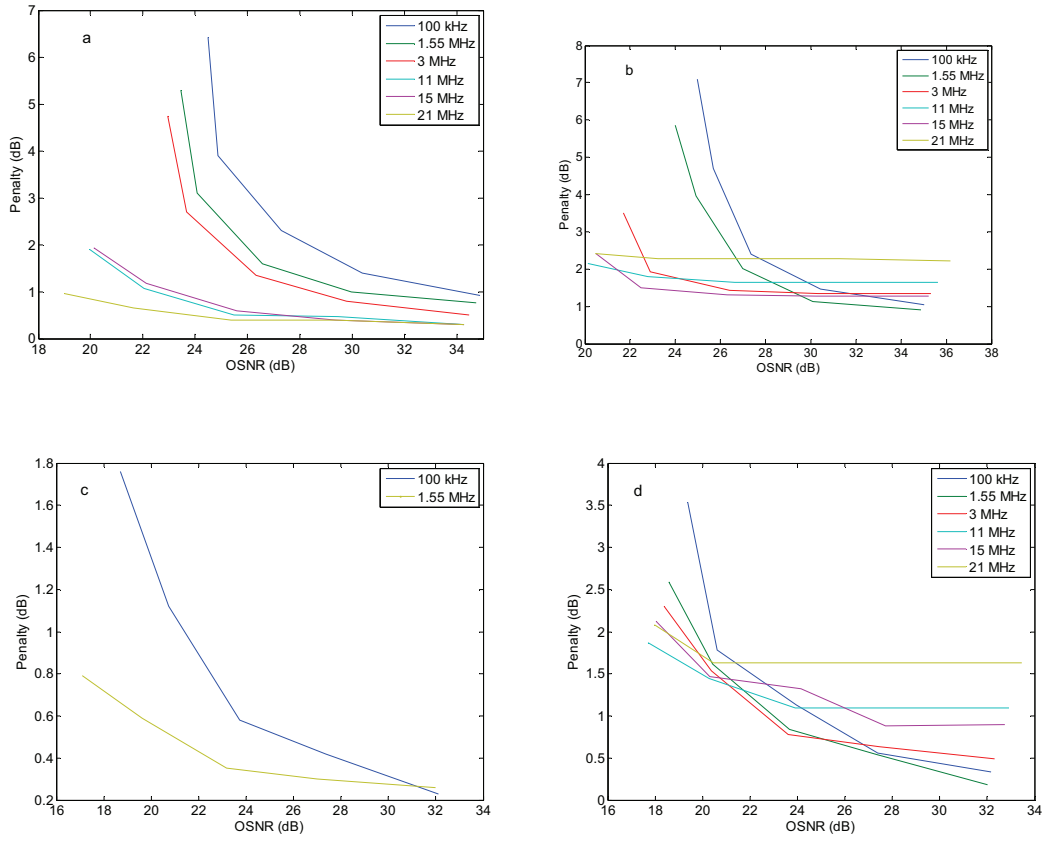

Fig. 2.5. Power Penalty due to type I Rayleigh for (a) 2^7-1 PRBS pattern, 6 dB ER, (b) 2^{31}-1 PRBS pattern, 6 dB ER, (c) 2^7-1 PRBS pattern, 13 dB ER, (d) 2^{31}-1 PRBS pattern, 13 dB ER

For the other datapattern and ER combinations the situation is not as straightforward. For the 2^7-1 PRBS pattern and 13 dB ER the pattern is still the same, with performance improving and penalty decreasing with each increasing value of high pass cutoff filter frequency, although less dramatically since less noise if concentrated at low frequencies. For the 2^{31}-1 PRBS pattern the situation is quite different. In this case the low frequency content, and thus baseline wander penalty, is significantly higher than for the 2^7-1 PRBS pattern. In this case the high pass filters are only worthwhile when the ROSNR is low enough that power penalty due to Rayleigh noise is more significant than the penalty due to baseline wander. Since the Rayleigh OSNR from Type I depends on the ratio of the CO launch power to the ONU launch power less the fiber loss, the optimal filter value will be a function of the link loss.

Sensitivity measurements were also taken at a lower 10^{-3} BER. Contrary to the results of [4], it was found that the addition of HPF led to a more significant improvement at low BERs. This was confirmed for both Type I and Coherent Rayleigh.

2.1.2.2. Coherent Rayleigh Noise Reduction from High Pass Filtering

High pass filtering of Coherent Rayleigh-signal beat noise has previously been demonstrated [4], and shown to be effective in only a narrow range of situations. Here it is shown through more thorough investigation with improved high pass filters that it is effective in a wide range of circumstances. Fig. 2.6 shows the penalty from Coherent Rayleigh under similar conditions to what were tested for Fig. 2.5.

Since Coherent Rayleigh has half roughly half as much power at DC (for an infinite ER signal), the high pass filtering of Coherent Rayleigh-signal beat noise is significantly less effective. While still effective for the short PRBS pattern, it is less so than for Type I noise. With the long PRBS pattern and high extinction ratio, high pass filtering never shows improvement before the error floor!

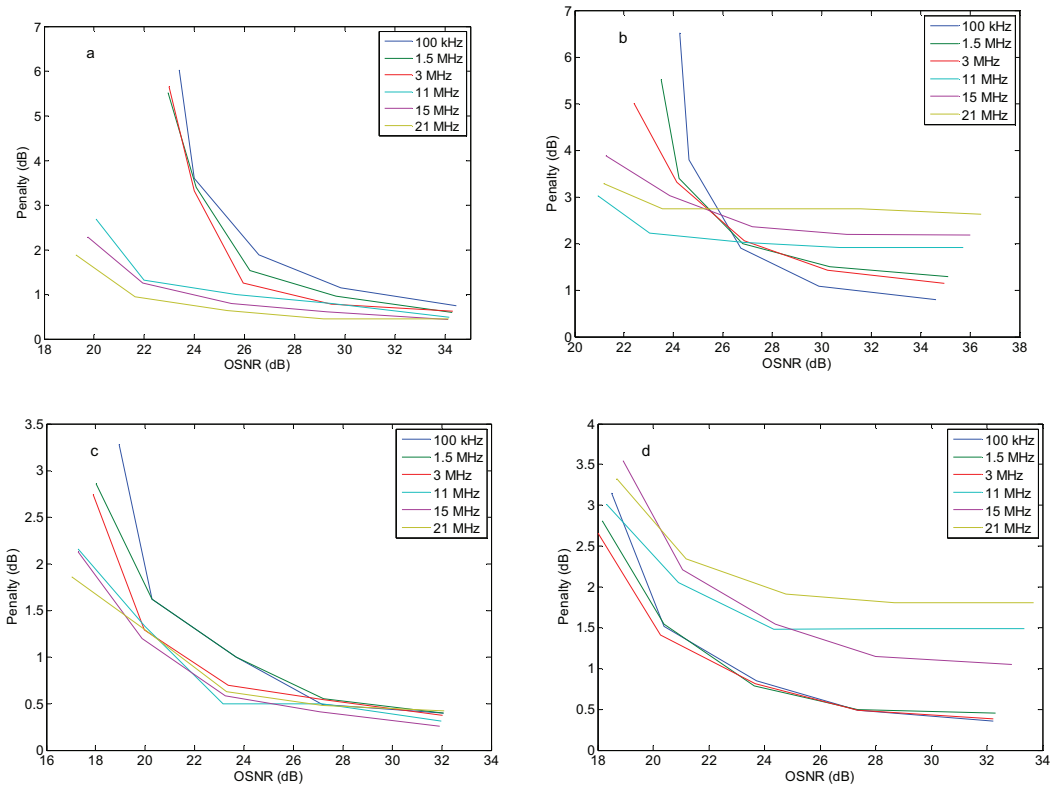

Fig. 2.6. Power Penalty due to Coherent Rayleigh for (a) 2^7-1 PRBS pattern, 6 dB ER, (b) 2^{31}-1 PRBS pattern, 6 dB ER, (c) 2^7-1 PRBS pattern, 13 dB ER, (d) 2^{31}-1 PRBS pattern, 13 dB ER

2.1.2.3. Type II Rayleigh Noise Reduction from High Pass Filtering

Experiments involving Type II Rayleigh are significantly different from Type I or Coherent Rayleigh Experiments. As described in section 2.1.1.3, these experiments require either a loop of some sort [2] or a series of cascaded modulators

[1] to isolate the effect of Type II from Type I Rayleigh or other noise sources. There is also the problem of the ROSNR due to Rayleigh being lower for Type II because it is reduced by remodulation by up to 3 dB. Regardless, using the setup in Fig. 2.4 we can isolate the effects to produce penalty vs. ROSNR curves as shown in Fig. 2.7. While difficult to compare numerically (this will be done in the next section) it is apparent that HPF improves the performance of the link in a qualitatively similar manner to Type I and Coherent signal beat noise. For a 2^7-1 PRBS pattern with limited low frequency content the penalty is reduced steadily with increased cutoff frequency for each ER, although more significantly for the more noise dominated low ER signal. For the longer 2^{31}-1 PRBS pattern and low ER case, improvement is seen up to 3 MHz of filtering consistently, but BLW penalties overwhelm the filtering improvement at high ROSNR values for higher cutoff frequencies. When the ER is improved to 14 dB there is no significant improvement from HPF.

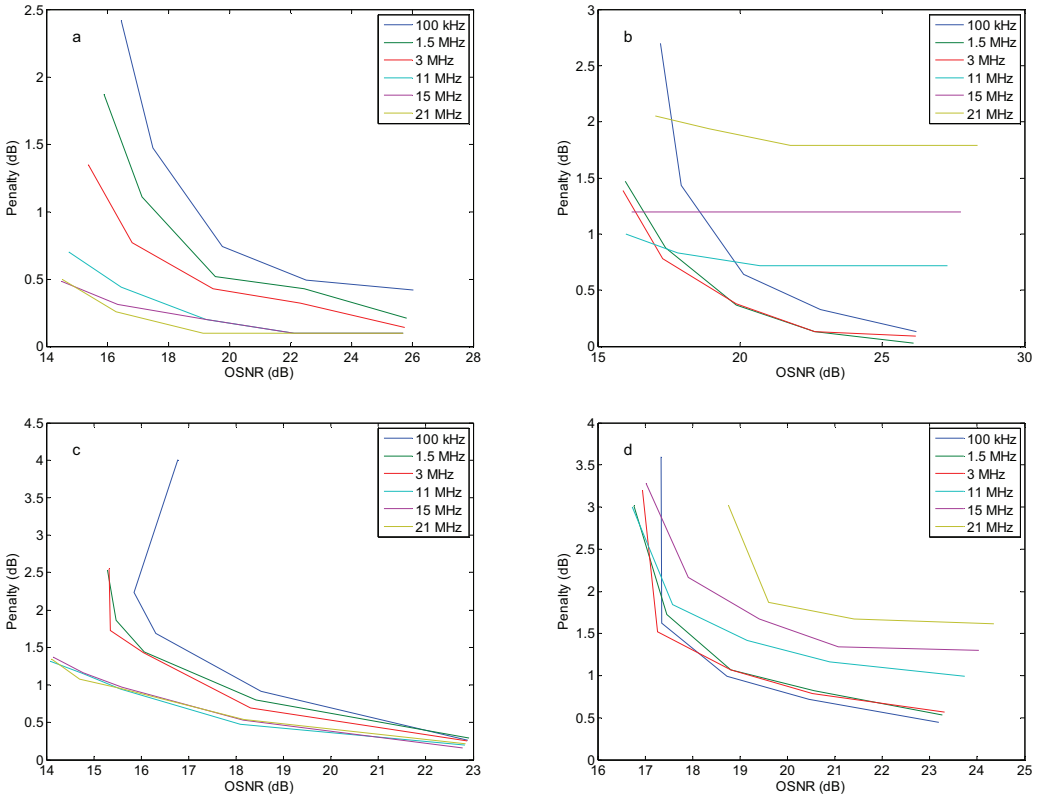

Fig. 2.7. Power Penalty due to Type II Rayleigh for (a) 2^7-1 PRBS pattern, 6 dB ER, (b) 2^{31}-1 PRBS pattern, 6 dB ER, (c) 2^7-1 PRBS pattern, 13 dB ER, (d) 2^{31}-1 PRBS pattern, 13 dB ER

2.1.2.4 Optimal Experimental High Pass Cutoff Frequency

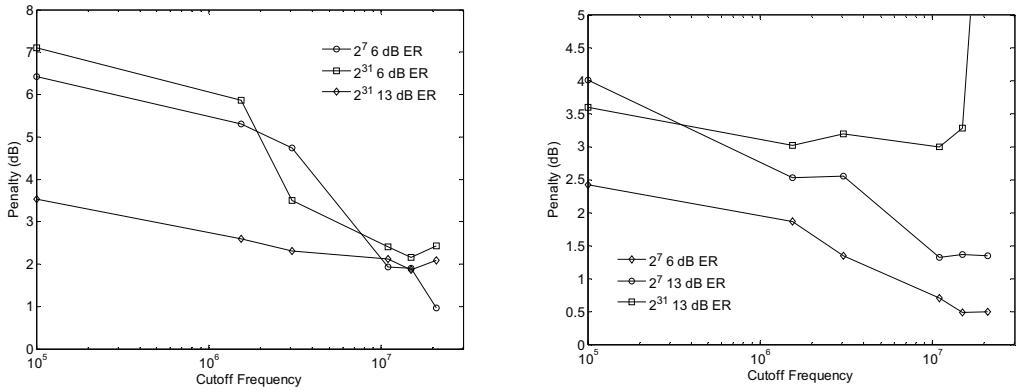

Fig. 2.8. Power Penalty for 10-^{9} BER for a constant noise input of -39 dBm for Type 1 Rayleigh (sensitivity ~-21dBm for 6 dB ER or -23 dBm for 13 dB ER, 27-1 PRBS pattern, left) and Power Penalty for 10-^{9} BER for a constant noise input of -36.8 dBm for Type 2 Rayleigh (sensitivity ~-21dBm for 6 dB ER or -23 dBm for 13 dB ER, right).

Fig 2.8 shows the power penalty due to the introduction of a constant Rayleigh noise power as a function of HPF cutoff frequency. Proper HPF requires a balance between Rayleigh noise that is reduced as the cutoff frequency of the filter is increased and baseline wander induced by the HPF attenuating long strings of marks or spaces. This can be seen with the 2^{31} bit pattern data, where the penalty increases with higher cutoff frequencies.

For a 10 Gb/s signal with a bit pattern of 2^7-1 bits the low frequency signal content is minimized such that baseline wander caused no significant penalty below 21 MHz, the highest cutoff frequency available. Optimal cutoff frequencies are expected to be in the 20-100 MHz range for a 2^7-1 PRBS signal at 10 Gb/s. This confirms the results shown in [5] using line coding and shows that they hold for type II Rayleigh. The result for 2^7-1 signals should be similar to that for 8B/10B coded

signals at a similar datarate. With lower datarates, broader sources, or other coding schemes (such as 64b/66b) the baseline wander penalty would be increased.

2.1.2.5 Impact of Decision Threshold

It is known that signal noise beating causes a shift to lower optimal decision voltage thresholds due to asymmetry of the noise levels on marks and spaces. Lower beat noise levels thus relax decision threshold sampling requirements. Fig. 8 shows the effect of using an optimal vs. 0V decision level. Results show that HPF reduces the requirement to sample at the optimal voltage due to Rayleigh, simplifying link requirements. The optimal threshold voltage reduction was most significant in cases where filtering was most effective, and least significant when little improvement was shown with filtering.

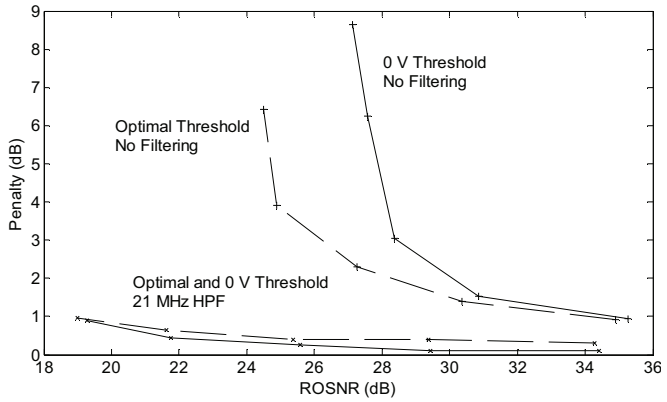

Fig. 2.9. Penalty comparison with and without optimal receiver voltage threshold, 6 dB ER 2^7-1 signal subject only to type I Rayleigh

2.2 Theoretical Model for Rayleigh Noise

In the previous section it was demonstrated that high pass filtering could significantly improve detection of an NRZ signal subject to all types of Rayleigh

noise. It was shown that Rayleigh noise was most effectively filtered when the signal had a low extinction ratio, causing a significant amount of power to be concentrated around DC. It was also found that the length of the transmitted signal played an important role in determining how much penalty was incurred due to filtering. In this section a model will be developed to predict the performance of a link subject to Rayleigh noise and HPF.

2.2.1. CLS-PON Link Model

The performance of a CLS-PON link dominated by backreflection noise was first modeled by Fujiwara. Arellano *et al* derived a model including the effect of discrete backreflection points and found a different value for optimal gain than the previous models [8]. This model, however, took a very broad treatment of the noise effects and did not account for specific signal parameters. A revised model from [2] explicitly considering the spectrum of Type I and Type II Rayleigh-signal beat noise, the modulation format, and signal extinction ratio was derived in [4], and the derivation is reproduced here for clarity.

2.2.1.1 Approach and Assumptions

Complete details of the derivation for the theoretical model can be found in [6]. The model is similar to the model proposed and verified by Fujiwara [1] to treat the impact of backreflections in a CLS-PON. However it explicitly considers the spectrum of the Type I and Type II Rayleigh-signal beat noise, the filtering effects at the receiver, and the impact of modulation format and extinction ratio. The fundamental approach is to approximate Rayleigh noise as a Gaussian noise source, and calculate the noise variance and signal levels of the marks and spaces

independently, and then calculate the BER from using the complementary error function. This approach also facilitates the incorporation of baseline wander penalty as shown in the next section.

The model is for a CW downstream light modulated with an on-off keyed (OOK) intensity signal at the ONU. It assumes that Rayleigh-signal beat noise is the dominant noise source, and ignores ASE, dispersion, thermal noise, shot noise, Brillouin noise, and all other noise factors. Intersymbol interference due to filtering effects will be addressed in the following section. Finally it assumes a flat, infinite bandwidth linear modulation at the ONU.

As discussed in section 2.1, the two types of Rayleigh noise have very different noise spectra. Different filtering techniques will remove each of these types of noise differently. The variance of signal-Rayleigh beat noise can be expressed as the integral of the convolution of the noise and signal power spectral densities (PSD), as follows:

$$\sigma^2_{sig-RB} = 2R_D^2\eta_{pol}\int_0^\infty \left(S_{sig}(f) * S_{RB}(f) + S_{RB}(f) * S_{sig}(f)\right)df \tag{2.2}$$

where σ^2_{sig-RB} is the signal-RB noise variance, R_D^2 is the receiver sensitivity, η_{pol} is the copolarization factor between the signal and noise (between 1/3 and 2/3), and $S_{sig}(f)$ and $S_{RB}(f)$ are the signal and Rayleigh noise spectra respectively. This states mathematically that Type I Rayleigh will be more concentrated at low frequencies, since it is the convolution of the noise, which is confined within the laser linewidth, and the signal, which has 50% or more of it's power within the linewidth of the source depending on the ER. Type II Rayleigh, however, is the convolution of

two signal PSDs, which moves as much as 50% of the noise away from low frequencies.

The spectrum of Type II Rayleigh is an open question. While it is largely reported as doubly broadened due to the remodulation process [1,2,4], this broadening effect was not experimentally verified. Similarly, initial simulations of the Rayleigh noise spectra suggest that the spectrum may not be doubly broadened, but something less, as shown in Fig. 2.10.

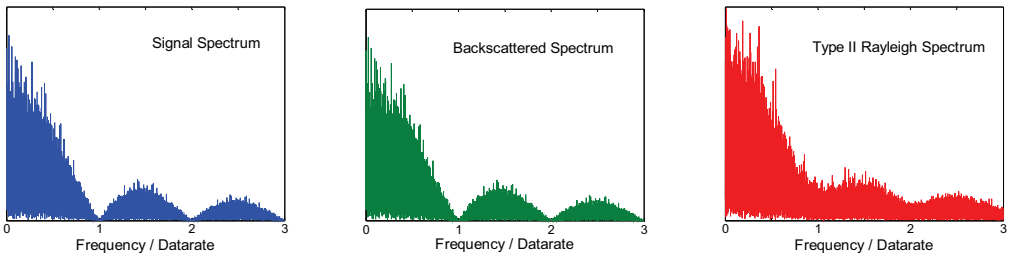

Fig. 2.10. Calculated spectrum of NRZ signal, backscattered signal, and remodulated, randomized noise as in Type II Rayleigh

Additionally, the case is made in [4] that since the spectral spreading occurs only on the edges of the marks and spaces, while the sampling occurs at the center of the bit period, the spectral spreading could be ignored. Because of these factors the spectrum of Rayleigh II will be treated as identical to the signal spectrum.

Accumulation of Rayleigh noise as a function of frequency depends primarily on the linewidth of the linewidth of the source at the CO, as shown in Fig. 2.11. As can be seen noise rapidly accumulates in the frequencies below the laser linewidth until reaching a plateau at roughly 50% for Type I Rayleigh and 25% for Type II Rayleigh. Coherent Rayleigh, which occurs with downstream modulated light, will have an accumulation similar to that of Type II Rayleigh. For all types of Rayleigh

the portion of Rayleigh noise blocked by a high pass filter will level off at roughly 10x the linewidth of the source, providing little benefit beyond this.

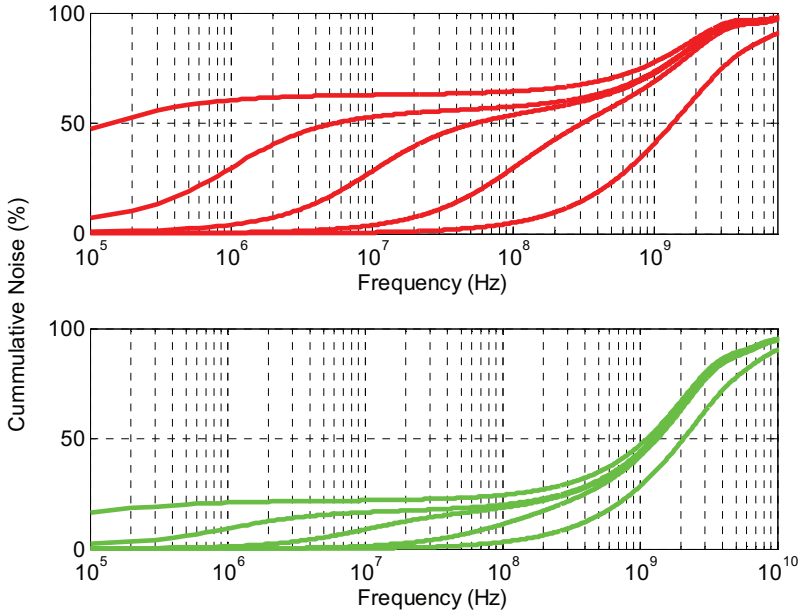

Fig. 2.11. Signal-Rayleigh Beat noise for Type I (top) and Type II (bottom) Rayleigh noise. The various lines show the accumulation of noise with frequency for 100 kHz, 1 MHz, 10 MHz, and 100MHz (from left to right) linewidth CO lasers.

Filtering of Rayleigh noise is treated by calculating the Rayleigh-Signal beat noise spectrum using 2.2 and assuming perfect brick wall filters. The sharp rolloff of single pole high pass filters such as coupling capacitors validates this assumption. It is incorporated into the expressions for variance by multiplying them by

$$\alpha_{RB} = 1 - \frac{\int_{f_{LFC}}^{f_{HFC}} S_{sig}(f) * S_{RB}(f) df}{\int_{0}^{+\infty} S_{sig}(f) * S_{RB}(f) df} \tag{2.3}$$

where α is the portion of Rayleigh noise that is filtered out and f_{LFC} and f_{HFC} are the low and high frequency (high and low filter) cutoff frequencies. A graphical

interpretation of the calculation of (2.3) is shown in Fig. 2.12 for a 6 dB ER, 2^7-1 PRBS NRZ (as used in this experiment) for Type 1 and Type 2 RB as a function of high pass filter cutoff frequency. The low pass filter is assumed to be at .75 times the datarate. Virtually all of the low noise blocked comes from the DC power caused by intensity modulation and falls within the laser linewidth.

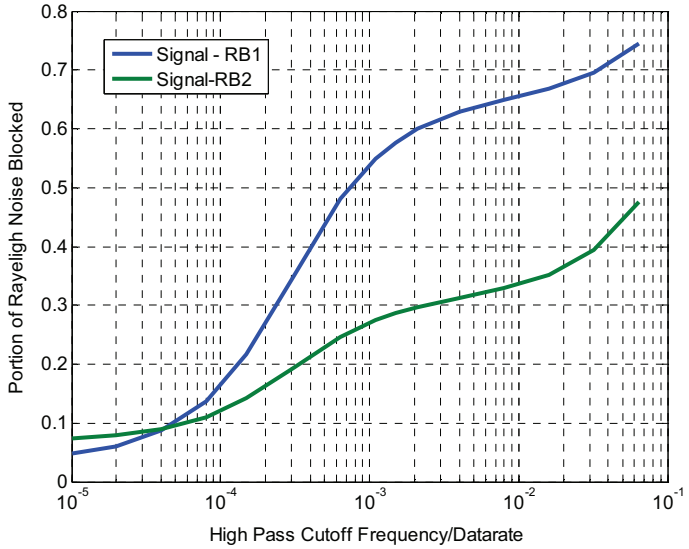

Fig. 2.12. Rayleigh Noise Blocking as a function of HPF Cutoff Frequency

2.2.2.2 Bit Error Ratio Calculation

By tracing the signal and noise roundtrip paths to the receiver, it is straightforward to compute the mean signal and noise levels. The signal power is given by

$$\langle P_S \rangle = P_L L^2 G\beta \xleftrightarrow{Average/Peak} \hat{P}_s = P_L L^2 G \tag{2.4}$$

where <> represents time average and ^ represents peak, P_L is the launch power at the CO, L is the single span loss, G is the ONU gain and β is the ratio of the peak mark power to the average power of the modulation given by

$$\beta = \frac{P_{ave}}{P_{pk}} = p_m d + \frac{1}{ER}\left(p_m(1-d) + (1-p_m)\right). \tag{2.5}$$

Here, p_m is the average mark probability (i.e. mark density, typically $p_m = 0.5$) and d is the duty cycle of the modulation (e.g. d = 1 for NRZ and d = 0.5 for 50% RZ). The expression for β in (2.5) is applicable to any intensity modulated optical signal, regardless of ER, mark density or duty cycle

The average and peak power from Type 1 RB will be

$$\left\langle P_{RB1} \right\rangle = P_L S_{RB} \xleftrightarrow{Average/Peak} \hat{P}_{RB1} = P_L S_{RB}\,. \tag{2.6}$$

Similarly Type II Rayleigh is given by

$$\left\langle P_{RB2} \right\rangle = P_L L^2 G^2 \beta^2 S_{RB} \xleftrightarrow{Average/Peak} \hat{P}_{RB2} = P_L L^2 G^2 \beta S_{RB} \tag{2.7}$$

where peak power is for a mark, and space power is this multiplied by the extinction ratio.

The mark and space signal powers are given by

$$\mu_1 = P_L L^2 G \tag{2.8}$$

$$\mu_0 = \frac{P_L L^2 G}{ER} \tag{2.9}$$

By plugging in the noise powers to the equation for noise variance, we find

$$\sigma_1^2 = {R_D}^2\left(2\eta_{RB1}(1-\alpha_{RB1})P_L^2 L^2 G S_{RB} + 2\eta_{RB2}(1-\alpha_{RB2})P_L^2 L^4 G^3 \beta S_{RB}\right) \tag{2.10}$$

$$\sigma_0^2 = R_D^2\left(\frac{2\eta_{RB1}(1-\alpha_{RB1})P_L^2 L^2 G S_{RB}}{ER} + \frac{2\eta_{RB2}(1-\alpha_{RB2})P_L^2 L^4 G^3 \beta S_{RB}}{ER^2}\right) \tag{2.11}$$

where η_{RB1} and η_{RB2} correspond to the copolarization of the signal with the RB noise component ($1/3 < \eta_{RB} < 2/3$) and term ($1-\alpha$) is the total unfiltered signal-RB beat

noise. The terms on the right represent Type I and on the left Type II Rayleigh noise.

To find the BER for the system we plug these mean and noise values into the standard equations

$$p_1 = Q\left(\frac{\mu_1 - z}{\sigma_1}\right) \qquad p_0 = Q\left(\frac{z - \mu_0}{\sigma_0}\right) \tag{2.12}$$

that will be used later to calculate the BER on a bit by bit basis. This approach gives the BER of an intensity modulated signal in a CLS-PON corrupted by beating between the signal and Type 1 and Type 2 RB. All relevant network parameters are accounted for including span loss, ONU gain, ER, Rayleigh return loss, degree of polarization and RB noise rejection in the receiver electronics (due to DC blocking and low pass filtering).

2.2.2.3 Optimal Gain Calculation

Assuming an infinite ER, the optimal gain can derived as

$$G_{opt} = \frac{1}{L\sqrt{\beta}}\sqrt{\frac{\eta_{RB1}}{\eta_{RB2}}}\sqrt{\frac{1-\alpha_{RB1}}{1-\alpha_{RB2}}} \tag{2.13}$$

Fig. 2.13 shows the maximum Q factor and what gain value achieves this Q factor calculated using (13) as a function of ER. It can be seen that optimal gain values are roughly 1 dB lower when appropriate high pass filtering is used. In [4] Fujiwara *et al*.calculated the special case for G_{opt} in which receiver filtering (both low and high frequency), degree of polarization, duty cycle and ER were neglected and showed that G_{opt} = L + 1.5 dB. Plugging into (2.13) shows that this generalized CLS-PON model simplifies to this special case assumption. As a general trend, as the receiver high pass filter cutoff frequency increases, G_{opt} decreases. This trend is physically

explained by the fact that as filtering preferential lly eliminates RB1 in its impact on the Q-factor, Type 2 RB begins to totally dominate reception. Since Type 2 RB grows with G^2, G_{opt} will tend to optimize for smaller values. As the high pass filter cutoff frequency increases, and α_{RB1} increases above and at a faster rate than α_{RB2}, the Q factor will optimize for a lower ONU gain value, as more R1 noise can be blocked. Similarly, as the extinction ratio decreases more noise will be concentrated at low frequencies, making R1 blocking more effective and optimizing the gain for a lower value.

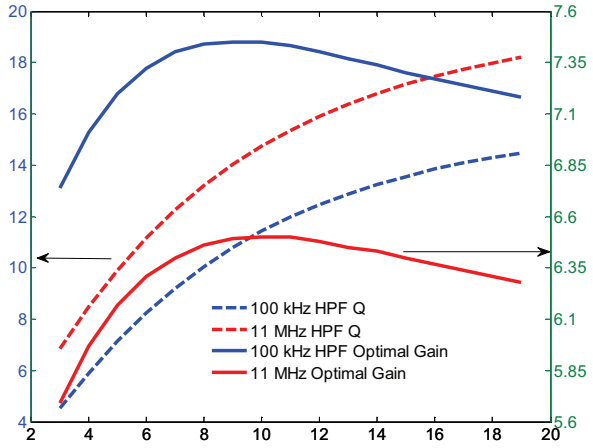

Fig. 2.13. Maximum Q and Optimal Gain vs. Extinction Ratio

2.2.2. Effect of Baseline Wander

With the impact of Rayleigh noise understood it is now necessary to create a model to predict the impact of high pass filtering on the data signals. When long strings of ones or zeros are transmitted through a blocking capacitor the mark or space level will degrade towards zero. This effect is referred to as DC or baseline wander (BLW)[9-13]. In contrast to low pass filtering effects, BLW in optical systems is poorly understood due to its pattern dependent nature. Low pass filtering

will cause the one and zero levels of an ideal noiseless signal to split into only two different levels, since the high frequency content of the signal is contained in each bit transition. BLW, however, causes the mark and space levels to split into a range of values depending on the input signal data pattern. For a deterministic data pattern these mark and space levels are also deterministic and can be calculated in a straightforward manner from the input signal. Fig. 2.14 shows a comparison of the measured and calculated mark and space levels for a 2^7-1 PRBS pattern at 1 Gb/s filtered with a 21 MHz HPF.

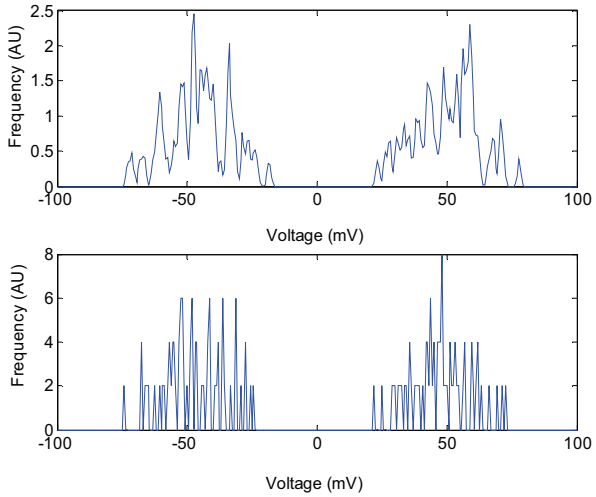

Fig. 2.14. Measured (a) and calculated (b) mark and space levels for a 2^7-1 length, 1 Gb/s PRBS signal filtered with a 21 MHz HPF. The filtering of the deterministic pattern leads to marks and spaces being spread to distinct voltage levels.

2.2.2.1 BER Calculation

A standard method for accounting for ISI due to low pass filtering is to scale the mark and space levels by a constant factor [4]. This is justified since there are only two possible levels for each, with equal probability. For BLW however there are

many possible signal levels with different frequencies depending on what input pattern is used, requiring a different approach.

One approach is to treat BLW as an additional Gaussian noise source and add it to the noise variances [9]. In long deterministic patterns such as 2^{23}-1 bit PRBS the data generates so many levels that they appear as a continuous, unbounded distribution. In random data patterns the BLW is unbounded and appears as a roughly Gaussian noise source, justifying this approach. When this random data is 8B/10B encoded the spread of mark and space values become significantly narrower and bounded (Fig. 2.14), limiting the BLW penalty. In this paper we propose an alternative method of calculating the BER by calculating the weighted bit error probability for each possible value of baseline wander.

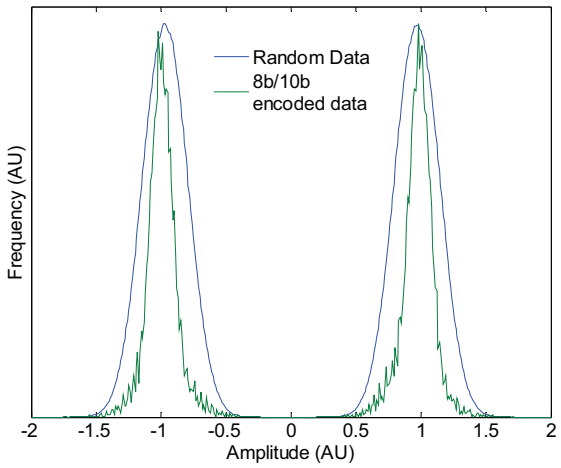

Fig. 2.15. Simulated histogram of mark and space levels for a 10 Gb/s random signal filtered at 100 MHz with and without 8B/10B encoding. The encoded data shows preference for specific signal values.

To determine the weighted BER of the system the mark and space levels of a noiseless, infinite bandwidth signal after a HPF are first calculated. Histograms of

mark and space levels for the simulated signal were compared to experimental data and found to agree at different datarates, filter values, and pattern lengths. The results for a 1 Gb/s signal filtered with a 21 MHz filter are shown for a 2^7-1 PRBS pattern in Fig. 2.13b and an 8B/10B encoded signal in Fig. 2.15.

2.2.2.2 BLW BER Experimental Confirmation

To verify the BLW model a simple experiment was performed by combining a high extinction ratio (>13 dB) 1 Gb/s signal with amplified spontaneous emission (ASE) from an erbium doped fiber amplifier (EDFA) filtered with a .5 nm optical bandpass filter. The noise and signal were combined in a 3 dB coupler, with one port leading to a PIN receiver that is then filtered with various HPFs. The other port of the coupler is connected to an optical spectrum analyzer (OSA) to directly measure the optical signal to noise ratio (OSNR) due to amplified spontaneous emission (ASE). The results are shown in Fig. 2.16. While the baseline values show some discrepancy due to the inaccuracy of power measurement using the OSA, the estimated penalty due to BLW is fairly accurate across OSNR values and high pass cutoff values.

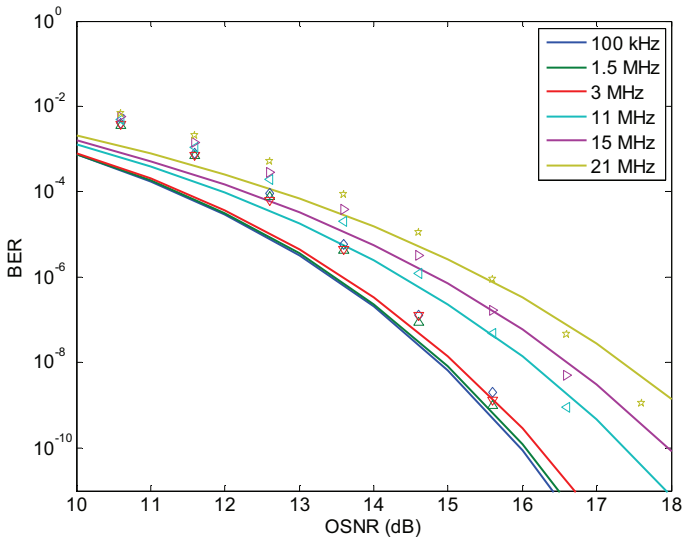

Fig. 2.16. BER vs $OSNR_{ASE}$ showing HPF penalty

2.2.2.3 Discussion

Fig. 2.17 demonstrates the impact of BLW on a noiseless signal as a function of high pass cutoff frequency. The impact is relatively low for random data below 10% of the signal amplitude to .001 times the datarate, increasing to 25% at .01 times the datarate. For 8B/10B encoded data the impact remains below 10% up to .01 times the datarate. A rule of thumb is thus that it is best to keep the high pass filter below .001 times the datarate for random data and .01 times the datarate for 8B/10B encoded data to minimize the impact of baseline wander.

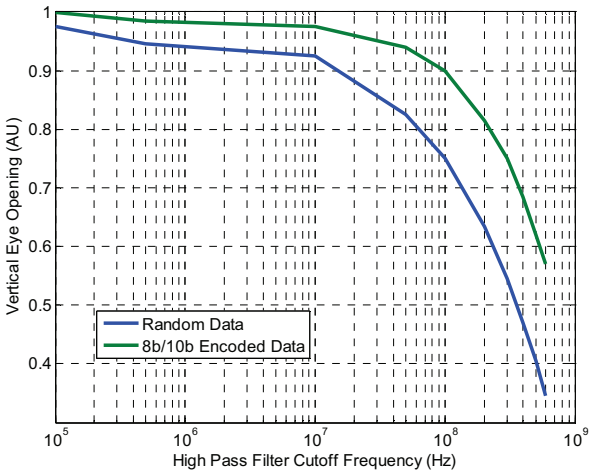

Fig. 2.17. Vertical Eye Opening of a noise-free, 10 Gb/s, unity amplitude signal as a function of filter cutoff frequency

2.2.3. Complete Theory Verification

The combination of the method for determining BER due to baseline wander with the theory developed in section 2.2.1 for calculating variance and signal levels due to Rayleigh-signal beat noise now allows us to predict the BER for a complete CLS-PON link under a variety of circumstances. Fig. 2.18-20 show the calculations for BER as a function of gain for receiver high pass filter values.

2.2.3.1 Experimental Design

To verify the accuracy of the combined CLS-PON noise model a link was constructed as shown in Fig. 2.18. The downstream CW is transmitted through standard SMF to the ONU, where it is amplified, modulated, and returned through a circulator back to the CO. The net gain of the ONU is controlled with an optical attenuator after the modulator. After transmission to the CO the signal is amplified again to maintain a constant signal power at the detector, negating the impact of thermal noise. The model predicts that the BER will be independent of launch power

if the link is dominated by Rayleigh noise and not ASE, thermal noise, or any other noise source. This prediction was tested and confirmed. The launch power was chosen to provide the maximum range of testable gain values between the SBS limit at the ONU (roughly 0 dBm launch power) and the signal necessary at the CO to maintain an ASE OSNR of better than 30 dB.

The extinction ratio was set at either 3 or 6 dB, the fiber length used was 25 or 50 km (5 or 10 dB of loss), and the received signal was filtered with high pass cutoff filters of 100 kHz, 1.55 MHz, 3 MHz, 11 MHz, 15 MHz, and 21 MHz, as used in section 2.1. A datarate of 5 Gb/s, well below the 10 Gb/s bandwidth of the signal generator and receiver, was employed to minimize the impact of ISI due to low pass filtering. Since the Rayleigh limited BER is dependent only on signal and noise levels, the only datarate dependent effect is baseline wander. BLW penalty was fairly small at 5 Gb/s, though it is still accounted for in the theoretical predictions. Low extinction ratios were used such that bit error ratios were measurable in a reasonable amount of time across the tested gain window over fiber distances that did not require clock recovery. Both types of Rayleigh noise were copolarized with the signal through the use of three polarization controllers and polarization beam splitters, such that the polarization of the downstream laser, incoming signal, and return signal could be independently controlled. Polarization control proved to be extremely difficult, given the 2/3 degree of polarization of Rayleigh noise and the polarization wander of the standard SMF employed. To account for this the degree of copolarization is fitted to the experimental data in the results.

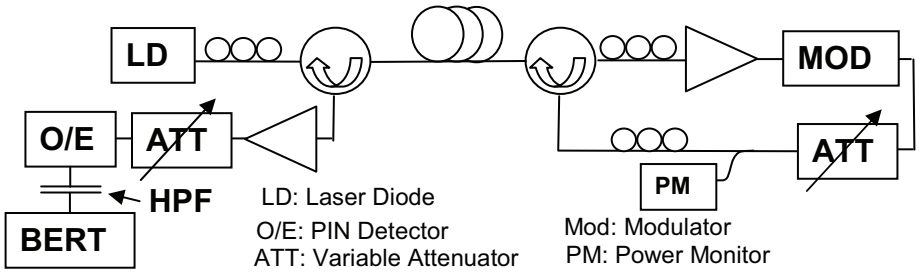

Fig. 2.18. CLS-PON link experimental setup.

2.2.3.2 Experimental Results

Experimental results are shown in Figs. 2.19-21. Key model predictions were verified by experimental data. First it is immediately apparent that BERs can be significantly improved with HPF, by several orders of magnitude, in almost all circumstances. While the model overestimates the improvement in BER at very low BERs in particular (Fig. 2.19), measured BERs were still significantly improved by HPF in all circumstances. Overestimates of the BER improvement at very low BERs are most likely the result of the model not taking into account the insertion loss and small group delay variation of the filters, the penalty due to ASE, dispersion, or thermal noise that become more significant at low BERs.

Secondly it can be seen that the optimal gain for a high pass filtered link deviates slightly from that predicted by the Fujiwara model prediction of Loss + 1.5 dB [2]. In Fig. 2.18 the optimal gain for a 5.2 dB loss shifts from ~6.5 dB for an unfiltered link to ~5.5 dB when a 20 MHz HPF is used. This is due to Type I Rayleigh-signal beat noise, which is dominant at low gain levels, being more effectively filtered by HPF than Type II Rayleigh-signal noise. Note that as shown in [8] this optimal gain value would be lower if backreflections were included in the experiment. While the optimal gain is shown to be measurably different with a

measurement resolution of 1 dB, the penalty for a misadjusted ONU gain is small. BERs were on the same order of magnitude for gain values in a 4-5 dB range around the optimal gain value.

A third prediction of the model verified by the experimental results is the effectiveness of filtering as a function of ONU gain. At lower values of gain, where signal-RB1 noise is the dominant noise source, HPF is found to be very effective. This is evidenced by the wide spacing between filter curves on each of the plots at lower than optimal gain values. At higher than optimal gain values the curves are closer together, indicating less improvement from filtering. This is due to the dominance of signal-RB2 at higher than optimal gain values, which has a broader spectrum and is less effectively filtered by high pass filtering at high cutoff frequency values than Type I Rayleigh.

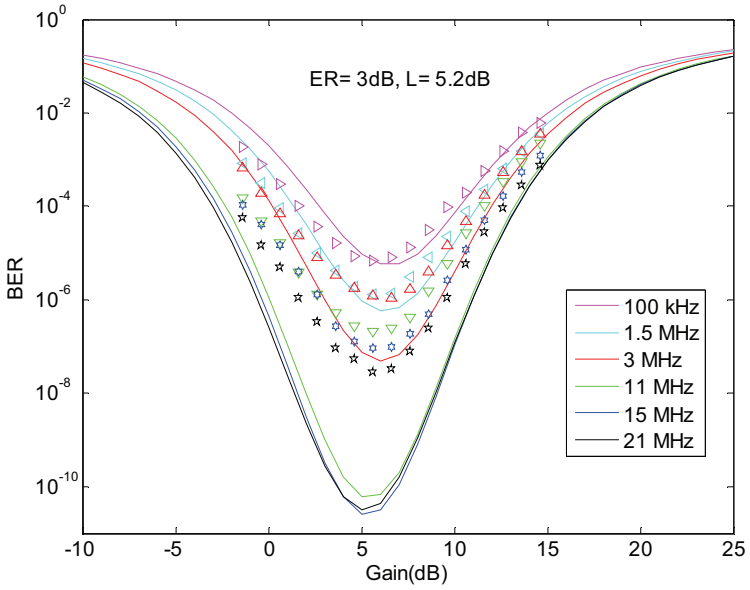

Fig. 2.19. Bit Error Ratio as a function of ONU gain for a 25 km link with ER of 3 dB.

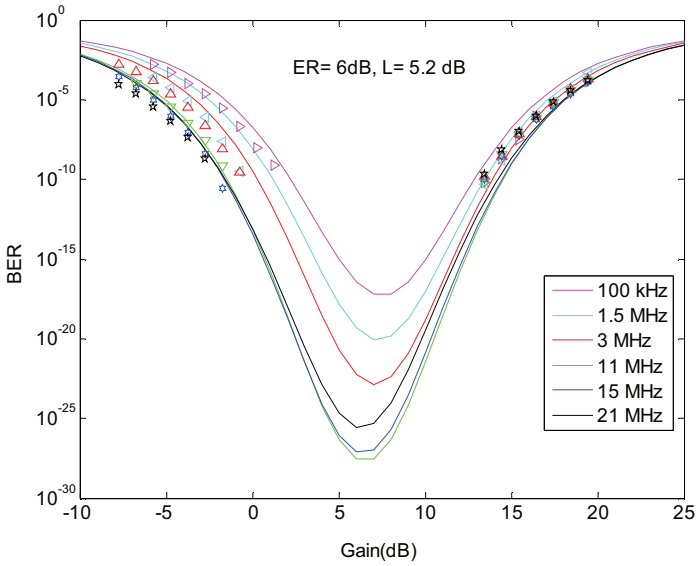

Fig. 2.20. Bit Error Ratio as a function of ONU gain for a 25 km link with ER of 6 dB.

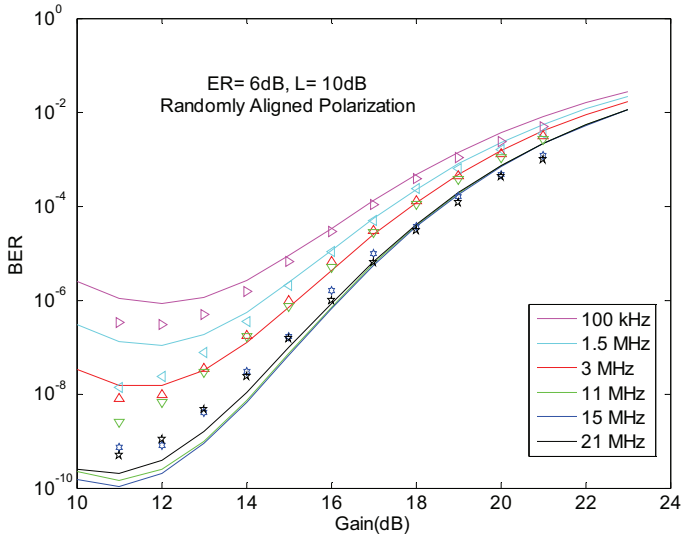

Fig. 2.21. Bit Error Ratio as a function of ONU gain for a 50 km link with ER of 6 dB, Rayleigh noise and signal randomly polarized.

2.2.4. Analysis and Discussion

2.2.4.1 Optimal High Pass Filtering

Optimal high pass filter cutoff frequency in a Rayleigh dominated link will be determined by the balance of Rayleigh noise elimination and BLW penalty. With an

accurate model in place for BLW we can now numerically calculate the optimal HPF cutoff frequency to minimize the BER for a given laser linewidth. Fig. 2.22 shows the results of numerical calculations of BERs taken at the optimal sampling threshold and ONU gain value for a variety of laser linewidth and HPF cutoff frequency values and using 8B/10B encoded data. The ER in the simulation was 6 dB, although the results were found to be qualitatively similar, including the location of the optimal cutoff frequency, for a 14 dB ER. Link loss was 10 dB, corresponding to 50 km of standard single mode fiber (SSMF).

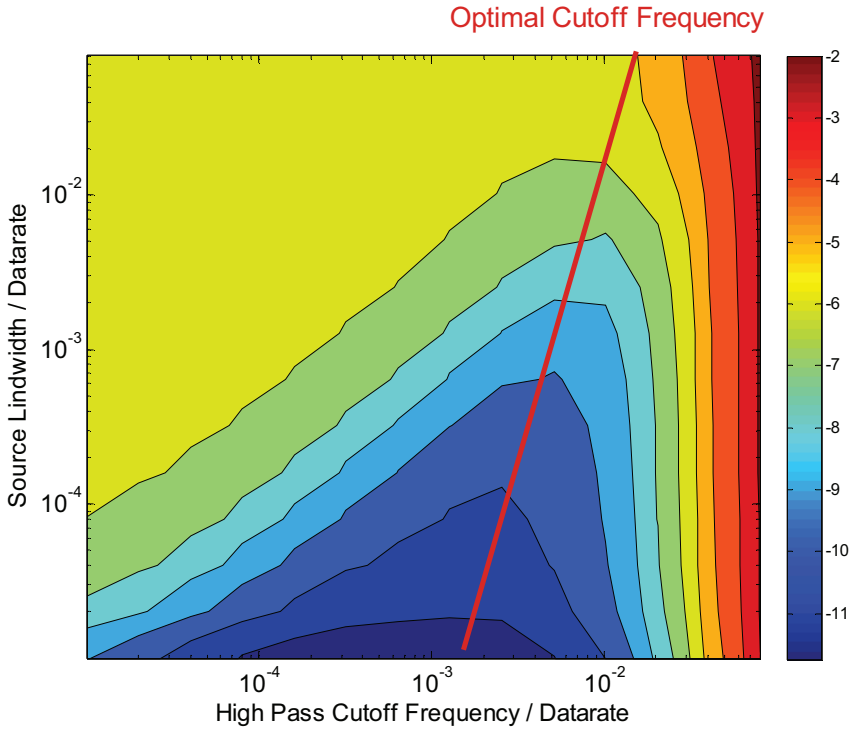

Fig. 2.22. Log of the BER for a Rayleigh Noise limited CLS-PON for a variety of source linewidth and HPF cutoff frequency values using an 8B/10B encoded signal.

From the results of section 2.2.1.1. we expect the noise blocking of the high pass filter to increase until roughly 10 times the linewidth of the source. From section

2.2.2.3. we expect the baseline wander penalty to be minimal when the cutoff frequency is below .01 times the datarate. Fig. 2.22 confirms these results, as the optimal high pass cutoff frequency is found to be around 10 times the datarate for narrow linewidth sources and .01 times the datarate for wide linewidth sources.

2.2.4.2 Effect of Source Linewidth and ONU Extinction Ratio

Two options to meet the low cost requirements of PONs are to use wide linewidth sources and low extinction ratio ONU modulators. A broader linewidth laser will allow the use of Fabry-Perot (FP) or possibly even Vertical Cavity Surface Emitting Lasers (VCSEL) at the CO. A lower extinction ratio modulator allows the use of electro-absorption modulators (EAM) or semiconductor optical amplifiers (SOAs) biased at non-optimal points and with lower bandwidths. Fig. 2.23 shows contour plots of the maximum link distance using a source linewidth and modulator ER indicated before Rayleigh noise will degrade the BER below 10^{-9}. The plot uses the optimal HPF cutoff values calculated in section 2.2.4.1.

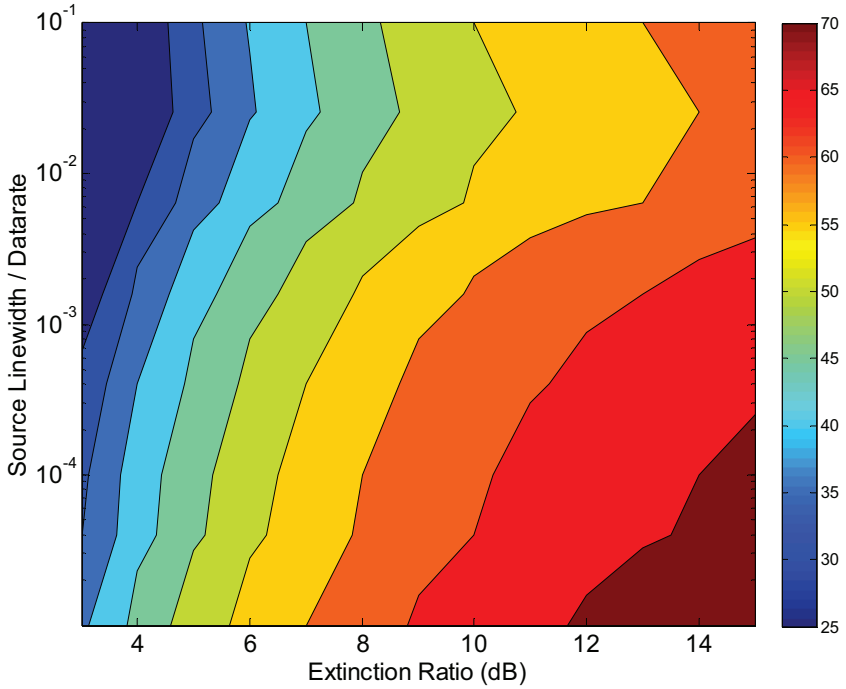

Fig. 2.23. Maximum Rayleigh Limited Link Reach for an NRZ OOK CLS-PON as a function of Source Linewidth / Signal Datarate and Extinction Ratio.

This calculation indicates that if optimal filtering and 8B/10B encoding are used as in Fig. 2.21, the linewidth of the source has significantly less impact than the receiver ER on achievable Rayleigh limited link distance. Future CLS-PON designers would be advised to use high ER modulators at the ONU and save cost through broader sources at the CO with line coding and appropriate receiver filtering.

2.2.4.3 Distance Improvement Due to Filtering

Fig. 2.24 shows the potential for improvement by using HPF. The curves are for 10 Gb/s data using a 1 MHz linewidth source and a 10 MHz HPF. As expected the improvement is most significant for low extinction ratios and 8B/10B encoded data. As you can see the improvement can be significant. Using HPF and 8B/10B

encoding, at an ONU ER of 4 dB the reach of the link can be increased by almost 50%.

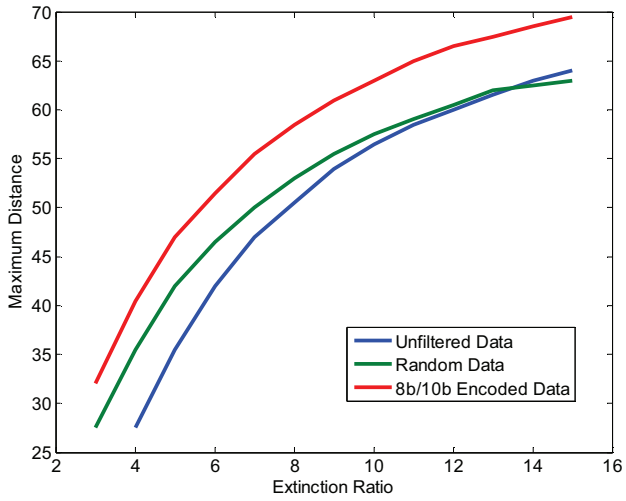

Fig. 2.24. Maximum Rayleigh Limited Link Reach for an NRZ OOK CLS-PON as a function of Extinction Ratio for a 10 Gb/s signal with a 1 MHz linewidth source and 10 MHz High Pass Filter.

2.3 Rayleigh Noise in Bidirectional Links

To this point we have only considered the effects of Rayleigh on a unidirectional data link in the sense that the downstream light has assumed to be continuous and unmodulated. In this section we will expand both the theoretical treatment and the experimental verification to the case where data is transmitted downstream as well as upstream. In both cases it will be fairly straightforward, demonstrating how robust the previous theory was.

2.3.1. Theoretical Impact of Rayleigh Noise in Bidirectional Links

In this section we will consider only an intensity modulated, on-off keyed link in which the downstream light is modulated with some small extinction ratio signal

and the upstream light in turn is modulated with a larger extinction ratio signal. The conclusions drawn, however, are as general as those in the previous section. As before no noise sources will be considered besides Rayleigh noise, and the components are assumed to be of infinite bandwidth. Having established appropriate guidelines for avoiding significant impact from baseline wander we will ignore its effects. A common technique to enhance transmission in these links is to transmit downstream at a higher datarate and retransmit at a lower datarate, allowing the higher frequency data to be filtered out at the CO receiver [15]. This technique will not be addressed in this theory, although a straightforward correction (noted later) would most likely suffice.

To determine the impact of Rayleigh noise on the bit error ratio of a bidirectional PON we will follow the same procedure as in section 2.2.2. First we must determine what portion of Rayleigh noise is actually present at the decision circuit, then determine the relative optical signal and noise power at the receiver to determine the BER using the Gaussian noise approximation

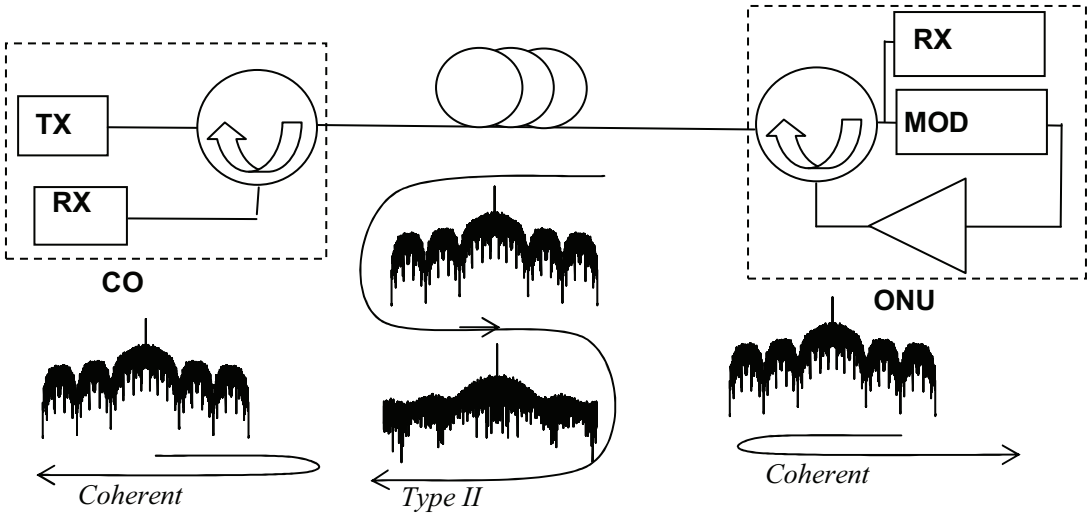

Fig. 2.25. Schematic Illustration of Rayleigh Noise Sources in Bidirectional PON.

Fig. 2.25 demonstrates the noise sources in a bidirectional PON. Note that instead of having Type I and Type II Rayleigh, the CO receiver is now afflicted with what we have previously called coherent and Type II Rayleigh. Similarly the ONU receiver is subject to only to coherent noise. For these cases the alpha parameter, corresponding to the portion of noise rejected by the electronic filtering, is still calculated according to (2.3). However, the spectrum of the coherent Rayleigh is identical to the transmitted downstream or upstream data, which causes a general broadening of the beat noise spectrum.

Following the procedure of section 2.2.2., but ignoring the average power and focusing only on the peak since there is no comodulated noise and signal now, we find that the *downstream* signal and noise powers are given, respectively by

$$\hat{P}_S = P_L L \tag{2.14}$$

where the respective symbols maintain their meanings from the previous derivation.

In this case β_D is specifically for the downstream signal, which will exclusively have a different extinction ratio if nothing else from the upstream signal. The average and peak power from coherent RB will be

$$\hat{P}_C = P_L L \beta_D G S_{RB} . \tag{2.15}$$

and there will be no other Rayleigh noise interfering with the signal.

The mark and space signal powers are given by

$$\mu_1 = P_L L \tag{2.16}$$

$$\mu_0 = \frac{P_L L}{ER_D} . \tag{2.17}$$

By plugging in the noise powers to the equation for noise variance, we find

$$\sigma_1^2 = R_D{}^2 \left(2\eta_{RBC} (1-\alpha_{RBC}) P_L^2 L^2 \beta_D \beta_U G S_{RB} \right) \tag{2.18}$$

$$\sigma_0^2 = R_D{}^2 \left(2\eta_{RBC} (1-\alpha_{RBC}) \frac{P_L^2 L^2 \beta_D \beta_U G S_{RB}}{ER_D} \right) . \tag{2.19}$$

This is sufficient now to calculate the Q factor and use the error function to estimate the BER.

Repeating the procedure for the *upstream* signal, but this time keeping track of the peak and average powers since it has comodulated signal and noise, we find

$$\left\langle P_S \right\rangle = P_L L^2 G \beta_D \beta_U \xleftrightarrow{Average/Peak} \hat{P}_S = P_L L^2 G \beta_D \tag{2.20}$$

$$\left\langle P_C \right\rangle = P_L \beta_D S_{RB} \xleftrightarrow{Average/Peak} \hat{P}_C = P_L \beta_D S_{RB} \tag{2.21}$$

$$\left\langle P_{RB2} \right\rangle = P_L L^2 \beta_D \beta_U^2 G^2 S_{RB} \xleftrightarrow{Average/Peak} \hat{P}_C = P_L L^2 \beta_D \beta_U G^2 S_{RB} \tag{2.22}$$

for the signal and noise powers. Using these we can derive

$$\mu_1 = \frac{P_L L^2 G}{ER_D} \tag{2.23}$$

$$\mu_0 = \frac{P_L L^2 G}{ER_D}. \tag{2.24}$$

$$\sigma_1^2 = R_D{}^2\left(2\eta_{RB1}(1-\alpha_{RB1})P_L^2 L^2 G\beta_D S_{RB} + 2\eta_{RB2}(1-\alpha_{RB2})P_L^2 L^4 G^3 \beta_D \beta_U S_{RB}\right) \tag{2.25}$$

$$\sigma_0^2 = R_D^2\left(\frac{2\eta_{RB1}(1-\alpha_{RB1})P_L^2 L^2 G\beta_D S_{RB}}{ER_U} + \frac{2\eta_{RB2}(1-\alpha_{RB2})P_L^2 L^4 G^3 \beta_D \beta_U S_{RB}}{ER_U^2}\right) \tag{2.26}$$

as the mark and space levels and noise variances. The important difference from the previous derivation here is the inclusion of the downstream extinction ratio and consequential change in both noise and signal powers. Note that in (2.24) and (2.25) the level of the mark has been assumed on the basis of a downstream transmitted space, and a space on that of a downstream transmitted mark. This gives the worst case scenario signal spacing and a pessimistic BER estimation. If filtering of the high datarate downstream data was assumed here we could use the average, calculated in the β parameter, to adjust the data instead and estimate the effect of filtering out the high frequency data.

2.3.2. Experimental Verification

In order to verify the predictions of this theory a link was constructed identical to the link illustrated in Fig. 2.18 except for a splitter and receiver after the ONU circulator and a modulator and amplifier between the CO modulator and laser. While calculations suggested that a 90/10 power splitter would be preferable in the ONU, a 50/50 splitter was used to ensure that a sufficient $OSNR_{ASE}$ was maintained. The

tests were performed at 1 Gb/s in order to make the results comparable to other tests that shall be performed in the next chapter. Using the rule of thumb for baseline wander established earlier, a 1.5 MHz low pass filter (.001 times the datarate) and 2^7-1 PRBS pattern was used to reduce the Rayleigh noise in all cases.

The most important parameter in this experiment is clearly the extinction ratio of the downstream signal. The ER of the upstream signal was chosen as 13 dB, which was the maximum that the MZM used was capable of. At first glance the equations seem to suggest that an ER below 3 dB, that is a majority of the CW light consumed by the upstream signal instead of the downstream signal, would be appropriate for two reasons. First, the downstream signal is subject to only one source of Rayleigh noise, and not type II Rayleigh, and so should be more robust. Second, the upstream signal, particularly the marks, is corrupted by the downstream signal. Fig. 2.26 shows what the theory predicts.

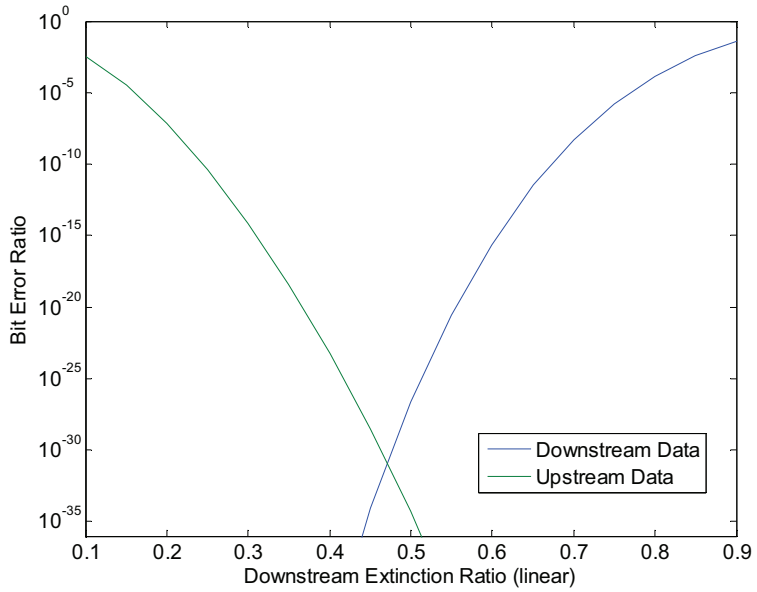

Fig. 2.26. Calculation of Bit Error Ratio of a bidirectional link as a function of downstream Extinction Ratio

This calculation is for a 25 km (5 dB loss) link using a 1.5 MHz filter and a 1 Gb/s signal. Note that the BERs are significantly underestimated because the theoretical data is not fitted to the intrinsic noise of the BERT system. The major prediction of Fig. 2.25 is that the optimal extinction ratio will be below 0.5, meaning that more than half of the available CW power at the launch will be used in the downstream modulation. This is the opposite of what was previously expected. Fig. 2.27 shows the results of the bidirectional experiment. Note that the downstream BERs come from a single trial, while the upstream BERs are the averaged result of several trials due to instabilities in the transmission system, possibly related to the copolarization of the noise and signal.

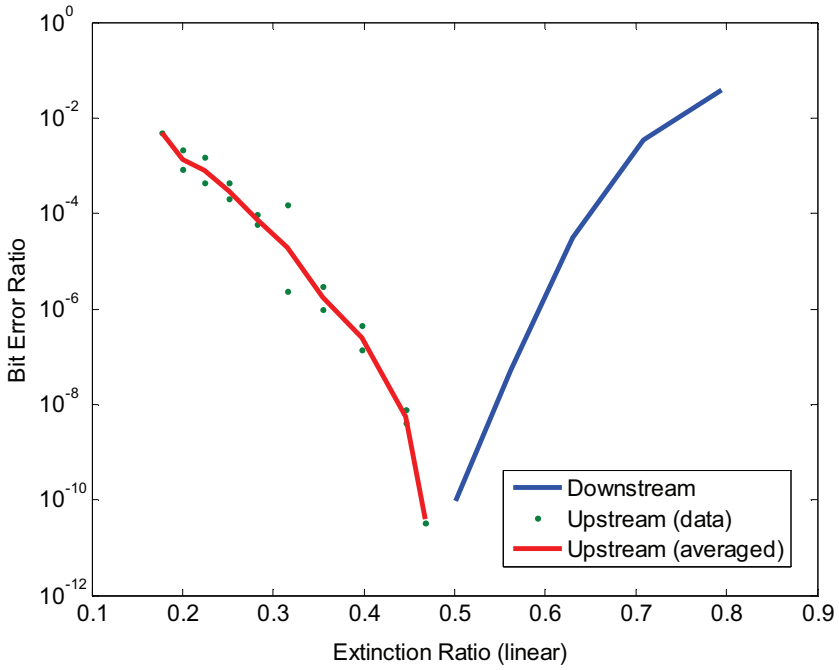

Fig. 2.27. Experimental Bit Error Ratios vs. Downstream modulated extinction ratio

The result clearly indicates that the theory was correct in predicting the optimal extinction ratio. Upon further examination of the equations it becomes apparent why the optimal downstream modulation depth would be greater than 50%. While there are more noise terms in the upstream data, the noise terms derive from signal-Rayleigh beating. Since the signal level is roughly twice as large on the downstream data it increases the electrical noise, which requires commensurately more power for the same bit error ratio.

2.4 Conclusion

The preceding chapter has shown, through intensive theoretical and experimental investigation, the potential for significant improvement in Rayleigh noise limited links using high pass filtering. These significant investments in

investigating the conditions under which HPF can provide improvement in these links is justified by the low cost and ease of implementation for high pass filters. Once the proper cutoff frequency for the high pass filter has been identified the benefit can be realized in the link literally for free.

The key contributions from this work are as follows:

- In section 2.1 it was demonstrated, experimentally, that an increase in Rayleigh noise immunity of up to 10 dB could be realized in certain situations using low pass filtering.
- In section 2.2.2 a novel method for determining the penalty due to baseline wander was developed and experimentally verified. This model is more relevant and accurate to modern fiber optic links than previous models.
- In section 2.2.3 the Rayleigh noise model developed in [4] and reproduced in section 2.2.1 was experimentally confirmed. This verified the significant improvement in Rayleigh noise immunity that high pass filtering could provide to an actual link.
- In section 2.2.4 calculations showed that HPF cutoff frequencies between 1 and 10x the source linewidth, and .001 (for random data) and .01 (for 8B/10B encoded data) times the datarate were optimal, serving as good rules of thumb for future CLS-PON designers.
- In section 2.3 the theory was expanded to apply directly to bidirectional intensity modulated links and this expansion was theoretically verified.

- The optimal downstream extinction ratio for Rayleigh limited (and generally optically noise limited) bidirectional links was found to be slightly above 3 dB.

To implement these results in a deployed commercial link would require more consideration of actual link parameters. For example in many circumstances differing modulation formats would be used for down and upstream data. For example a subcarrier multiplexed signal has been employed in the downstream direction with the carrier reused in an on-off keyed signal in the upstream direction. This scheme will be reviewed more thoroughly in Chapter 3. This method will more significantly impact both the effectiveness of high pass filtering and the effect of baseline wander. These techniques will be further complicated by the use of sophisticated optical filtering techniques. However, as long as low cost intensity modulators at the ONU are used there will be a carrier component to reflected noise. As long as some carrier Rayleigh noise is present this high pass filtering method should be relevant.

ACKNOWLEDGEMENT

Section 2.1 is, in part, a reprint of the material in "Improved High Pass Filtering for Passive Optical Networks", published in *Photonics Technology Letters*, 2010 by D. Jorgesen, C. F. Marki, and S. Esener. Section 2.2 is, in part, a reprint of "Analysis of High Pass Filtering of Rayleigh Noise Limited Central Light Source Passive Optical Networks", submitted to the *Journal of Lightwave Technology*, 2010.

The dissertation author was the primary investigator and first author of these publications, but would like to thank Dr. Christopher Marki and Prof. Sadik Esener for their helpful suggestions.

2.5 References

[1] G. Talli, D. Cotter, and P.D. Townsend, “Rayleigh backscattering impairments in access networks with centralised light source,” *Electron. Lett* , vol. 42, no. 15, pp. 877–878, 2006.

[2] M. Fujiwara, J. Kani, H. Suzuki, and K. Iwatsuki, ”Impact of backreflection on upstream transmission in WDM single-fiber loopback access networks”, *J. Lightwave Technol*., vol. 24, pp. 740–746, 2006.

[3] C.F. Marki, F.A. Marki, and S.C. Esener, “Reduction of interferometric optical crosstalk penalty via DC blocking,” *Electron. Lett.*, vol. 43, no. 11, pp. 644–646, 2007.

[4] C.F. Marki, “Design and Optimization of Bidirectional and Optical Logic Systems in the Presence of Noise”, Ch. 4, Ph.D. dissertation, Dept. Elect. Eng., Univ. California, San Diego, La Jolla, CA, 2007.

[5] A. Chiuchiarelli, M. Presi, R. Proietti, G. Contestabile, P. Choudhury, L. Giorgi, and E. Ciaramella, “Enhancing Resilience to Rayleigh Crosstalk by Means of Line Coding and Electrical Filtering,” *IEEE Phot. Tech Lett*, vol. 22, no. 2, pp. 85–87, Jan. 2010.

[6] R. Staubli and P. Gysel, “Crosstalk penalties due to coherent Rayleigh noise in bidirectional optical communication systems”, *J. Lightwave Technol.*, vol. 9, pp. 375–380, 1991.

[7] G. Talli, C.W. Chow, and P.D. Townsend, “Modeling of Modulation Formats for Interferometric Noise Mitigation”, *J. Lightwave Technol,* vol. 26, no.17, 2008.

[8] C. Arellano, K-D Langer, and J. Prat, “Reflections and Multiple Rayleigh Backscattering in WDM Single-Fiber Loopback Access Networks”, *J. Lightwave Tech.*, vol. 27, no.1, 2009.

[9] G. A. Sefler and P. K. Pepeljugoski, "Interferometric noise penalty in 10-Gb/s Ethernet LAN links," *IEEE Phot. Tech. Lett.*, vol. 14, pp. 113-115, 2002.

[10] Z. Ghassemlooy, “Investigation of the baseline wander effect on indoor optical wireless system employing digital pulse interval modulation”, *IET Communications*, vol.2, pp. 53-60, 2008.

[11] Maxim, "NRZ Bandwidth-LF Cutoff and Baseline Wander," in Appl. Note HFAM-09.04.

[12] £. OELIWCZYÑSKI and P. Krehlik, “Optimisation of low frequency characteristics of digital optical links”, *Opto-Electronics Rev.*, vol. 11, pp. 27-29, 2003.

[13] N. Sommer, I. Lusky, and M. Miller, “Analysis of the Probability Distribution of the Baseline Wander Effect for Baseband PAM Transmission with Application to Gigabit Ethernet”, *Proc. 11th IEEE International Conference on Electronics, Circuits and Systems*,pp. 89-92, 2004.

[14] J. Bromage, P. J. Winzer, and R.-J. Essiambre, "Multiple Path Interference and its Impact on System Design," in *Raman Amplifiers for Telecommunciations 2*, M. N. Islam, Ed. New York: Springer-Verlag, 2004, pp. ch. 15.

[15] Wooram Lee, M. Y. Park, S. H. Cho, Jihyun Lee, Chulyoung Kim, Geon Jeong, and B. W. Kim, “Bidirectional WDM-PON Based on Gain-Saturated Reflective Semiconductor Optical Amplifiers”, *IEEE Phot. Tech. Lett.*, vol. 17, no. 11, pp. 2460-2462, 2005.

3. Improved Transmission Techniques for CLS-PON

In this section several alternate techniques for optimizing central light source passive optical network (CLS-PON) design are presented. As we see throughout this thesis the combination of extreme cost pressure and the asymmetrical, bidirectional nature of the CLS-PON link combine to require alternative link designs and methods. As discussed in Chapter 1, the desire to deploy optical networking units (ONU) to subscribers instead of maintaining them within service provider networks demands ONUs that are very low cost yet extremely reliable under a variety of circumstances. In the first two sections two methods will be discussed increase the bandwidth of a link using a low cost reflective semiconductor optical amplifier (RSOA), which is an attractive option for CLS-PONs. In the third section we will explore the possibility of alternately using the in-phase and quadrature components of a microwave subcarrier to improve the bidirectional performance of a CLS-PON.

3.1 Transmitter Predistortion for RSOA PON

3.1.1 Background on Equalization

The ONU in a CLS-PON must generally do three things: amplify, modulate, and retransmit an incoming CW or modulated downstream lightsource. In Chapter 2 these functions were achieved with an erbium doped fiber amplifier (EDFA), a lithium-niobate Mach-Zender modulator (MZM), and an optical circulator to experimentally produce an ideal ONU. In an actual link these functions can be combined much more cost effectively with a reflective semiconductor optical

amplifier (RSOA). RSOAs are low cost, wavelength independent across the C and L bands, can be directly modulated, are intrinsically reflective, and provide gain [1]. The main drawback of RSOAs is their low modulation speed due to long gain recovery times, limiting their single channel performance to 2.5 GHz [2]. One technique to improve the performance of low modulation bandwidth components is to use equalization.

Equalization is the process of using a frequency dependent gain to boost the high frequency content of a signal, which can counteract the low frequency roll-off of system components and increase overall system datarates. It is widely used in electronic communications, most notably on backplane interconnects that suffer from frequency dependent attenuation. Electronic data processing, including adaptive equalization and maximum likelihood sequence estimation (MLSE) [3], has been used in optical communications for some time. Historically it has been used to combat differential modal dispersion (DMD) in multimode fibers, polarization mode dispersion in single mode fibers (PMD), and chromatic dispersion (CD) and laser chirp compensation [3,4]. As silicon processing circuits have evolved to handle higher datarates the use of these circuits in optical networks has also advanced. Next generation optical communication systems will almost certainly use significant advanced detection digital signal processing, not only for equalization and error detection but inherently to detect the polarization and phase of differential polarization quadrature phase shift keyed (DP-QPSK) or quadrature amplitude modulated (QAM) signals [5].

In this section we will limit the discussion to analog real-time equalization of standard on-off keyed (OOK) intensity signals. This technique can be used to offset the low modulation bandwidth of low cost optical components. There are two main techniques for performing high speed adaptive equalization: feed forward and decision feedback [3]. Both techniques involve adding a weighting term accounting for degraded high frequency components to the signal before the receiver. In feed forward equalization (FFE) a weighted sum of the preceding bits is added to each received or transmitted signal. This technique can be used at the receiver between the photodetector and the decision circuit, or at the transmitter before the modulation device. Decision feedback equalization (DFE) is performed by making a decision at the receiver as to what a bit is, and then added to the following bit. For example if a mark is detected the following bit will have the signal slightly reduced to account for any power from the mark that may have leaked into the next bit period. This technique can only be used at the receiver, and its use may lead to cascaded errors since the detection of an erroneous bit will cause the wrong feedback signal to be sent, possibly causing burst errors.

For CLS-PONs using an RSOA as the ONU modulator, equalization can be used to offset the low modulation bandwidth of the RSOA. Cho et al demonstrated that 10 Gb/s operation was possible using a 2.2 GHz RSOA with electronic postprocessing receiver equalization and forward error correction (FEC) [6]. They found a penalty of 2.5 dB for the equalized RSOA signal. Papagiannakis et al extended this to show 10 Gb/s operation of a 2.5 GHz RSOA circuit using an offset optical filter and receiver equalization [7]. In this experiment the RSOA was seeded

locally, and so Rayleigh noise was not considered. Later Omella expanded this study to include downstream transmission, although Rayleigh noise was still not properly considered [8].

In the frequency domain equalization can be considered as a high pass filter, ideally the inverse of the low pass filtering function of the system. For this reason equalization is not effective with direct laser modulation since the relaxation oscillations in a laser will cause it to have a nonlinear filter function. A DFE or FFE can be seen as a high pass amplifier, or a high pass filter cascaded with an amplifier. It will boost both the signal and high frequency noise. A passive equalization filter, however, will only attenuate the low frequency portion of the signal without boosting the high frequency content of it. This is only useful if a limiting or saturated amplifier is employed, or if it done *before* the low frequency link component. A high pass filter will only attenuate strings of marks or spaces without boosting the isolated marks and spaces.

An alternative method of electronic impairment mitigation to receiver equalization is transmitter pre-emphasis, where the high frequency components of the RSOA driving signal are emphasized to provide an open transmitted eye. The driving power of the RSOA is limited by the heat dissipation capability of the RSOA. By pre-emphasizing the high frequency components before the RSOA this means that higher datarates can be transmitted through the RSOA. There are also benefits of this technique in that noise and dispersion from transmission are not enhanced by the receiver equalizer, and that power and heat can be transferred from the power and heat limited central office to the less restrictive optical networking unit. In the

sections that follow it will be shown that up to 5 Gb/s performance is possible from a 1.2 GHz bandwidth RSOA using this transmitter pre-distortion technique.

3.1.2 Experimental Setup

A commercial RSOA from CIPhotonics with a bandwidth of 1.24 GHz (Fig. 3.2) was used. The frequency response of the device shows no relaxation oscillations and falls off uniformly. The device was driven using an Accelerant Networks AN6420 transceiver chip with built in bit error ratio tester mounted on a proprietary communications testboard. The BERT chip is a .13 micron CMOS device designed for testing backplane interconnects. It has an integrated transmitter equalizer with single stage feedforward and five stage feedback filter, providing a boost of up to 19 dB at the Nyquist frequency (2.5 GHz). In this experiment only the leader and first trailing tap were set using an iterative method for a boost of 12.5 dB at 2.5 GHz. The effect of the equalizer is to act as a high pass filter, offsetting the effect of the low frequency roll off of the RSOA, as shown in Fig. 3.1. The integrated BERT provides byte error ratios. For the purpose of making this work comparable it will be assumed that the bit error ratio is the same as the byte error ratio divided by eight, meaning that in each errant byte only one bit was wrong.

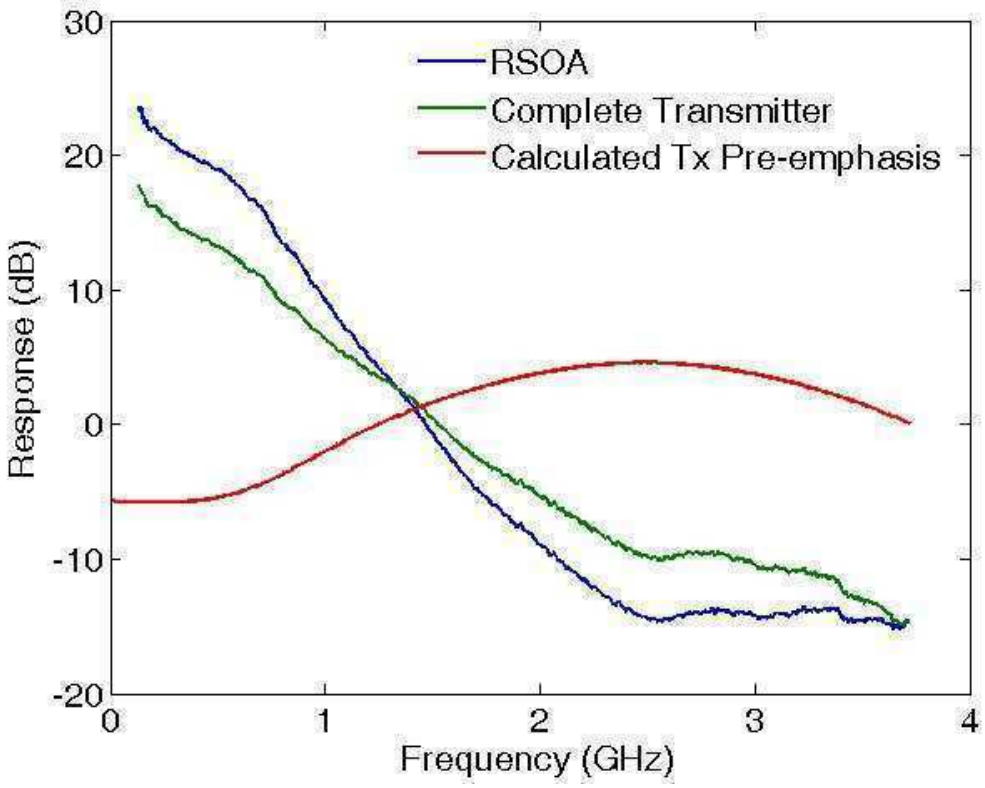

Fig. 3.1. Frequency Response of RSOA, pre-emphasis equalization high pass filter, and complete transmitter frequency response.

The experimental setup is shown in Fig. 3.2. The pre-emphasized signal coming from the chip was amplified by a 10 dB Picosecond preamplifier and a 14 dB Marki Microwave low noise power amplifier to increase the p-p amplitude of the signal to 3.9 Vrms(Fig 2.3). This level of amplification is necessary to offset the high pass filtering of the predistorted signal. Higher levels of gain are the tradeoff for increasing the bandwidth. The signal was applied to the RSOA through a bias tee with a 100 mA bias current. A DFB laser (Agilent 83434A) tuned to 1551 nm was injected through a circulator into the RSOA through a 400 pm bandwidth tunable optical filter with an insertion loss of 2.6 dB. For unidirectional measurements the

circulator output was transmitted over 20 km of SMF with a loss of 5.8 dB. For the bidirectional experiment the filter was removed and the laser light was launched through a circulator, into 20 km of SMF, reflected from the RSOA, and data was collected at the third port of the circulator.

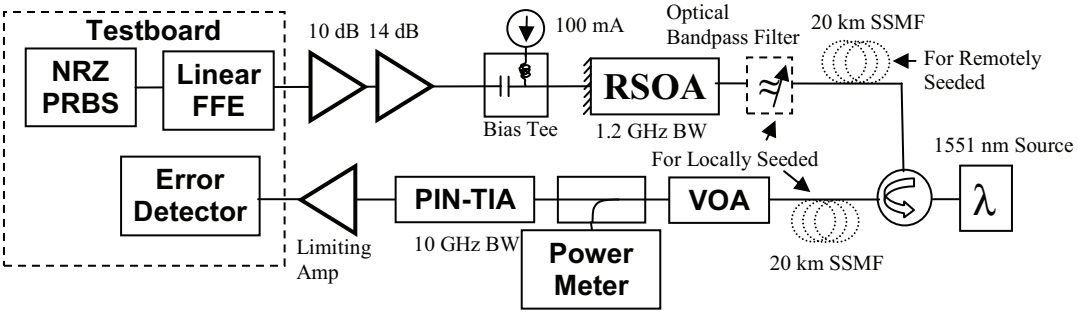

Fig. 3.2. Experimental setup for investigation of transmitter pre-distorted RSOA CLS-PON

3.1.3 Experimental Results

The driving signal was shown to adequately compensate the low frequency roll off of the RSOA to produce error-free eyes in back to back operation, as shown in Fig. 3.3c and 3.4a. RSOA dynamics are governed by the semiconductor rate equations, which decrease the electron lifetime with increasing current and the photon lifetime with increasing input power. Thereforethe performance of the RSOA improves with increased injection power, yielding a power penalty of ~5 dB for an injection power of 6.2 dBm. With a lower injection power of -4.8 dBm an error floor is observed just below 10^{-9} BER. As can be seen from the eye diagram in Fig. 3.3c, the error floor is caused because the predistortion filter cannot compensate for the poor high frequency performance of the RSOA with low light injection, causing isolated marks to have lower peak amplitude than desirable. This bandwidth

dependence on input light power for an RSOA is a significant detriment to use in a CLS-PON link, where the input power would be dependent on link distance and operation is desired at as high a bandwidth as possible.

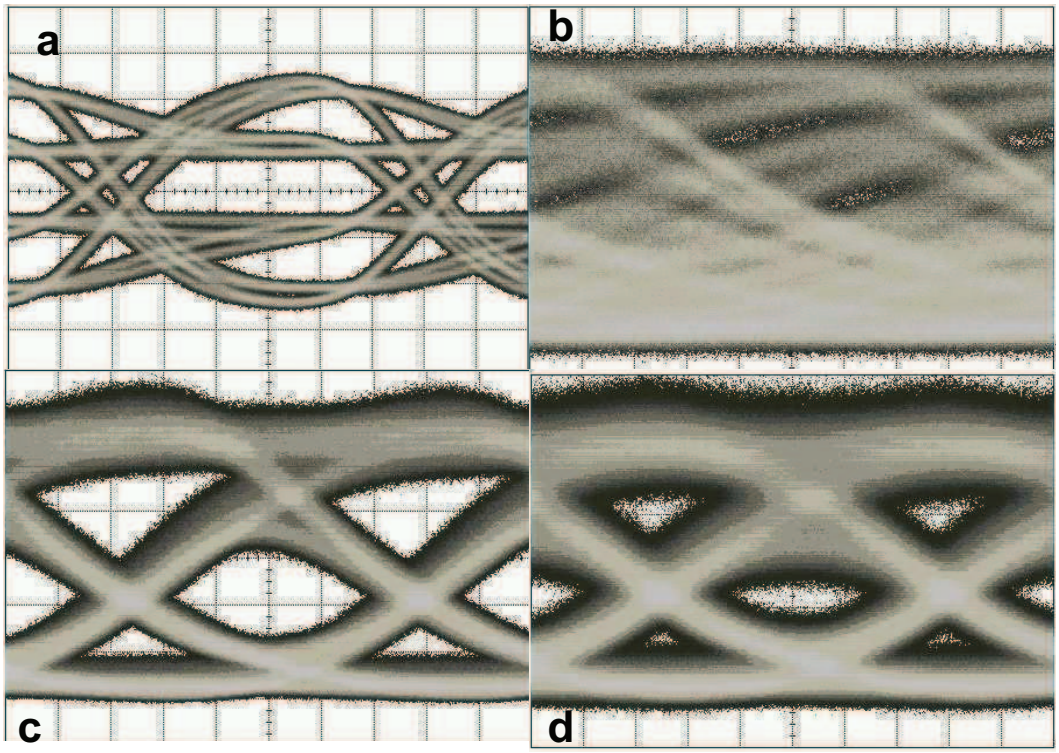

Fig. 3.3. Eye diagrams for a) the pre-distorted signal, b) the RSOA output with an undistorted signal at 5 Gb/s, c) the RSOA output with a predistorted signal and d) the eye diagram after 20 km of fiber

To test the signal quality without seed light Rayleigh or stimulated Brillouin backscatter, the signal was transmitted through 20 km of SMF and the BER was measured again. As shown in Fig. 3.4b the signal demonstrates an error floor for all injection powers and a penalty of about 6 dB over the ideal case, which had virtually no penalty for fiber transmission. Since the ASE is removed by the tunable optical filter, the dominant noise sources are most likely high dispersion caused by the chirp

of the SOA transmitter (particularly on isolated marks). At the injection levels to the fiber (.2, 1.2, and 2.1 dBm for injection powers of -4.8, 0, and 6.2, respectively) the Rayleigh backscatter will be ~33 dBm [9]. With an RSOA gain of ~10 dB on this reflected noise, it becomes significant to interfere with the error free operation of the signal.

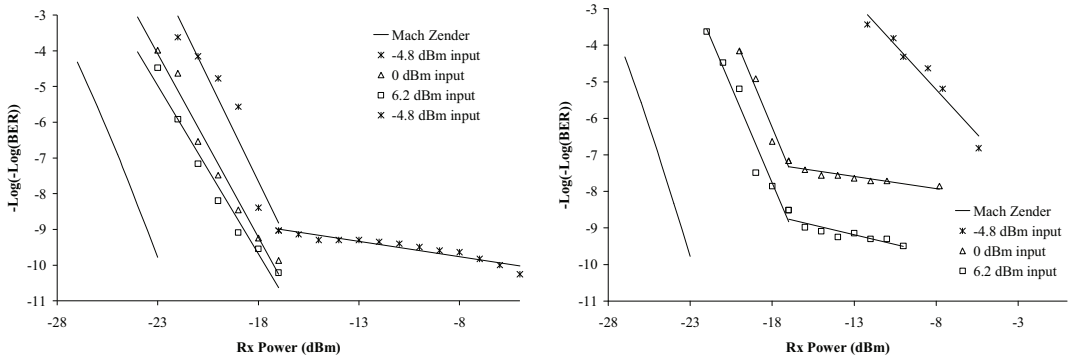

Fig. 3.4. Bit error ratio for pre-distorted 5 Gb/s RSOA operation back to back (left) and after 20 km of SMF (right)

As seen in Chapter 2 the Rayleigh noise performance of a CLS-PON is independent of the launched power, but does depend on the gain at the ONU side of the link. Because the modulation bandwidth of the RSOA increases with input light power this means that it makes sense to launch as much power as possible down the link. The limit to this is the onset of stimulated Brillouin scattering, which becomes the dominant noise source above a certain threshold. This is shown in Fig. 3.5 where it is seen that the optimal launch power is at 8 dBm, which is significantly higher than the power level at which SBS becomes the dominant backscattered noise source. Even at high levels of SBS the modulation bandwidth improvement of the RSOA offsets the increased noise levels to provide improved performance.

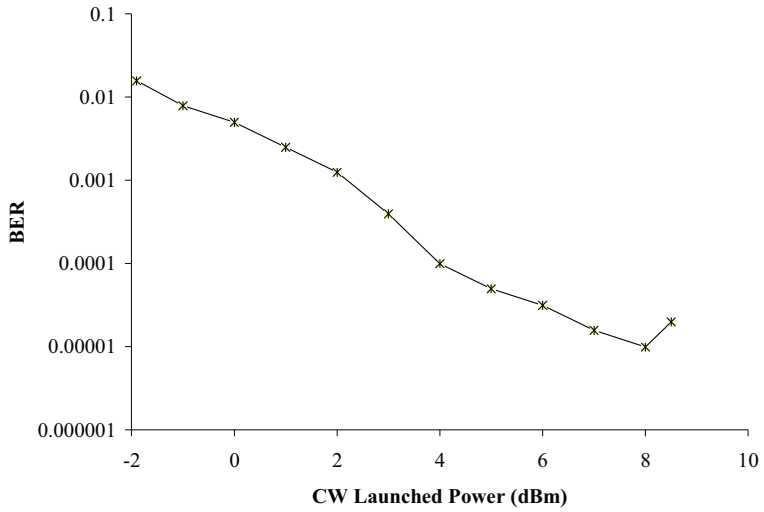

Fig. 3.5. Bit error ratio for pre-distorted 5 Gb/s RSOA fully bidirectional 20 km CLS-PON as a function of CO launch power

3.1.4 Equalization Discussion

We have seen in this section that pre-distortion can provide a significant improvement for the transmitter modulation bandwidth. This comes mainly at the cost of increased power consumption by the amplifiers at the ONU. A more thorough study would be required to demonstrate what noise sources dominate the link when the pre-distorted RSOA is used. The major unknown is the chirp induced in the RSOA due to the pre-distorted signal. The dispersion of an ideal NRZ signal at 5 Gb/s over standard SMF would be less than 1 ps. If the pre-distorted signal causes a large amount of chirp then a significant penalty could be induced. This effect was exploited by Pappagiannakis in [7] to convert the phase modulation (chirp) from the RSOA into amplitude modulation using the edge of an optical filter. It isn't clear whether or not this is a viable option for realistic link implementations.

3.2 Four Level Intensity Modulation for RSOA CLS-PON

3.2.1 Introduction to Multilevel Modulation

When transmitting information over long distances optical links are typically limited by transmission impairments such as chromatic or polarization mode dispersion, or by amplified spontaneous emission noise from the inline EDFAs. Over the shorter distances required by PONs the limiting factor is the modulation bandwidth of the low cost components employed. As we saw in the last section the datarate of these links can be increased by using equalization. Another technique to increase the datarate of a low modulation bandwidth transmitter that can be used independently or in conjuction with equalization is multilevel modulation.

Multilevel modulation is the standard for many electronic communication schemes. Wireless and low bandwidth wireline communications typically use multilevel, quadrature modulation formats such as 16, 64, or 256 quadrature amplitude modulation (QAM), 8 to 16 symbol phase shift keying (PSK), and multilevel amplitude shift keying (ASK). Most of these modulation techniques require access to both the phase and amplitude of the received electric *field*. In electrical systems this only requires some sort of phase locked loop to perform carrier recovery because of the low carrier frequency. In optical systems the extremely high carrier frequency mandates that either an external laser at a similar wavelength beat against the incoming signal (heterodyne) or the incoming signal beat against itself (homodyne) to generate the phase. While recent techniques using digital processing [5] to perform coherent demodulation, there is still considerable expense in generating coherent transmission that is beyond the cost range of CLS-PON systems.

For this reason only intensity modulated signals will be considered in this thesis in regards to CLS-PONS.

There are two general methods for performing multilevel modulation using intensity only modulation. The first, direct intensity modulation, will be considered in this section. The second, quadrature modulation of a microwave subcarrier, will be considered in the next section. Direct four level intensity modulation offers several benefits over standard on off keying in that it provides an increased datarate with the same channel bandwidth and same bandwidth components. This benefit comes at the cost of decreased sensitivity, or more stringent signal to noise requirements.

3.2.2 Experimental Setup

An experiment was performed to determine whether datarate enhancement could be achieved by using a four level pulse amplitude modulation technique instead of a standard binary transmission technique. The setup was very similar to that used in section 3.1.2. The actual physical setup is shown in Fig. 3.6. The chips used, an Accelerant Networks AN6420, produced a four level amplitude modulated signal, received it, and detected errors. It is identical to the system used in [10]. It is imperative for error free operation that each of the components be extremely linear. In particular the driving amplifier, receiver, and receiver amplifier must all be linear. The linear operation of the RSOA is assumed. It is particularly difficult to find a high speed linear commercial receiver as most commercial receivers are packaged with a limiting amplifier. A further difficulty is that the PAM-4 is designed for electrical interconnects, which require symmetric logic levels. The optical system, by nature of the Poisson distributions of the light levels, performs better with uneven spacing of

the logic levels. [11]. The signal was enhanced by the use of transmitter pre-distortion, as in section 3.1, to further improve the bandwidth of the modulator. It is not clear how the equalization affects the optimality of the drive levels of the modulator.

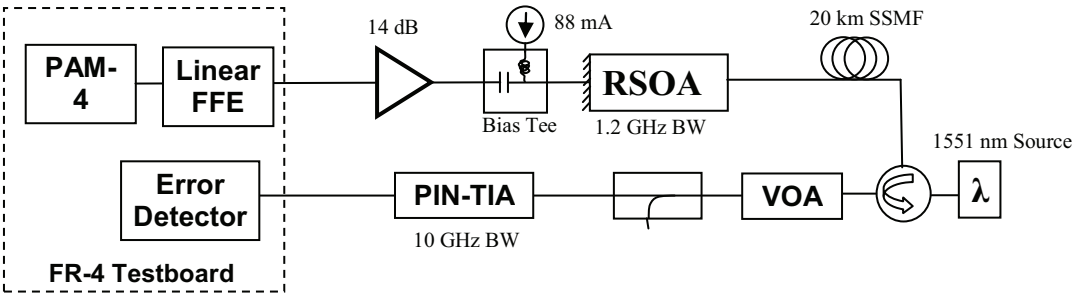

Fig. 3.6. Experimental setup for investigation of four level intensity modulated RSOA CLS-PON

3.2.3 Results

As can be seen from Fig. 3.8, 5 Gb/s (2.5 GSymbols/s) operation of PAM-4 RSOA PON is possible, although it does not show improvement over the equalized 5 Gb/s NRZ system. As you can see, however, the system can operate up to 8 Gb/s (4 GS/s) using PAM-4. The top eyes in this situation are open, but the noise on the bottom level inhibits operation. This is a case where if unequal distributions could be applied to the RSOA, improved performance is likely. The bias on the RSOA was adjusted to provide the best possible intensity level spacing, but was limited by the linearity of the RSOA and the relationship between the modulation bandwidth and the input power and current.

As can be seen in Fig. 3.7 the RSOA was capable, when driven with an optimal signal, of producing marginally open eyes up to 8 Gb/s (4 GS/s). This is

slightly less than double the datarate that was possible with a pre-distorted signal, which was shown in the previous section to be 5 Gb/s. Testing at higher rates was not possible because the BERT chips were only capable of generating driving signals up to 8 GS/s when driven in PAM-4 mode. As was predicted there are difficulties due to the required asymmetry that was not provided by the electrical driving signal.

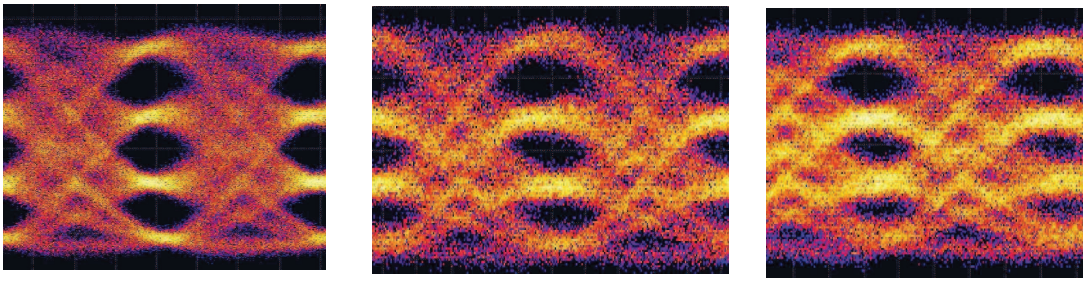

Fig. 3.7. Four level intensity modulated eyes with no transmission distance, at (left to right) 5 Gb/s (2.5 GS/s), 7.5 Gb/s (3.75 GS/s), and 8 Gb/s (4 GS/s)

Despite the relatively open eyes, the four level signal was incapable of transmitting low bit error ratio signals. As can be seen in Fig. 3.8 a very high power level was required to achieve error-free transmission, around 18 dBm higher than was required for equalized OOK transmission. After 20 km of unidirectional transmission (source light was seeded locally) the signal is barely capable of producing a bit error ratio above 10^{-3}. Fully bidirectional transmission was not possible.

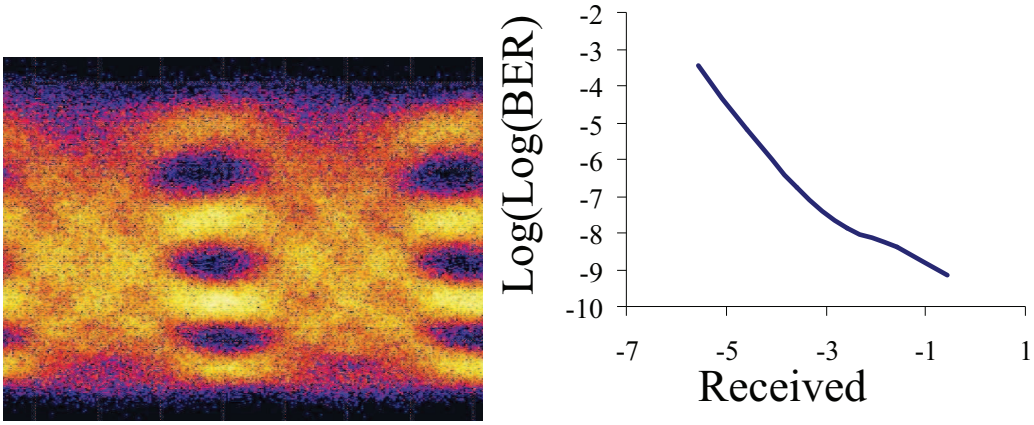

Fig. 3.8. Left) Four level intensity modulated signal at 5 Gb/s after 20 km of unidirectional transmission. Right) Back to Back sensitivity of 5 Gb/s four level signal.

3.2.4 Discussion

It is important to note that these experiments were performed using suboptimal experimental conditions, with a poor understanding of the noise sources and optimal driving conditions for the RSOA. Further understanding was gained in the experiments comprising Chapter 2, and the main sources of noise (Rayleigh noise, stimulated brillouin scattering) could be significantly reduced. Further the necessary amplifiers for proper four level modulation were not available at the time of the experiments, and an extremely linear receiver, which is necessary for proper four level intensity modulation, was not available. Another confounding factor was the use of the integrated BERT chip. The chip automatically determined the appropriate phase and voltage threshold for sampling, sometimes leading to erratic results. These results cannot generally be directly compared to experiments performed using a more traditional bit error ratio tester.

Regardless of these impediments, the great disparity between the BERs from OOK signals and the four level modulation signals suggests that this transmission method has significant drawbacks. Considering that negative intensity modulation levels are not available, the additional signal to noise ratio required will almost always negate any improvement in datarate that might be achievable from this method. The additional hardware and tuning requirements, as well as reduced system margins, will inevitably outweigh any possible benefits, rendering this method generally impractical. In the next section we will explore a more sophisticated and promising method for improving link performance using advanced intensity modulation formats.

3.3 Bidirectional PON Using Quadrature Subcarrier Multiplexing

3.3.1 Introduction to Subcarrier Multiplexing (SCM)

As mentioned in section 3.2.1. the use of low cost intensity modulators in a CLS-PON limits the modulation formats to intensity only, preventing the use of phase information in transmission. One method to work around this problem that also allows the provision of multiple channels on a single wavelength in a CLS-PON is microwave subcarrier multiplexing (SCM). In this scheme the data is initially mixed with a microwave carrier within the modulation bandwidth of the intensity modulator (up to 2.5 GHz using the equalized RSOA of previous sections). This modulated carrier is used to drive the intensity modulator. At the receiver end a photodiode detects the signal, the carrier phase is recovered using a phase locked loop, and the signal is recovered by mixing the incoming signal with the recovered carrier.

Among the benefits of this method are that multiple users can share the same wavelength simply by modulating and demodulating at a unique carrier frequency for that wavelength. A single broadband photodiode can be used to detect the signals from all different users simultaneously with the signals demultiplexed with different mixers after the photodiode. The main disadvantage is that twice the bandwidth is required to transmit a simple one-phase OOK signal, since the signal spectrum on the microwave carrier has two sidebands, and the carrier in turn produces two sidebands in the optical spectrum, as seen in Fig. 3.9. Fortunately a significant advantage of this method is that any arbitrary modulation format can be used on the data, and both the amplitude and microwave phase of the signal are available once the microwave carrier is recovered.

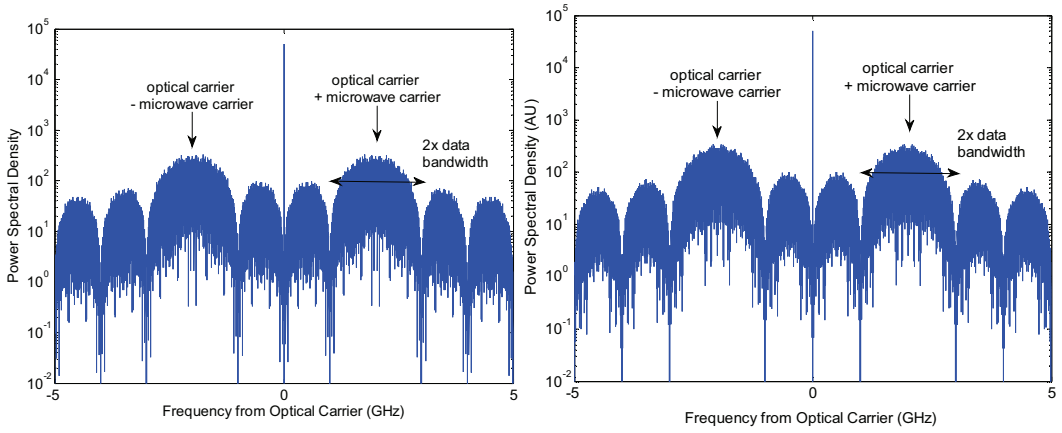

Fig. 3.9. Left) Optical spectrum of an intensity modulated, subcarrier multiplexed NRZ-OOK modulated signal. Right) Optical spectrum of an intensity modulated, subcarrier multiplexed quadrature amplitude modulated signal with twice the datarate. While the spectra are virtually identical, the signal to the right has twice as much data.

The modulation format we will use to exploit this feature is quadrature amplitude modulation. When a carrier frequency is used the property of orthogonality can be exploited to double the datarate of a signal without increasing it's bandwidth, as seen in Fig. 3.10. While the optical spectra of the two signals is identical, the signal on the left has a datarate of 1 Gb/s while the signal on the right has twice the datarate. This is because the cosine and sine components of a wave are orthogonal, such that when one is at a maximum amplitude the other is at zero amplitude, such that signals placed on two waves with a phase difference of 90° will not interfere with each other [12]. This allows a doubling of the datarate without the same OSNR penalty as four level intensity modulation since the two signals are orthogonal. In fact there is a 3 dB improvement if coherent signaling is performed on the optical carrier since half of the noise will be out of phase and thus eliminated on demodulation.

In a CLS-PON the subcarrier multiplexing technique can be used in many ways. It was initially proposed in [13] as a method for reusing the optical carrier from the downstream intensity signal. If the downstream signal is subcarrier multiplexed the carrier will still be present at the ONU, which can be remodulated and transmitted upstream at baseband without interfering with the downstream signal, and these techniques have been used to demonstrate bidirectional data transmission up to 1.25 Gb/s using narrow optical filtering [14-18].

Several studies have been performed demonstrating improved Rayleigh immunity from the subcarrier multiplexed scheme [19-20]. The fundamental reason for this improvement is similar to the reason that Rayleigh noise can be effectively

low pass filtered from an intensity modulated signal. Imagine the simplest SCM CLS-PON scenario in which a downstream CW signal is modulated at the ONU with an NRZ-OOK data signal on a microwave carrier that is at least as high as the datarate. In this case the spectrum of the type I Rayleigh noise, type II Rayleigh noise, and signal will look like the diagrams in Fig. 3.10.

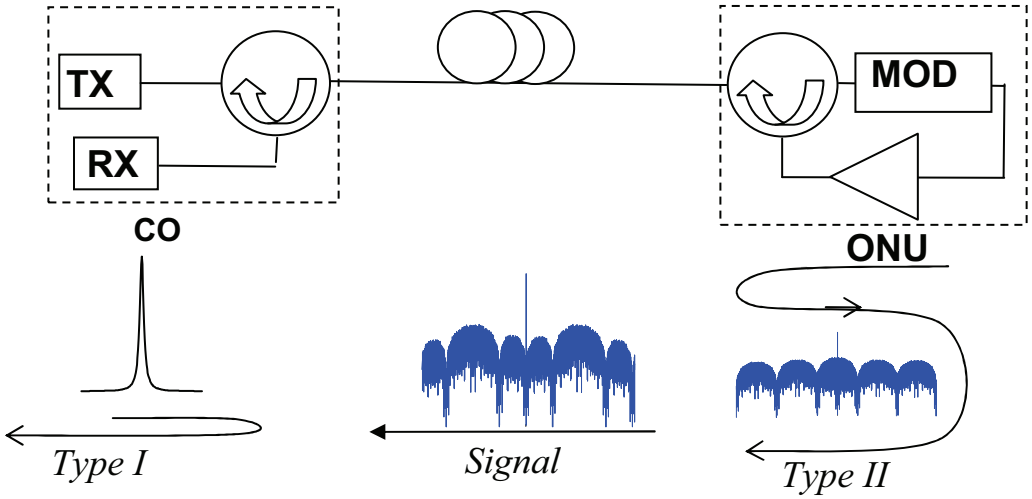

Fig. 3.10. Spectrum of signal and Rayleigh noise for a simple SCM CLS-PON

It is easy to see from this diagram that the type I Rayleigh, the reflected CW carrier from the CO, will be completely out of the optical bandwidth of the received signal. It can be filtered either optically with a very narrow filter, or half of the signal-type I beat noise can be filtered using a high pass filter without any signal penalty. Since all the information is contained within one optical sideband, one sideband can be eliminated with the carrier without penalty. The signal has information in both sidebands. After it is reflected from the fiber and amplified in the ONU, it is modulated again which spreads the carrier component to the signal bands and the signal component to higher and lower bands. In this case half of the noise

will be directly overlapping the signal. Half of the noise will be optically completely out of band, however, shifted either higher out of band or lower into the carrier band. Again it can either be optically filtered or electrically filtered with a combination of low and high pass filters before and after the receiver mixer. Using this technique the Rayleigh noise can be significantly mitigated.

3.3.2 Bidirectional System Concept

The use of quadrature components on a subcarrier is generally used to increase the bandwidth of a unidirectional link. In a bidirectional link, however, it can be used to transmit information in both directions simultaneously. This is schematically illustrated in Fig. 3.11. First the downstream data is translated from the baseband to a microwave carrier frequency using a mixer. This carrier is then intensity modulated onto a CW laser source with some modulation depth. This signal is transmitted to the ONU where the carrier is recovered (the data is essentially microwave BPSK at this point, so carrier recovery is straightforward). The ONU uses the recovered carrier to translate its own data to the same microwave carrier frequency, *but with a phase shift of 90° to the original carrier*. This phase shift is the key to the system, as the upstream data is now orthogonal to the originally transmitted data.

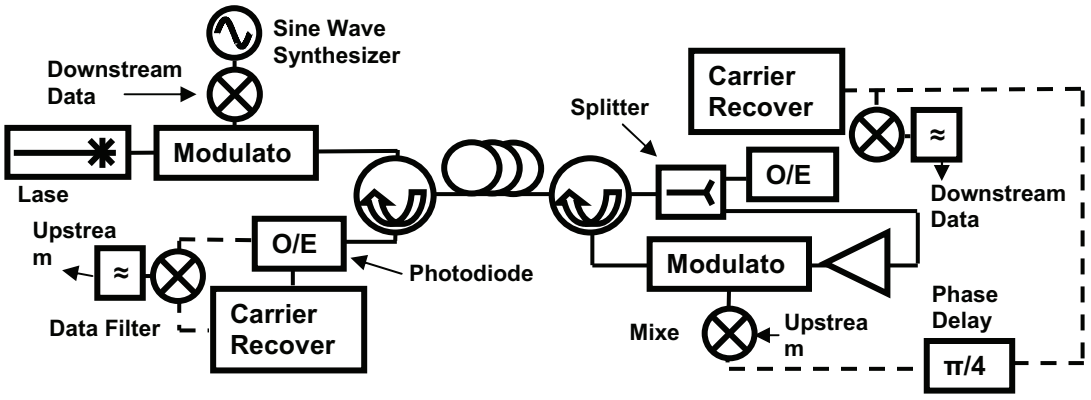

Fig. 3.11. Schematic Diagram of Proposed Bidirectional Subcarrier Multiplexed PON

The new data is transmitted upstream to the CO, where it is recovered using either the original sine wave generator or a recovered carrier from the received data. As we shall see in the experimental results section, this system is much less sensitive to the downstream extinction ratio than the OOK system analyzed initially in Chapter 2. This is for two reasons. First, the superposition of the optical wave means that even assuming that a perfect infinite extinction ratio is used on the downstream transmission, there is still power in each bit. In fact the amount of optical energy in each bit is equal to half of the originally transmitted power under this condition. This is because the transmission scheme is essentially phase modulation of the superimposed carrier. Secondly, the receiver at the CO can filter out the downstream transmitted data, since it is orthogonal to the upstream data. Thus the upstream data is less sensitive to the magnitude of the downstream data.

The main advantage of this scheme is that it will provide an improved general noise resistance to OOK modulation. This is demonstrated by Figs. 3.12-13. On the downstream side, while the average total transmitted power for a given ER is the same, the power transmitted is the same for marks and spaces if SCM is used. Since

the photodetector is a square law detector this means that the total signal-optical noise beat noise will be lower for a subcarrier signal than for an OOK signal. On the upstream side there is a penalty for subcarrier for this same reason. OOK has a hard zero, and thus has a high noise tolerance for zeros. Subcarrier has no such benefit, but it should make up for it because of the ability to eliminate the downstream data from the signal when the carrier phase is set such as to eliminate both the downstream signal and any noise present in the orthogonal microwave phase, which should be roughly half of the noise.

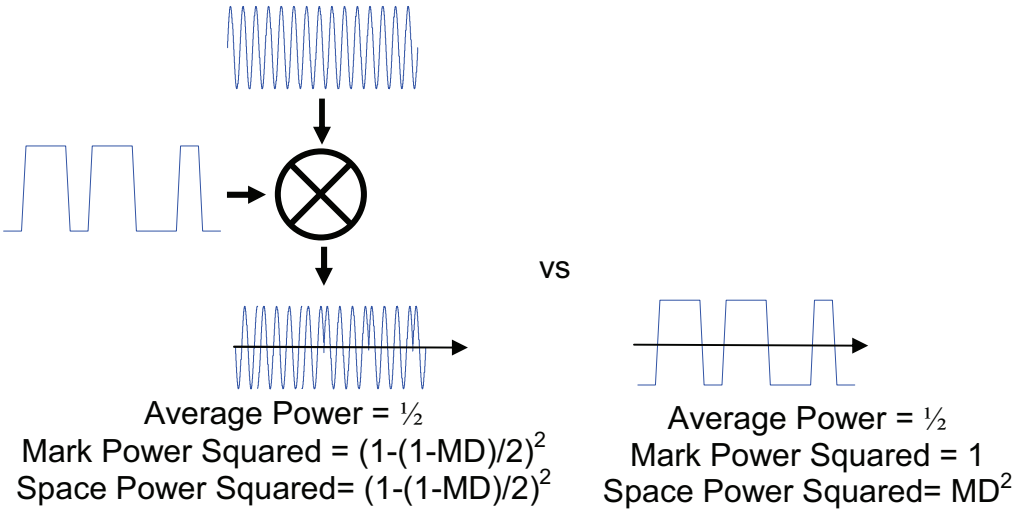

Fig. 3.12. Schematic illustration of downstream transmission showing reduced average squared power, indicating improved noise performance, for SCM modulation

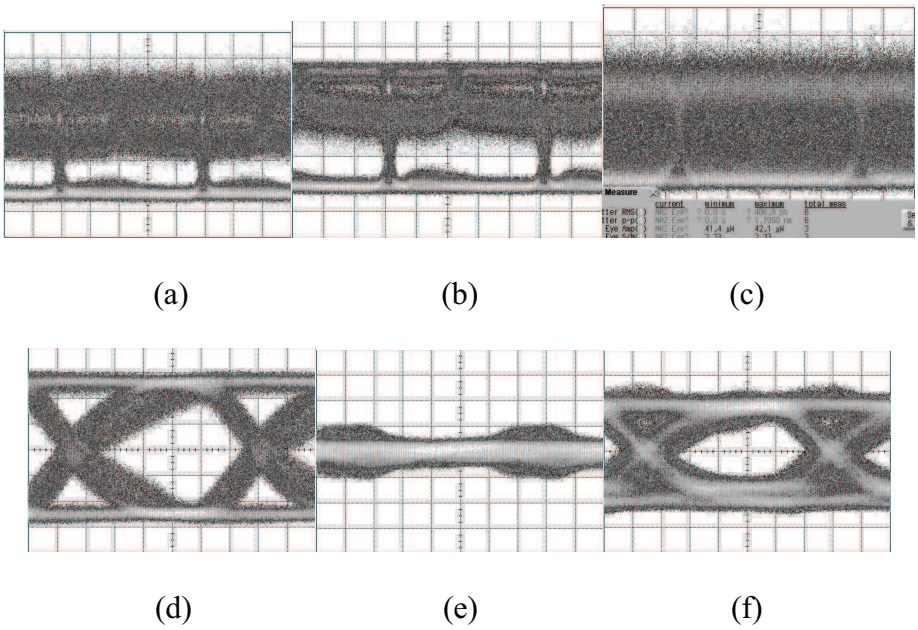

Fig. 3.13. Eye diagrams from upstream signals. a) OOK optical eye diagram translates to b) OOK electrical eye diagram. c) SCM optical eye diagram translates to d) SCM electrical eye diagram, which is the sum of e) the canceled downstream signal and f) the transmitted upstream signal if the carrier phase is set properly.

This scheme also provides improved immunity to Rayleigh noise. The Rayleigh noise spectra present in the quadrature modulated PON are shown in Fig. 3.14. The portions in dashed boxes are the desired signal. In the optical reception and downconversion process, only the information surrounding the carrier frequency within the receiver data filter will be detected. This means that the CW portion of the Rayleigh backscattering noise, which is still quite significant, will be filtered out. Furthermore the modulation of the light with higher frequency upconverted signal will lead to Rayleigh noise that does not fall at the CW carrier to be pushed further out of the received band and this will also be largely filtered out in the downconversion and receiving process. Considering the already significant noise immunity introduced by quadrature modulation it is expected that this scheme will be

significantly more resistant to Rayleigh noise than OOK methods. To predict this immunity would require the calculation of the cross correlations of each of the noise and signal spectra, an exercise that is outside the scope of the present work.

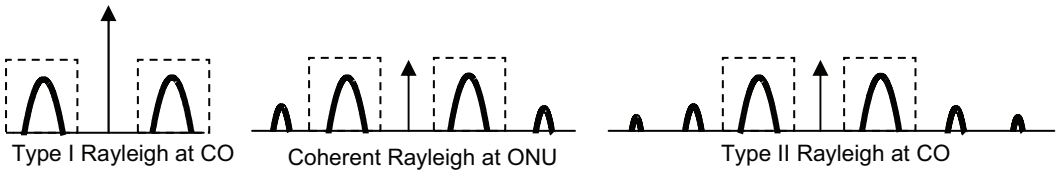

Fig. 3.14. Illustrated spectra of Rayleigh noise sources in quadrature modulated PON

An interesting outcome of this scheme is that if the CO mixer is driven by an LO that is 90° out of phase with the upstream carrier it is possible to recover the original data. This is because when the upstream carrier has an amplitude of ½ the downstream data will be a maximum or minimum, and thus it is still present and detectable. Considering that an infinite downstream ER can be used this means that it is possible to have both signals present in equal powers in the upstream signal. One application of this technique is to reuse the same light for a three point network by transmitting the signal on from the ONU to a receiver that is not at the CO. In this technique the ONU would receive the CO signal, and the third point would receive both the CO and ONU signals. Note that this is impossible in the OOK method since half of the bits are extinguished completely by the ONU modulator.

3.3.3 Experimental Demonstration of Noise Immunity

Two experiments were performed to determine the performance of the proposed scheme in comparison to the bidirectional OOK methodology. The first demonstrated general susceptibility to noise, as evaluated by injection of ASE. The

second was susceptibility to Rayleigh noise and link operation, evaluated by building an actual link.

3.3.3.1 Experimental Design

A system of separate signal and noise generation was built to determine the relative noise immunity of each signaling scheme. The setup is shown in Fig. 3.15. The ER of the downstream signal was set by the bias and signal amplitude of the first MZM. The mark level was fixed and the space level increased to decrease the ER. The downstream linear ER for OOK signaling was evaluated at 0.45, 0.38, and 0.2. These values were chosen to find the value closest to the optimal ER, at which point the upstream and downstream signals were equally susceptible to noise. It was found for the RSOA modulator the optimal ER was 0.2, while for the MZ modulator the optimal ER was 0.38.

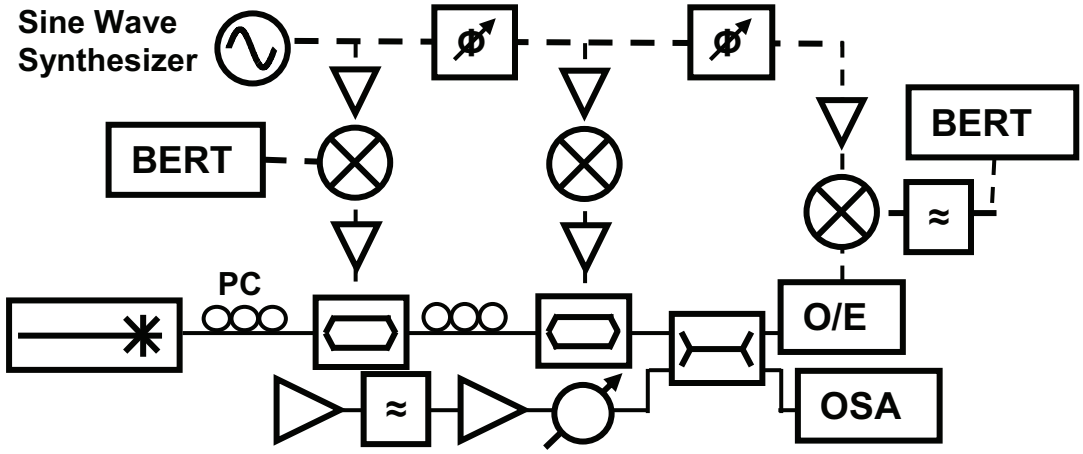

Fig. 3.15. Experimental Setup for determining noise immunity. For RSOA experiments the second MZM was replaced with a circulator and the RSOA. PC – Polarization Controller, VOA – Variable Optical Attenuator, BERT – BER Tester, φ – Variable Phase Delay

The subcarrier signals were generated by upconverting a 1 Gb/s data signal with a 2.5 GHz carrier using a Marki T3 triple balanced mixer driven with an A126EQP amplifier. This output was amplified using an AP-110 amplifier, which is a lower cost amplifier since it does not have to operate at DC, to drive either the MZM or RSOA. Microwave phase shifters were used on the receiver and transmitter sides to maximize the signal, and in the case of the upstream signal minimize crosstalk, by observing the eye diagram of the received signal.

The RSOA used was the same CIP RSOA used in previous experiments in this chapter. It was biased with a current of 96 mA and driven with a peak to peak voltage of 4 V in order to maximize the modulation bandwidth, which was nominally only 1.2 GHz. Remarkably the subcarrier signal, with a bandwidth from 2 to 3 GHz, was capably modulated onto the optical carrier using the low speed RSOA.

3.3.3.2 Experimental Results and Discussion

The results of the experiment are shown in Fig. 3.16. Since the ER was selected to equalize the noise immunity between the upstream and downstream signal, the curves for each signaling system are grouped together. To the farthest right are the curves for the bidirectional OOK using an MZM for the upstream modulator and an ER of 0.38, which is the system most susceptible to noise. In contrast the far left has the curves for orthogonally modulated data using an MZM for the upstream modulator. In this case the optimal ER is 0. The reasons for the noise immunity and selection of ER are those discussed in the previous section. As can be seen the improvement gained by using the subcarrier method can be significant. At low BERs this method is immune to up to 9 dB of increased noise!

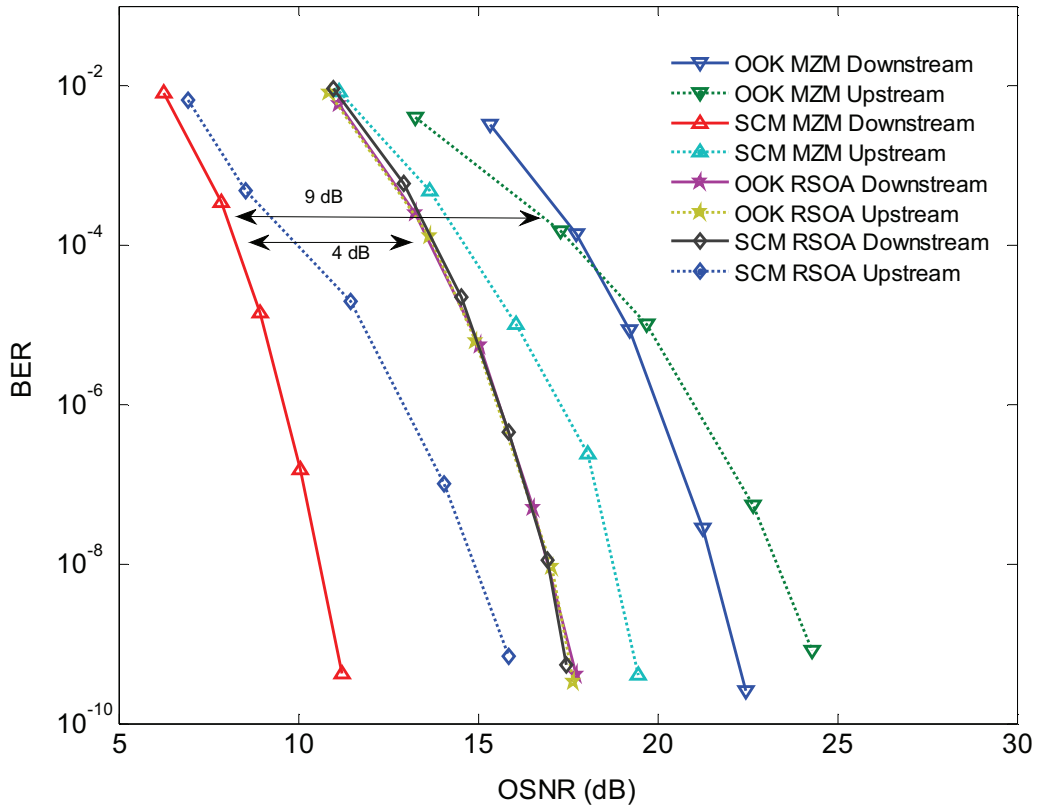

Fig. 3.16. BER vs OSNR for various modulation formats. Downstream transmission is marked with a solid line, and upstream transmission with a dashed line.

In the middle of these extremes are the curves due to the RSOA OOK and SCM modulation. The curves for downstream OOK, upstream OOK, and downstream SCM are almost overlapping. There is a small penalty for the upstream SCM signal. There are two main factors causing this deviation from the MZM case. The first is that the RSOA makes an excellent modulator for OOK signals because it generates hard zeros and in saturation causes the squeezing of both noise and signal levels on the marks. The second effect is the limited modulation bandwidth of the RSOA, which causes the subcarrier signal to be distorted and introduces errors. Conversely the nonlinear nature of the saturated SOA bequeaths no benefit to the

SCM signal as it introduces further distortion and the SCM signal sees no benefit from the hard zeros. It is surprising that despite these limitations the signal still produces wide open eyes with noise immunity superior to that for the MZM OOK case. This effect would be mitigated with the use of high modulation bandwidth and linear SOAs.

3.3.4 Experimental Link Demonstration

3.3.4.1 Experimental Design

The link was built to reproduce the schematic diagram shown in figure 3.11 and is nearly identical to the link employed at the end of chapter 2 to test the OOK link, with the significant differences being the electrical driving system being replaced with the subcarrier system, the replacement alternately of the ONU modulator with the RSOA, and the length of the fiber. The setup for the RSOA is shown in Fig. 3.17. Experiments were performed using the MZM modulator at 50 km and the RSOA at 5 km. While the RSOA was capable of transmitting at 20 km successfully using the SCM scheme and error-free using OOK, the low relative gain of the RSOA prevented proper setting of the link gain and thus made a fair comparison of the two schemes impossible at this length.

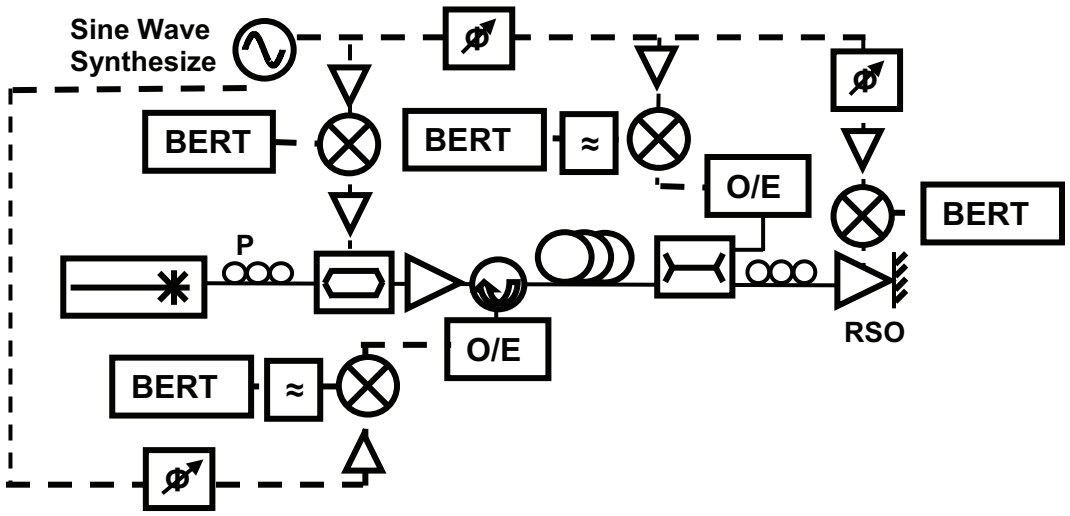

Fig. 3.17. Experimental setup for bidirectional transmission using RSOA.

For the MZM case the gain for each link was set to roughly the loss of the fiber + 1 dB, as shown as a rule of thumb in Chapter 2, and then fine tuned to minimize the BER. For the RSOA the gain was maximized, with a bias of 96 mA and driving signal of 4 V p-p as before, to maximize the modulation bandwidth. Conversely the polarization of the ONU was set to maximize the BER, indicating co-polarization of the signal and Rayleigh noise.

3.3.4.2 Experimental Results and Discussion

Results of the RSOA link, including eye diagrams, are shown in Fig. 3.18. These results do not provide a great deal of information, however, since both systems performed admirably at a 5 km distance. The OOK signal was capable of very low BERs across a wide range of modulation depths (MD, defined as the ratio of the space level to the mark level for OOK, or the ratio of the carrier low to the carrier high for SCM). Despite having the worst eye diagram of all the link combinations, the upstream OOK signal was the most resilient to different MDs. As seen at the end

of Chapter 2 the downstream signal requires a greater portion of transmitted light than the upstream signal due to the upstream signal having hard zeros. With the selection of a proper sampling voltage this means that the extremely noisy upstream OOK signal is still capable of error free transmission, although any deviation from the optimal sampling voltage will cause significant errors. In this limited circumstance it appears that both systems would be feasible, and since OOK is more economical, it would be more desirable.

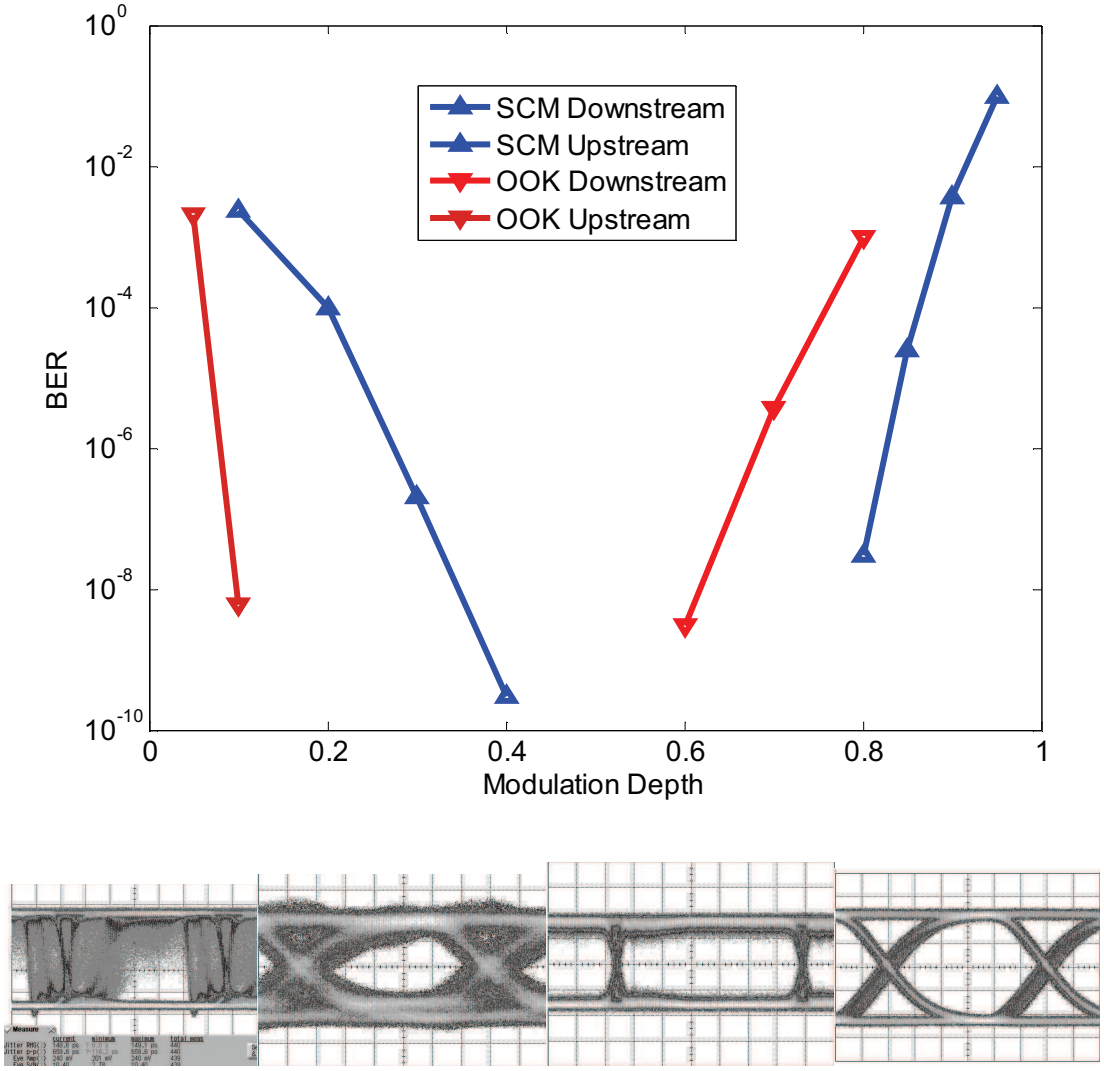

Fig. 3.18. Bidirectional BERs for an RSOA link at 5 km. Downstream transmission is on the right and upstream on the left. Eye diagrams are in the same order as the curves (left to right): OOK upstream, SCM upstream, OOK downstream, SCM downstream

Fig. 3.19 shows the results for using MZMs as both the downstream and upstream transmitters. This case is significantly different. In this 50 km link the OOK signal struggles, mustering an optimal BER of worse than 10^{-5} when an optimal MD is chosen. This is due to the high susceptibility of the OOK signal to Rayleigh

noise. For the SCM modulated signal, however, performance is excellent. The downstream signal is undetectable until an MD of 0.7, but it rapidly becomes error free at an MD of 0.5. The upstream signal doesn't show up on the chart, only as an eye diagram, because it is error free across the entire range of MD values! Therefore, given these modulators and a distance of 50 km, a designer would be unable to employ OOK signaling, but would be able to use SCM modulation. Unfortunately the RSOA did not provide sufficient gain to evaluate its performance at 50 km. However, because of the MZM SCM systems noise margin of 1-7 dB over the OOK RSOA, it seems likely that it would be capable of a significant distance improvement over this alternative scheme as well.

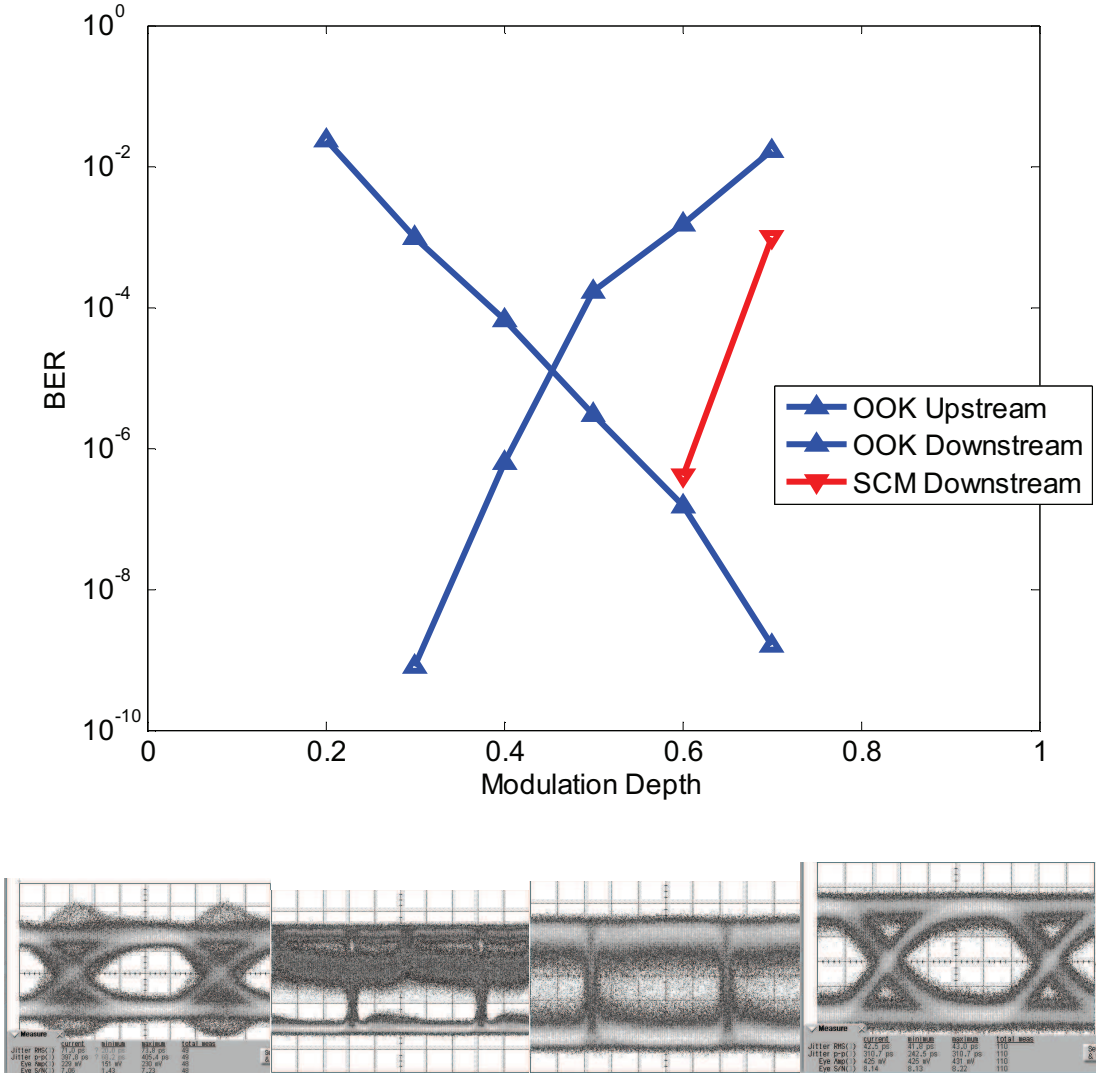

Fig. 3.19. Bidirectional BERs for an MZM link at 50 km. Downstream transmission is on the right and upstream on the left. Eye diagrams are in the same order as the curves (left to right): SCM upstream (error free at all MDs), OOK upstream, OOK downstream, SCM downstream

3.3.5 Quadrature Subcarrier Modulation Conclusion

It has now been demonstrated that significant improvement can be realized by employing quadrature modulation in a bidirectional link if given an ONU with sufficient gain and modulation bandwidth. It is reasonable to assume that RSOAs

will continue making gains in gain-bandwidth product that may allow deployment in links. For the short distance links that PONs will primarily be used to serve, however, current RSOAs or couple SOA-EAM devices should provide sufficient gain-bandwidth products. While the benefits of this system may not justify the cost for short distances where NRZ modulation will suffice, the method of split quadrature modulation deserves further investigation. As orthogonal frequency division multiplexing (OFDM) and other subcarrier based techniques gain understanding it would be beneficial to determine whether better signal crosstalk reduction is provided by using separate frequencies with electrical filtering for upstream and downstream signal distinction as in previous works, or orthogonal phase modulation as demonstrated in this work.

3.4 Conclusion

This chapter has been concerned with the experimental investigation of various signaling techniques to improve the transmission performance of passive optical networks. The first contribution of the work was to demonstrate that transmitter pre-distortion for RSOAs could expand the modulation bandwidth and allow generation of open eye diagrams at datarates up to 4x the 3 dB modulation bandwidth of the RSOA. With further study of link noise mechanisms and optimization it is expected that this technique would be a viable alternative or possible enhancement to receiver side equalized links.

Next the chapter investigated the use of four level intensity modulation to increase the bandwidth of the RSOA link. While the RSOA was capable of

generating open four level eye diagrams, the reduced noise immunity of this scheme caused it to underperform standard binary NRZ transmission. This investigation however led to the investigation of four level modulation using a microwave subcarrier and orthogonal modulation.

The third and most significant contribution of this chapter was the invention and investigation of separate modulation of the I and Q components of a microwave carrier in an intensity modulated, bidirectional, lightwave reuse passive optical network. It was shown that this scheme demonstrated significantly improved noise immunity to OOK signaling of up to 9 dB for MZM modulators and 4 dB for saturated RSOA modulators. Finally it was shown that this noise improvement led to successful error free transmission for this scheme in a bidirectional 50 km link that OOK signaling could not achieve.

ACKNOWLEDGEMENT

Section 3.3 is, in part, a reprint of the material in "of "Bidirectional Quadrature Subcarrier Modulation for Central Light Source PONs", to be submitted to *Photonics Technology Letters*, 2010.

The dissertation author was the primary investigator and first author of these publications, but would like to thank Dr. Christopher Marki and Prof. Sadik Esener for their helpful suggestions.

3.5 References

[1] P. Healey, P. Townsend, C. Ford, L. Johnston, P. Townley, I. Lealman, L. Rivers, S. Perrin, and R. Moore, "Spectral slicing WDM-PON using wavelength-seeded reflective SOAs", *Elec. Lett.*, Vol. 37, 19, pp. 1181–1182, 2001.

[2] P. Chanclou, F. Payoux, T. Soret, N. Genay, R. Brenot, F. Blache, M. Goix, J. Landreau, O. Legouiezigou, and F. Mallécot, "Demonstration of RSOA-based remote modulation at 2.5 and 5 Gbit/s for WDM PON", *Proc. OFC 2007*, paper OWD1.

[3] Yu, Q., Shanbhag, A., "Electronic Data Processing for Error and Dispersion Compensation", *J. Lightwave Tech.*, vol. 24, no. 12, pp. 4514-4525, 2006.

[4] K. Azadet, E. F. Haratsch, H. Kim, F. Saibi, J. H. Saunders, M. Shaffer, and L. Song, M-L Yu, "Equalization and FEC Techniques for Optical Transceivers", *IEEE J. Solid-State Circuits*, vol. 37, no. 3, pp. 317-327, 2002.

[5] M. G. Taylor, "Algorithms for Coherent Detection", *Proc. OFC 2010*, paper OThL4.

[6] K.Y. Cho, Y. Takushima, and Y.C. Chung, "10-Gb/s Operation of RSOA for WDM PON", *IEEE Phot. Tech. Lett.*, vol. 20, 18, pp. 1533-1535, 2008.

[7] I. Papagiannakis, M. Omella, D. Klondis, A. Birbas, J. Kikidis, I. Tomkos, and J. Prat, "Investigation of 10-Gb/s RSOA-Based Upstream Transmission in WDM-PONs Utilizing Optical Filtering and Electronic Equalization", *IEEE Phot. Tech. Lett.*, vol. 20, 24, pp. 2168-2170, 2008.

[8] M. Omella, I. Papagiannakis, B. Schrenk, D. Klonidis, J.A. Lázaro, A.N. Birbas, J. Kikidis, J. Prat, and I. Tomkos, "10 Gb/s Full-Duplex Bidirectional Transmission with RSOA-based ONU Using Detuned Optical Filtering and Decision Feedback Equalization", *Opt. Express*, vol. 17, 7, pp. 5008-5013, 2009.

[9] C.F. Marki, "Design and Optimization of Bidirectional and Optical Logic Systems in the Presence of Noise", Ch. 4, Ph.D. dissertation, Dept. Elect. Eng., Univ. California, San Diego, La Jolla, CA, 2007.

[10] J.E. Cunningham, D. Beckman, X. Zheng, D. Huang, T. Sze, A.V. Krishnamoorthy, "PAM-4 Signaling over VCSELs with 0.13 CMOS Chip Technology", *Opt. Exp.*, vol. 14, 25, pp. 12028-12038, 2006.

[11] G. Papen and R. Blahut, *Lightwave Communication Systems*, Draft A, Prentice-Hall, 2007.

[12] P. J. Winzer and R.-J. Essiambre, “Advanced Optical Modulation Formats”, *Proc. IEEE*, vol. 94, 5, pp. 952-985, 2006.

[13] J.-M. Kang and S.-K. Han, “A novel hybrid WDM/SCM-PON sharing wavelength for up- and down-link using reflective semiconductor optical amplifier,” *IEEE Photon. Technol. Lett*., vol. 18, no. 3, pp. 502–504, Feb. 2006.

[14] Z. Xu, Y. J. Wen, W.-D. Zhong, M. Attygalle, X.-F. Cheng, Y. Wang, T. H. Cheng, and C. Lu, “WDM-PON architectures with a single shared interferometric filter for carrier-reuse upstream transmission,” *J. Light. Tech.,* vol. 25, pp. 3669–3677, Dec. 2007.

[15] M. Attyglle, N. Nadarajah, and A. Nirmalathas, “Wavelength reused upstream transmission scheme for WDM passive optical networks,” *Electron. Lett.*, vol. 41, pp. 1025–1027, Sep. 2005.

[16] J. Yu, O. Akanbi, Y. Luo, L. Zong, T. Wang, Z. Jia, and G.-K. Chang, “Demostration of a novel WDM passive optical network architecture with source-free optical network units,” *IEEE Photon. Technol. Lett.*, vol. 19, no. 8, pp. 571–573, Apr. 2007.

[17] Zhaowen Xu, Yang Jing Wen, Wen-De Zhong, Tee Hiang Cheng, M. Attygalle, Xiaofei Cheng, Yong-Kee Yeo, Yixin Wang, and Chao Lu, “Characteristics of Subcarrier Modulation and Its Application in WDM-PONs”, *J. Light. Tech.*, vol. 27, no. 12, pp. 2069-2076, 2009.

[18] C.W. Chow, G. Talli, A.D. Ellis, and P.D. Townsend, “Rayleigh Noise Mitigation in DWDM LR-PONs Using Carrier Suppressed Subcarrier-Amplitude Modulated Phase Shift Keying”, *Optics Express*, vol. 16, no. 3, pp. 1860-1866, 2008.

[19] A. Chowdhury, Hung-Chang Chien, Ming-Fang Huang, Jianjun Yu, and Gee-Kung Chang, “Rayleigh Backscattering Noise-Eliminated 115-km Long-Reach Bidirectional Centralized WDM-PON With 10-Gb/s DPSK Downstream and Remodulated 2.5-Gb/s OCS-SCM Upstream Signal”, *IEEE Phot. Tech. Lett.*, vol. 20, no. 24, pp. 2081-2083, 2008.

[20] C.W. Chow, C.H. Yeh, C.H. Wang, F.Y. Shih, and S. Chi, “Rayleigh Backscattering Performance of OFDM-QAM in Carrier Distributed Passive Optical Networks”, *IEEE Phot. Tech. Lett.,* vol. 20, no. 22, pp.1848-1850, 2008.

[21] Zhaowen Xu, Yang Jing Wen, Wen-De Zhong, Tee Hiang Cheng, M. Attygalle, Xiaofei Cheng, Yong-Kee Yeo, Yixin Wang, and Chao Lu, "Characteristics of Subcarrier Modulation and Its Application in WDM-PONs", *J. Light. Tech.,* vol. 27, no 12, pp.2069-2076, 2009.

4. Applications of VCSELs in PONs

As we have seen in previous chapters the main driving consideration in passive optical network (PON) design is equipment, maintenance, and operation cost. One method for lowering overall link cost mentioned in Chapter 2 is to replace traditional long haul communication components such as distributed feedback (DFB) lasers, mach-zender modulators (MZM), and erbium doped fiber amplifiers (EDFA) with lower cost components such as vertical cavity surface emitting lasers (VCSEL), electro-absorption modulators (EAM), and semiconductor optical amplifiers (SOA). What these components have in common is that they are fabricated using integrated circuit technology instead of as a collection of discrete components.

Since integrated circuit (IC) technology was invented fifty years ago, it has continuously penetrated further into applications traditionally dominated by discrete components, dramatically reducing costs and improving performance. Integration in photonic components has lagged significantly behind electronics significantly for two major reasons. First because light cannot be conducted through wires in the way electrons can. This limits the size of photonic components by requiring a minimum bend radius from waveguides, on the order of tens of millimeters for standard single mode fiber (SSMF) [1] to tens of microns for high index silicon waveguides [2]. The second reason is that silicon, which has been the workhorse of the electronics industry due to its mechanical stability, ease of manufacturing, and low cost, is not a direct bandgap material and thus will not emit light through a direct recombination process. Because of this fact emitters and amplifiers in the low loss 1550 nm communication

band are typically made from Indium-Gallium-Arsenic-Phosphide quaternary quantum well structures. This is the case for both the VCSELs and reflective SOAs (RSOA) used in these experiments.

The use of these integrated circuit technologies has several implications for the design of PONs. When the semiconductor devices are to be used as modulators there is a tradeoff between optical output power and modulation bandwidth, limiting the driving frequency of the RSOA in chapter 3 for example. In the ideal ONU unit in chapter 2 the amplification was done by an EDFA while the modulation was done by a lithium-niobate MZM. Since the amplification and modulation are combined in an RSOA there is a tradeoff between increasing the length or width of the device to increase the gain and decreasing it to reduce the capacitance of the diode and thus increase the modulation bandwidth.

4.1 VCSEL as CO Source Laser

4.1.1 VCSEL CO Transmitter

It was identified early in the development of the PON that a major impediment to implementation is the identification of a low cost multi-wavelength source [5]. Because they are fabricated in planar arrays, and because the wavelength can be set using graded depositions and other fabrication methods, it is feasible for an array of VCSELs to meet this demand. Further, since VCSELs can be directly modulated this is a promising low cost solution. Fig. 4.1 illustrates a sample CO transmitter that could meet these demands.

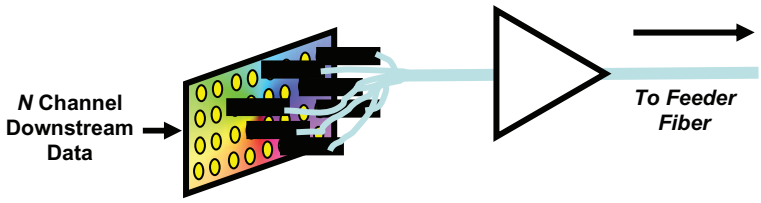

Fig. 4.1. Schematic Illustration of Potential VCSEL Based CO Downstream Data Source

Using this scheme an array of VCSELs would be fabricated and tested on die. An appropriate set of wavelengths would be selected, and those VCSELs that had the correct wavelength and the best operating characteristics would be fiber coupled. The temperature of the entire array would be kept constant, and to a certain extent the precise wavelength can be tuned with the bias current. The downstream signals would be amplified together using a single EDFA. Note that there is nothing in this scheme that would prevent advanced intensity modulation formats from being used, such as subcarrier multiplexed or analog RF modulation.

4.1.2 Effect of VCSEL Linewidth

The only major effect that is beyond fabrication, and thus within the scope of this thesis, is the effect from having a broader linewidth than Fabry-Perot or Distributed Feedback lasers. While the linewidth of a typical DFB is on the order of MHz, the linewidth of a VCSEL is on the order of hundreds of MHz. This will create two major differences for link design between the two laser choices. The first is a delayed onset of stimulated Brillouin scattering (SBS). Fig. 4.2 shows the onset of SBS as a function of fiber input power for two a DFB (linewidth of 3 MHz maximum) and a VCSEL (unknown linewidth, typically on the order of 300 MHz [6]).

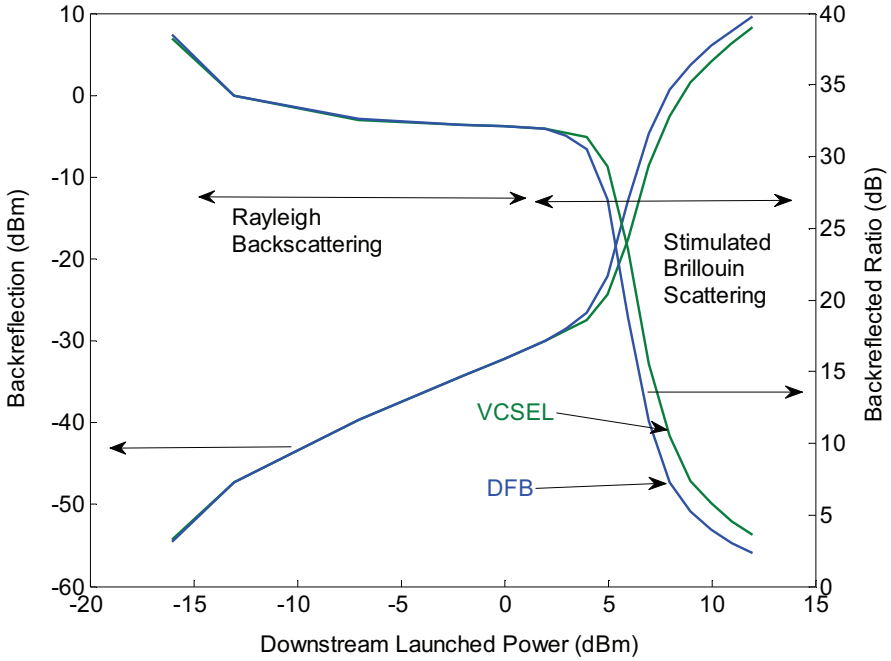

Fig. 4.2. Measured Backreflection as a Function of Launch Power

As can be seen, the onset of SBS is delayed for the VCSEL over the DFB. Unfortunately this offset is only by less than 2 dB. Fig. 4.3 shows the maximum Rayleigh noise limited distance for a single directional link using 8B/10B encoding and high pass filtering.

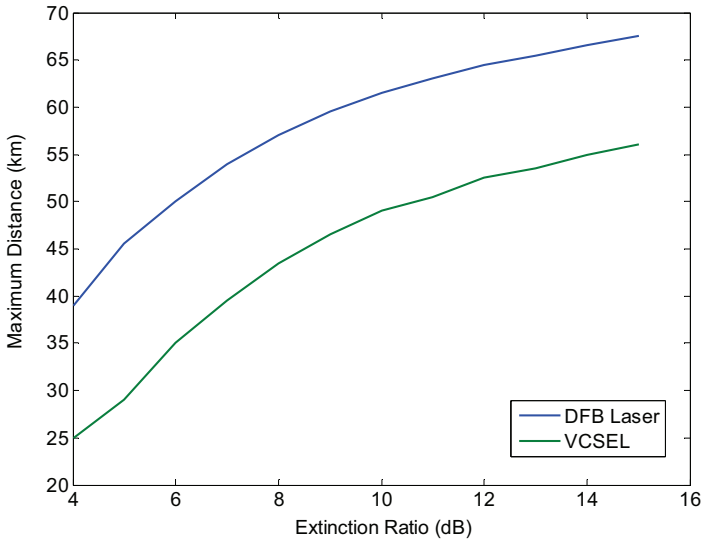

Fig. 4.3. Rayleigh Limited Link Reach for unidirectional CLS-PON

This figure shows very clearly the detriment of using a higher frequency source laser such as a VCSEL. Nonetheless, for high extinction ratio modulators it may be the most practical choice.

4.2 Vertical Cavity Semiconductor Optical Amplifier as ONU Modulator

4.2.1 Introduction to VCSOAs

Recently a good deal of research has been performed [7-22] to study the use of the vertical cavity laser structure as an amplifier because of it's lower cost, ease of fabrication, and easier installation than the edge coupled semiconductor amplifier. Most vertical cavity structures are constructed to operate at the 850 nm wavelength the GaAs material system emits at due to the relative ease of constructing GaAs dielectric mirror stacks compared to those of InGaNAs. The dominance of long

wavelengths at communication wavelengths has led to the development of VCSOA technology at 1300 and 1550 nm [15], [20-21]. Long wavelength injection locked VCSELs have been shown to demonstrate very large modulation bandwidths, and thus have been employed as the ONU transmitter in prototype PONs [23-25]. Injection locking a VCSEL requires significant optical injection power, however, causing the ONU to have a net loss unless additional amplification is employed. For this reason it is desireable to investigate whether the VCSEL structure can be operated below the lasing threshold current, in the amplifying mode as a VCSOA, for the ONU transmitter.

It is expected that operating in the high gain region of the VCSOA will present significant challenges. The modulation bandwidth of the VCSOA/VCSEL is dependent on the level of both current and light injection, as described by the rate equations [25]. VCSOAs are only capable of providing high gain when they are operated below threshold (around 2 mA for the 1550 nm VCSELs used in this experiment) and with a low level optical input (typically below 10 μW (-20 dBm) input and 100 μW (-10 dBm) output). If a typical PIN photodiode with -17 dBm sensitivity at 10 Gb/s is used, this indicates that there is an extremely narrow noise margin. However, if an avalanche photodiode (APD), pre-amplifier, distribution node amplifier, or lower datarate is used there should be sufficient power for a narrow noise margin.

4.2.2 Experimental Investigation

In order to evaluate the ability of VCSOAs to operate as ONU modulators a simple experiment was performed. A 1550 nm VCSEL rated for 2.5 Gb/s modulation

speed from Raycan (South Korea) was soldered to an SMA connector. The VCSEL was biased with a bias T and driven with a signal generator. No amplifier was necessary since the driving voltage of the VCSEL was less than 1 V. Bias was set in three different regions: reverse, below threshold, and above threshold. In reverse bias the VCSEL acts as a vertical cavity electro-absorption modulator (VCEAM), which is interesting for very short reach interconnects but not generally for PONs as it introduces significant losses. Below threshold the VCSEL operates as an amplifier, producing gain to small incoming signals. Above threshold it acts as an injection locked laser, which has a high modulation bandwidth but is lossy. The eye diagrams that result from modulating the VCSEL in each of the different regimes are shown in fig. 4.4.

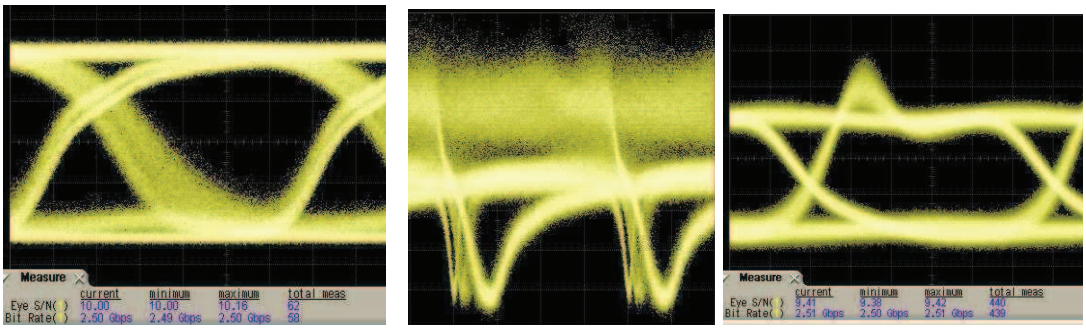

Fig. 4.4. Eye diagrams of modulated vertical cavity structure in reverse biased (left, as an EAM), above threshold (right, as an injection locked VCSEL), and below threshold (middle, as a VCSOA). Eye diagrams for the VCEAM and VCSEL are taken at 2.5 Gb/s, while the VCSOA is at 500 Mb/s.

As the eye diagrams show, modulation at 2.5 Gb/s is easily achieved both in the reverse biased regime, as an EAM, and above threshold, as a VCSEL. When the device is biased as a VCSOA, however, the device cannot handle modulation even at 500 Mb/s. This is not a relic of a poorly chosen bias point, driving current, or optical

injection power. It is pervasive across the parameter space as long as the VCSEL is forward biased below threshold. In addition to having insufficient modulation bandwidth to operate at reasonable datarates, the VCSOA demonstrates wild nonlinearities that cause the signal to completely disintegrate. These nonlinearities will be the subject of the next section.

4.3 Bistability in VCSOAs

4.3.1 Introduction to Bistability

Bistability refers to a general phenomenon whereby a system has hysteresis of some value depending on previous conditions. For optical bistability of an amplifier this means that the output power of the system depends not just on the input power and current, but also whether the input power and current were increased or decreased to get to the current state. For the VCSOAs studied here bistability is what causes the instabilities when a data pattern is applied to the electrical signal. Since the rising and falling edges cause the device to transition chaotically to different states, depending also on the data pattern, a chaotic output pattern is observed.

All-optical Boolean logic has been a heavily researched topic for several decades due to its potential impact in optical information processing (OIP) including areas such as optical signal processing (OSP), optical computing, and optical packet switching [28-30]. Although a multitude of techniques exist which achieve OIP including cross gain modulation (XGM) and cross phase modulation (XPM) in semiconductor optical amplifiers (SOA) [31], four wave mixing (FWM) in highly nonlinear fiber [32], intensity bistability in Fabry-Perot laser amplifiers (FPLA)

[33,34] and polarization bistability in Vertical Cavity Surface Emitting Lasers (VCSEL) [35], no clear technology candidate has emerged for large-scale OIP because of shortcomings in terms of speed, power, size, large scale integrability and cost of logic elements. Over recent years, intensity bistable VCSOAs have received interest for applications in optical signal processing at 850 nm [36-41]. Owing to their gain and highly nonlinear resonant structure, 850 nm VCSOAs have been shown to achieve critical functionalities such as re-amplification and reshaping (2R) [36], optical inversion [42], self-sustained ring oscillation [37], and optical flip-flop [38]. Most importantly, as a mature technology platform, 850 nm VCSOAs offer an excellent tradeoff in terms of speed, power, size, integrability, and cost. Contrastingly, work in 1550 nm VCSOAs is still nascent as a result of the greater difficulty in fabricating 1550 nm VCSELs. Nevertheless, VCSEL/VCSOA research is ongoing in the telecom band for its potential economic impact [20-21].

Recently, Hurtado et al. [43] observed optical bistability in 1550 nm VCSOAs. The operating conditions necessary to achieve bistable switching were stringent with large switching power of 150 μW for counterclockwise and 600 μW for clockwise bistability. The narrow operating range is explained, among other factors, by the large insertion loss (20 dB) suffered when coupling into and out of the device. In order to compete with alternative technologies and to justify the use of bistable VCSOAs in commercial telecom applications, the switching power must be reduced. In this experiment, we experimentally observe optical bistability with fiber pigtailed 1550 nm VCSOAs with switching powers as low as 2 μW, two orders of magnitude smaller than previously reported and comparable to that of 850 nm devices.

Moreover, we observe, for the first time in VCSOAs, all three types of bistability: counterclockwise, clockwise, and butterfly. We begin by offering a physically intuitive explanation for the existence of the various forms of bistablity in reflection mode VCSOAs and then confirm that all three types can be observed experimentally by changing either the current bias of the device or the injected wavelength into the device. We find that optical bistability is readily achievable in our devices over a wide range of bias currents and wavelength detuning. These results help substantiate the claim that VCSOAs can be a key technology for future OSP applications at 1550 nm.

4.3.2 Theory of Bistability

Optical bistability is the ability of a device to operate in two stable states, depending on the input history. When light is injected into the active resonant cavity carriers are consumed, resulting in gain through the process of stimulated emission. The accompanying drop in the carrier concentration leads to an increase in the refractive index of the cavity through the Kramers-Kronig relationship. This refractive index change, in turn, leads to a red-shift in the peak resonant wavelength of the cavity.

When the injected light is detuned towards the longer wavelength side of the gain window, carrier depletion shifts the cavity resonance towards the injected wavelength causing positive feedback. The combination of this dispersive non-linearity and gain saturation within the cavity leads to a counterclockwise bistability in the transmitted intensity [29]. Whereas transmission mode devices only exhibit counterclockwise bistability, it has been known for some time that dispersive bistable

laser diodes operated in reflection mode also exhibit two additional forms of bistability known as butterfly and clockwise bistability [30,34]. Butterfly and clockwise bistability are manifested through the careful balance between the incoming and outgoing intensities in the laser amplifier cavity [30,33,34,44].

Equations describing the bistable phenomenon were first developed by Adams *et al* [33] and are given by Hurtado *et al* [44] as:

$$
\begin{aligned}
I_{av} &= \frac{(1-R_t)(1+R_b e^{gL_c})(e^{gL_c-1})}{(1-\sqrt{R_t R_b}\, e^{gL_c})^2 + 4\sqrt{R_t R_b}\, e^{gL_c} \sin^2\phi} \frac{P_{in}}{P_x g L_c} \\
P_R &= \frac{(\sqrt{R_t} - \sqrt{R_b} e^{gL_c})^2 + 4\sqrt{R_t R_b}\, e^{gL_c} \sin^2\phi}{(1-R_t)(1+R_b e^{gL_c})(e^{gL_c-1})} I_{av} P_y g L_c \\
gL_c &= \frac{\Gamma g_0 L_c}{1+(I_{av}/I_s)} - \alpha_i L_c \\
\phi &= \phi_0 + \frac{\Gamma g_0 L_c b}{2}\left(\frac{I_{av}/I_s}{1+I_{av}/I_s}\right)
\end{aligned}
\qquad 4.1
$$

Where I_{av} is the intensity inside the cavity, P_{in} is the optical power input at the front facet, P_R is the reflected power, R_t and R_b are the top and bottom mirror reflectivities, respectively, gL_c is the single pass gain of the cavity, φ is the single pass phase delay of the cavity, Γ is the optical confinement factor, $\alpha_i L_c$ is the single pass absorption loss, b is the linewidth enhancement factor, and I_s is the saturation intensity at which point the roundtrip gain becomes 1. These equations can be solved using a stepwise solver and treating them as a set of coupled equations. However, since they are highly nonlinear and the reflected power is not a single valued function of the input power, these equations can be very difficult to solve. By careful inspection we can see that the nonlinearity comes from the combination of the phase being dependent on

the intensity inside the cavity (as a result of the consumption of carriers) and the intensity and reflected powers being dependent on the $\sin^2$ of the phase.

Physical insight into the existence of butterfly and clockwise bistability is gained when one considers that, in steady state, incoming and outgoing intensities must equate [33] as described by the more basic equation:

$$I_{ref} = I_{in} + gL_c \cdot I_{av} - I_{trans} \qquad 4.2$$

where I_{in} is the input intensity, I_{av} is the average intensity inside the cavity, gL_c is the single pass gain, and I_{trans} is the transmitted intensity. Effectively, the total intensity outside the cavity through I_{ref} and I_{trans} must equal the total intensity inside the cavity (I_{in} and gL_c*I_{av}). As stated above, dispersive nonlinearity and gain saturation always combine to cause counterclockwise bistability for I_{trans}. Since I_{in} is a linear term, the behavior of I_{ref} can ultimately be understood by determining gL_c*I_{av} and solving (4.2).

Fig. 4.5 demonstrates how both counterclockwise and clockwise bistability can arise by assuming $gL*I_{av}$ exhibits counterclockwise bistability. Physical insight into this complex balancing of the terms in (4.2) can be garnered when one considers two extremes of operation: first when the current bias is high (e.g. ~99% of threshold) and the wavelength detuning is small and second when current bias is reduced (e.g. ~90% of threshold) and wavelength detuning is large. As depicted by the solid lines in Fig. 4.5, at high values of bias and low values of detuning, the second term in (4.2) dominates due to larger gain, and the reflected intensity, I_{ref}, mimics the S shaped counterclockwise solution of $gL*I_{av}$.

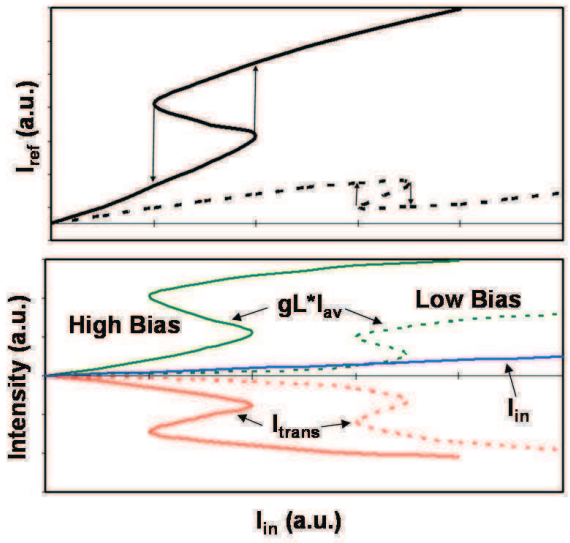

Fig. 4.5. Illustration of (4.2) explaining the existence of clockwise bistability in reflection mode VCSOAs. Solid curves represent higher bias-lower detuning case which generates counterclockwise hysteresis in I_{ref}. Dotted curves represent lower bias-higher detuning case which generates clockwise hysteresis in I_{ref}. The transition between these two regimes generates butterfly hysteresis.

As the bias is reduced and the detuning is increased (depicted by the dotted lines), the bistable functional form of I_{trans} grows larger than gL_c*I_{av} due to reduced gain and thus begins to dominate the right side of (4.2). By summing the S-shaped -Itrans and gL_c*I_{av} terms and the linear I_{in} term, Fig. 4.5 shows that I_{ref} results in a clockwise hysteresis loop (dashed black curve). During the transition region between counterclockwise and clockwise bistability, when gL_c*I_{av} and I_{trans} are of comparable magnitude, I_{ref} exhibits butterfly bistability in which both discontinuous transitions fall from higher to lower powers.

It is worth noting that while I_{trans} will always exhibit counterclockwise bistability though the effects of dispersive nonlinearity and gain saturation, it is not generally true that gL_c*I_{av} is always counterclockwise bistable. As was shown in [44],

gL_c*I_{av} can also exhibit butterfly and clockwise bistability (see Fig. 5 in [44]). Nevertheless, this fact does not distract from the physical interpretation above that it is the careful balancing of (4.2) which yields the complex bistability curves observed in the reflected intensity.

4.3.3 Experimental Design

The fiber-coupled experimental setup used to study the bistable switching properties of the 1550 nm devices is shown in Fig. 4.6.

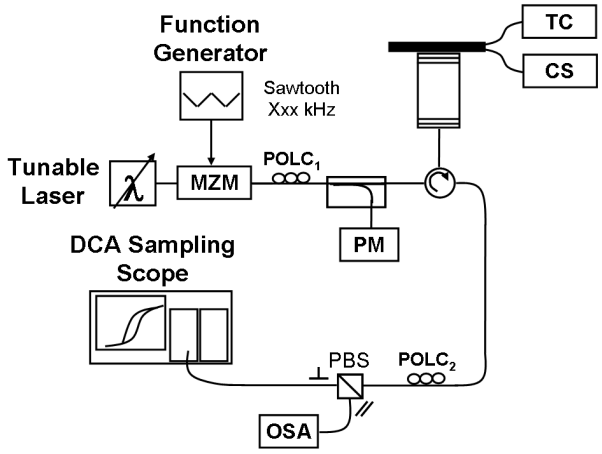

Fig. 4.6. Experimental Setup to study bistabilty in 1550 nm VCSOA.

A single mode 1550 nm fiber pigtailed VCSEL from Raycan (Korea) was used for the demonstration. The VCSEL had a threshold current of 1.99 mA, a peak gain of about 11 dB for an optical input of 1 μW at a wavelength of 1542.290 nm on the stronger gain axis, and a peak gain of about 7 dB for the weaker gain axis for an input of 1 μW and a wavelength of 1542.830 nm. The 3 dB gain windows were approximately 8 GHz wide for an input of 1 μW and around 12 GHz wide for an

input of 10 μW. This intensity dependent gain window bandwidth is consistent with previous work with 850 nm VCSOAs [36,40].

Tunable laser light is first intensity modulated using a Mach Zehnder modulator (MZM) driven by a 50 kHz sawtooth wave. This allows for real-time plotting of the input-output characteristics of the VCSOA by using the processing functionalities of the digital communication analyzer (DCA) sampling scope. After the MZM, the injected light is aligned in polarization to the strong gain axis of the VCSOA via a polarization controller ($POLC_1$).

The light is then injected into a fiber coupled 1550 nm VCSOA via a circulator. The VCSOA output is passed back through the circulator and then through $POLC_2$ and a polarization beam splitter (PBS). The PBS helps facilitate polarization alignment to the stronger gain axis of the VCSOA and rejects the amplified spontaneous emission (ASE) in the polarization orthogonal to the signal. The input-output characteristics are plotted on the sampling scope. The current source (CS), temperature controller (TC), power meter (PM) and optical spectrum analyzer (OSA) are used to carefully control and monitor VCSOA bias current, temperature, input optical power and polarization alignment, respectively.

4.3.4 Results

As described above, Fabry-Perot bistability theory predicts that, for a given bias current (I_{bias}), counterclockwise bistability will onset first as the input wavelength is red-shifted with respect to the amplifiers peak resonant wavelength. Upon further detuning, the input-output characteristics will transition to butterfly and then clockwise bistability. Experimental observation of this transition can be seen in

Fig. 4.7. Clearly, at larger detuning butterfly and clockwise bistability can be obtained at the expense of higher switching powers and wider hysteresis windows.

In a similar manner, the transition between all three bistable regimes can be observed if the wavelength detuning is kept constant and the bias current is swept as shown in Fig 4.8. Physically, as the bias current is decreased, the resonant peak of the amplifier blue shifts. This effectively causes the wavelength detuning to increase thereby resulting in butterfly and clockwise bistability. Consistent with Fig. 4.7, Fig. 4.8 clearly shows that counterclockwise bistability has the lowest switching powers and narrowest hysteresis windows.

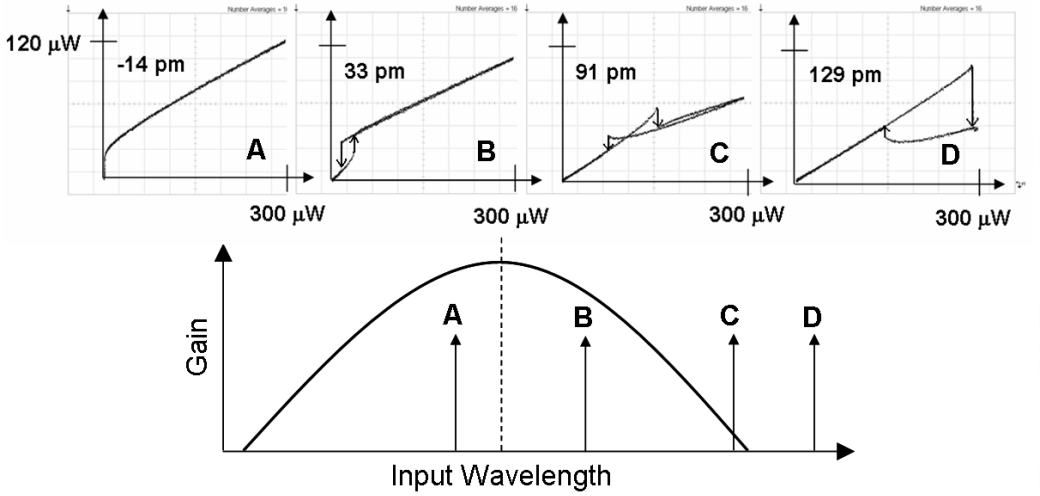

Fig. 4.7. All three types of bistability in a 1550 nm VCSOA for constant Ibias = 0.96*Ith. Wavelength detuning is swept towards longer wavelengths. A is for no bistability. B is counterclockwise bistability. C is butterfly bistability. D is clockwise bistability.

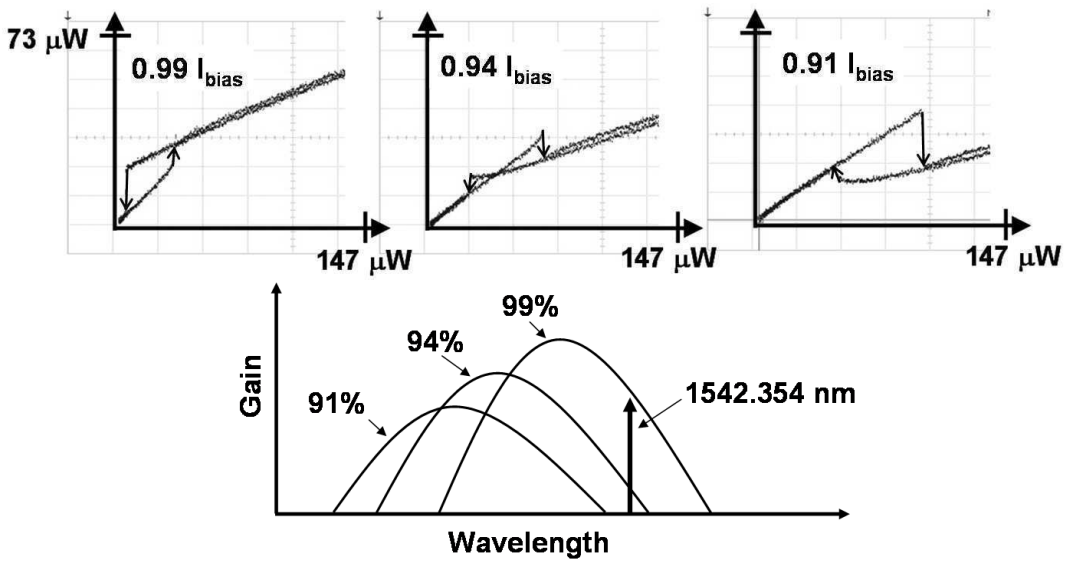

Fig. 4.8. All three types of bistability for constant wavelength 1542.354 nm . Ibias is swept. 99%*Ith shows counterclockwise bistability. 94%*Ith shows butterfly bistability. 91%*Ith shows clockwise bistability.

Since it is desirable in signal processing applications to have minimal power dissipation per gate, we next seek to find the minimum bistable switching power achievable in our device. In Fig. 4.8, counterclockwise bistability is plotted as a function of wavelength detuning for a fixed bias current of 0.99*Ith. Again, as the detuning is swept towards longer wavelengths, the bistable switching power shifts towards higher values and the overall widths of the hysteresis windows increases. Most importantly, we find that a minimum switching power of 2 μW can be obtained for a wavelength detuning of 27 pm. Compared to previously published results on 1550 nm VCSOA [43], this represents a two order of magnitude improvement in minimum possible switching power. We attribute this improvement mainly to the fact that our fiber pigtailed VCSOA has significantly better input-output coupling compared to the free space coupling losses present in previous studies. We estimate

our coupling losses to be about 3 dB, yielding a 17 dB improvement over that used in [43]. For this reason, it is evident that sound packaging and integration methods must be developed to minimize input-output coupling losses for future VCSOA-based OSP.

Table. 4.1. Comparison of switching power for different devices.

Switching Peak Power	Device Type	Reference
~200 µW	1550 nm External Cavity Semiconductor Laser	Pakdeevanich *et al*, J. Quant. Elec., 35, pp 1894-1903, 1999.
~175 µW	1550 nm VCSOA	Hurtado *et al*, Elec. Lett. 42, pp. 483-484, 2006.
~2 µW	850 nm VCSOA	Wen *et al*, Opt. Exp. 10, pp. 1273-1278, 2002.
~2 µW	1550 nm VCSOA	Marki *et al*, Opt. Exp. 15, pp. 4953-4959, 2007.
~30 nW	980 nm VCSEL	Mori *et al*, Appl. Phys. Lett. 88, 101102, 2006.

This demonstrated µW switching is readily achievable and represents an important advantage of VCSOAs over traveling wave SOA optical logic technologies based on XGM and XPM [31]. Table 4.1 shows a comparison of minimum demonstrated switching power for a variety of devices. As can be seen the 2 µW switching power represents a 100x improvement over previous switching technologies at the 1550 nm wavelength. It was recently shown that polarization bistability in VCSELs can achieve switching powers on the order of 100 nW [35] for a 100 MHz switching frequency. While such a low switching power is advantageous, it was also shown that the required switching power increased with increasing switching frequency (~80 µW peak power for 10 GHz) owing to the narrow sensitivity region of the wavelength detuning characteristics [35]. Since polarization

bistabilty is also known to be susceptible to self-heating effects [45,46], we believe dispersive bistability in VCSOAs may offer a viable alternative for OIP applications. Furthermore, we believe that optimization of the VCSOA structure may further reduce the switching power to sub-μW levels.

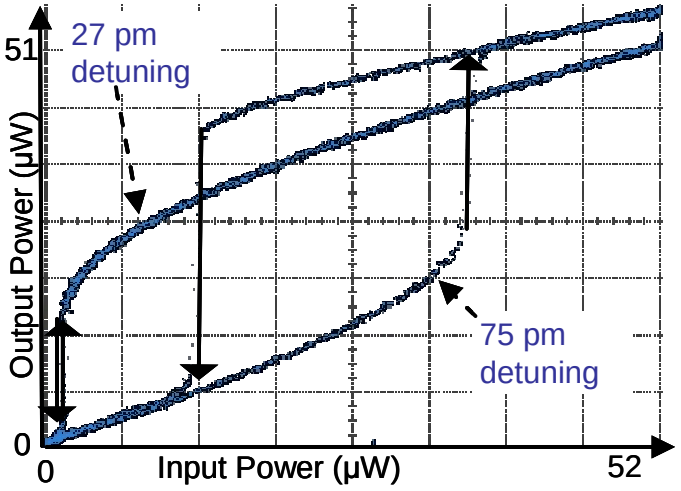

Fig. 4.9. Counterclockwise Bistability for 0.99*Ith.

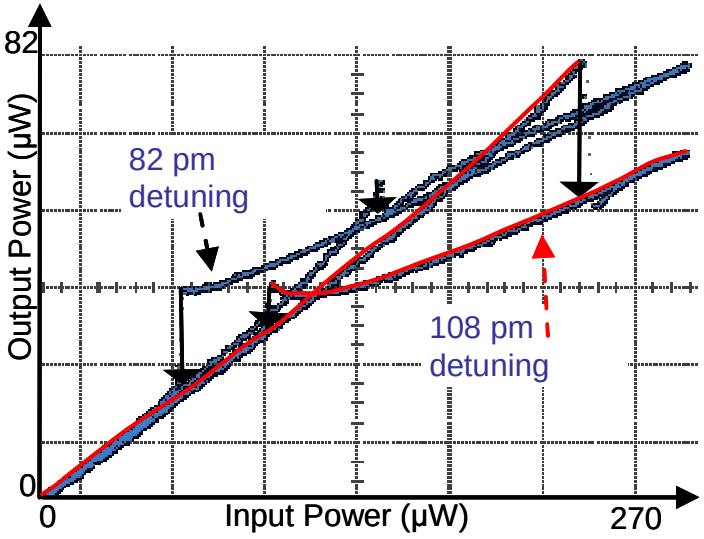

Fig. 4.10. Butterfly Bistability for 0.99*Ith.

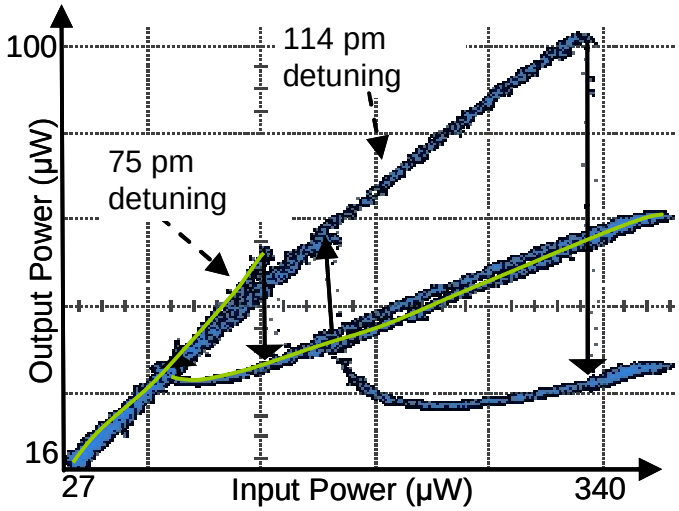

Fig. 4.11. Experimental Clockwise Bistability for 0.89*Ith.

In terms of the bistable sensitivity of our devices to operating conditions, we find that all three forms of bistability manifest over an extremely wide range of bias currents and wavelength detuning. This contrasts with previously reported results which showed a relatively small range of operating conditions to achieve bistable switching [43]. As we can see in Figs. 4.9-4.11, all three forms of bistability exist over tens of pm of detuning.

Constrastingly, the results in [43] showed very narrow hysteresis windows. We attribute the improvement primarily to the improved coupling efficiency of our fiber pigtailed devices. Additional modeling using the technique described in [36] also indicates that the existence of bistability in VCSOAs in critically dependent on device properties such as top/bottom mirror reflectivity, linewidth enhancement factor, cavity confinement and overall gain. These factors may further explain why our tested devices exhibit much stronger bistability. Our measurements show counterclockwise bistability visible from 83% I_{th} to 122% I_{th}, butterfly bistability from 81% I_{th} to 114% I_{th}, and clockwise bistability from 66% I_{th} to 108% I_{th} where

the upper end of the bistability for clockwise and butterfly bistability is limited by the available input power of the setup. We also obtain hysteresis windows as large as 119 μW (54-173 μW) for counterclockwise and 164 μW (89-253 μW) for clockwise bistability, only limited by the available input power of the system. The robustness and flexibility of these devices to exhibit bistable behavior over a wide range of operating conditions is of practical interest for possible future applications.

4.3.5 Electrical Input Nonlinearity

A drawback of the VCSEL structure for use as an ONU modulator is the narrow wavelength window in which it operates. The idea of wavelength reuse is rendered obsolete if the VCSEL can only operate at a single wavelength. Fortunately the wavelength of the VCSEL can be tuned by bias current at a fixed temperature, or by varying the temperature at a fixed bias current. Fig. 4.11 shows the lasing and orthogonal polarization outputs of a VCSEL with a fixed wavelength input on the orthogonal (non-lasing) polarization and a square wave electrical input at 50 MHz. The input power was 136 μW and the average output power was 293 μW. The square wave voltage is 913 mV peak to peak (current is ~ 4.565 mA), and the currents listed beneath the traces indicate the bias current. The square wave causes localized heating in the VCSEL which leads to a periodic variation in the locking wavelength, which causes it to lock at a specific point in time. This can be seen in the output of the VCSEL as a dip in the lasing polarization when it locks to the orthogonal polarization.

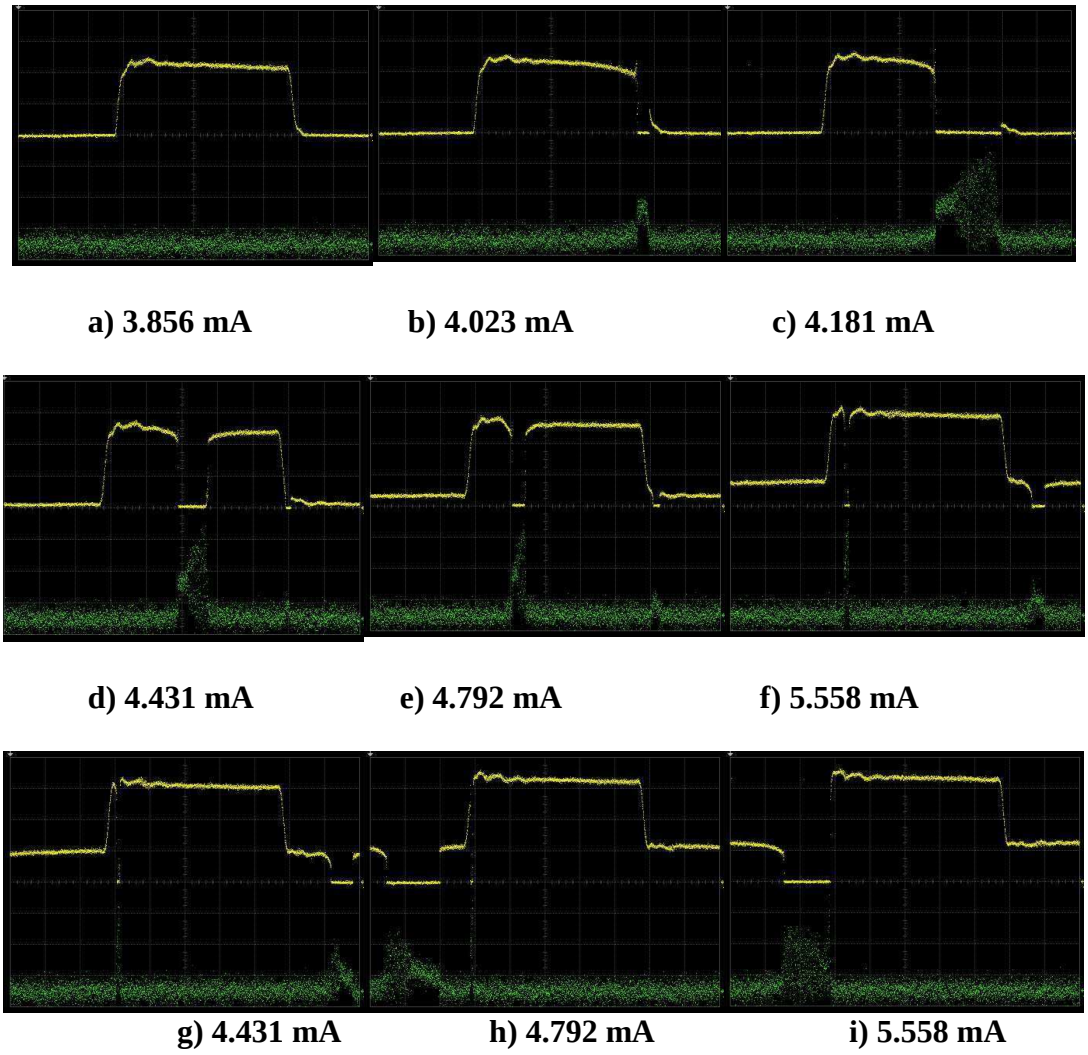

a) 3.856 mA **b) 4.023 mA** **c) 4.181 mA**

d) 4.431 mA **e) 4.792 mA** **f) 5.558 mA**

g) 4.431 mA **h) 4.792 mA** **i) 5.558 mA**

Fig. 4.12. Lasing polarization (top) and orthogonal polarization (bottom) output of a VCSEL with light injected into the orthogonal polzarization. Different currents correspond to the bias current the square wave is applied to.

By using the technique demonstrated in Fig. 4.12, it is possible to sweep the operation wavelength of the VCSEL to a specific wavelength of operation. The spike in output power from the orthogonal polarization, or alternatively the spike in current/voltage that occurs on the drive signal when a VCSEL is injection locked (see e.g. [47]), indicates that the VCSEL is injection locked and that the ONU can be operated in this state. Another potential application of this technology is as a

wavelength meter for a single wavelength input. Fig. 4.13 shows the 3 dB locking range of the device as a function of optical input power. There is a tradeoff as the input power goes up, the locking range increases. This means that for precise wavemeter readings it is desirable to have a low optical input power, while for operation as an ONU modulator it is desirable to have a high optical input power.

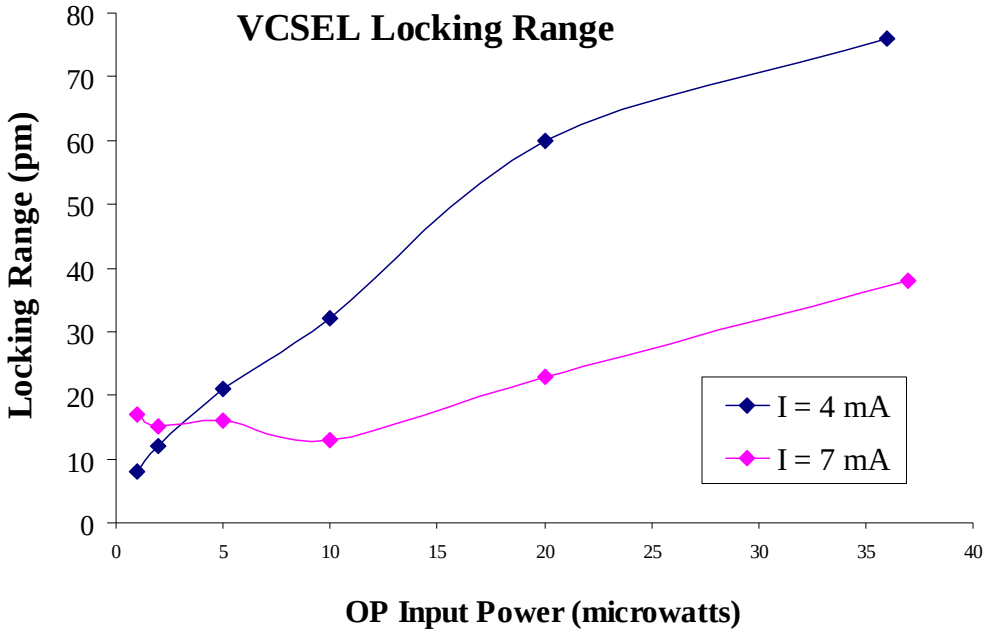

Fig. 4.13. Locking range of a 1550 nm VCSEL as a function of input power for two different bias currents.

4.4 Conclusion

This chapter began by investigating the use of vertical cavity semiconductor optical amplifiers as ONU modulators in PONs. It was quickly found that regardless of other concerns these devices made unsuitable candidates because of a significant instability of the optical cavity. The subsequent section was devoted to exploring this instability and led to the significant contributions contained in the chapter. The first

of these was a demonstration of all possible types of optical bistability in 1550 nm VCSOAs, including clockwise, counterclockwise, and previously unobserved butterfly bistability. The second contribution was the observation of bistability at dramatically lower optical input powers than previously observed in 1550 nm VCSOAs, at power of 2 μW, which is two orders of magnitude lower than previously observed. In addition electrical bistability was observed, which has a possible benefit as a wavelength meter or as a mechanism for matching the device to an incoming wavelength for using injection locked VCSELs in a light reuse network. It is hoped that this work will contribute positively to the future development of optical logic and low power optical information systems.

ACKNOWLEDGEMENT

Section 4.3 is, in part, a reprint of the material in "Observation of counterclockwise, clockwise and butterfly bistability in 1550 nm VCSOAs," from *Optics Express*, 2007 and "Low power optical bistability in 1550 nm VCSOAs," presented at CLEO, Baltimore, MD. The dissertation author and C. F. Marki contributed equally to the first authorship of these publications.

Special thanks is warranted to Dr. Pengyue Wen, Dr. Haijiang Zhang, and Prof. Sadik Esener for their contributions to this research.

4.5 References

[1] Cornell, Inc. “Corning SMF-28e+ Optical Fiber with NexCor Technology Product Information”, http://www.corning.com/WorkArea/showcontent.aspx?id=27659, retrieved July 2, 2010.

[2] J. Cardenas, C.B. Poitras, J.T. Robinson, K. Preston, Long Chen, and M. Lipson, “Low Loss Etchless Silicon Photonic Waveguides”, *Optics Express*, vol. 17, no. 6, pp. 4752-4757, 2009.

[3] C.W. Chow, L. Xu, C.H. Yeh, H.K. Tsang, W. Hofmann, and M.C. Amann, “40-Gb/s Upstream Transmitters Using Directly Modulated 1.55 µm VCSEL Array for High-Split-Ratio PONs”, *IEEE Phot. Tech. Lett*., vol. 22, no. 5, pp. 347-349, 2010.

[4] T.B. Gibbon, K. Prince, C. Neumeyr, E. Ronneberg, M. Ortsiefer, and I.T. Monroy, “10 Gb/s 1550 nm VCSEL Transmission Over 23.6 km Single Mode Fiber with No Dispersion Compensation and No Injection Locking for WDM PONs”, in *Optical Fiber Communication Conference and Exposition (OFC) and National Fiber Optic Engineers Conference (NFOEC)*(Optical Society of America, Washington, DC, 2010), JThA30.

[5] N.J. Frigo, P.P. Iannone, P.D. Magill, T.E. Darcie, M.M. Downs, B.N. Desai, U. Koren, T.L. Koch, C. Dragone, H.M. Presby, and G.E. Bodeep, “A Wavelength-Division Multiplexed Passive Optical Network with Cost-Shared Components”, *IEEE Phot. Tech. Lett.*, vol. 6, no. 11, pp. 1365-1367, 1994.

[6] Sang-Yuep Kim, N. Sakurai, H. Kimura, and H. Hadama, “VCSEL-Based Coherent Detection of 10-Gbit/s QPSK Signals Using Digital Phase Noise Cancellation for Future Optical Access Systems”,*Proc. Optical Fiber Communication*, 2010.

[7] S. Calvez, A.H. Clark, “1.3 µm GaInNAs Optically-Pumped Vertical Cavity Semiconductor Optical Amplifier”, *Elec. Lett.*, vol. 39, no. 1, pp. 100-102, 2003.

[8] Pengyue Wen, Michael Sanchez, M. Gross, and S. Esener, “Observation of Bistability in a Vertical-Cavity Semiconductor Optical Amplifier (VCSOA)”, *Optics Express*, vol. 10, no. 22, pp. 1273-1278, 2002.

[9] E.S. Bjorlin and J.E. Bowers, “Noise Figure of Vertical-Cavity Semiconductor Optical Amplifiers”, *IEEE J. Quant. Elec.*, vol. 38, no. 1, pp. 61-66, 2002.

[10] E.S. Bjorlin, J. Geske, and J.E. Bowers, “Optically Preamplified Receiver at 10 Gbit/s using Vertical Cavity SOA”, *Elec. Lett*., vol. 37, no. 24, pp. 1474-1475, 2001.

[11] E.S. Bjorlin, B. Riou, P. Abraham, J. Piprek, Y.J. Chiu, K.A. Black, A. Keating, and J.E. Bowers, "Long Wavelength Vertical-Cavity Semiconductor Optical Amplifiers", *IEEE J. Quant. Elec.*, vol, 37, no. 2, pp. 274-281, 2001.

[12] J. Piprek, S. Bjorlin, and J.E. Bowers, "Design and Analysis of Vertical-Cavity Semiconductor Optical Amplifiers", *IEEE J. Quant. Elec.*, vol. 37, no. 1, pp. 127-134, 2001.

[13] T. Kimura, S. Bjorlin, H.F. Chou, Q. Chen, S.M. Qu, and J.E. Bowers, "Optically Preamplified Receiver at 10, 20, and 40 Gb/s Using a 1550-nm Vertical-Cavity SOA", *IEEE Phot. Tech. Lett.*, vol. 17, no. 2, pp. 456-458, 2005.

[14] Michael Sanchez, Pengyue Wen, M. Gross, and S. Esener, "Polarization Anisotropy in Vertical-Cavity Semiconductor Optical Amplifiers", *Optics Letters*, vol. 29, no. 16, pp. 1888-1890, 2004.

[15] A.H. Clark, S. Calvez, N. Laurand, R. Macaluso, H.D. Sun, M.D. Dawson, T. Jouhti, J. Kontinnen, and M. Pessa, "Long-Wavelength Monolithic GaInNAs Vertical-Cavity Optical Amplifiers", *IEEE J. Quant. Elec.*, vol. 40, no. 7, pp. 878-883, 2004.

[16] T. Kimura, S. Bjorlin, J. Piprek, and J.E. Bowers, "High-Temperature Characteristics and Tunability of Long-Wavelength Vertical-Cavity Semiconductor Optical Amplifiers", *IEEE Phot. Tech. Lett.*, vol. 15, no. 11, pp. 1501-1503, 2003.

[17] E.S. Bjorlin, T. Kimura, and J.E. Bowers, "Carrier-Confined Vertical-Cavity Semiconductor Optical Amplifiers for Higher Gain and Efficiency", *IEEE J. Selec. Top. Quant. Elec.*, vol. 9, no. 5, pp. 1374-1385, 2003.

[18] N. Laurand, S. Calvez, M.D. Dawson, and A.E. Kelly, "Slow-Light in a Vertical Cavity Semiconductor Optical Amplifier", *Optics Express*, vol. 14, no.15, pp.6858-6863, 2006.

[19] N.S. Chen and S.F. Yu, "Design and Analysis of Large-Area Vertical-Cavity Semiconductor Optical Amplifiers with Anti-Resonant Reflecting Optical Waveguide", *IEEE J. Light. Tech.*, vol. 24, no. 1, pp. 526-535, 2006.

[20] N. Laurand, S. Calvez, M.D. Dawson, and A.E. Kelly, "Index and Gain Dynamics of Optically Pumped GaInNAs Vertical-Cavity

Semiconductor Optical Amplifiers", *Appl. Phys. Lett.*, vol. 87, no. 23, p. 231115, 2005.

[21] N. Laurand, S. Calvez, M.D. Dawson, A.C. Bryce, T. Jouhti, J. Konttinen, and M. Pessa, "Performance Comparison of GaInNAs Vertical-Cavity Semiconductor Optical Amplifiers", *IEEE J. Quant. Elec*., vol. 41, no. 5, pp. 642-649, 2005.

[22] G.D. Cole, E.S. Bjorlin, Q. Chen, C.Y. Chan, S.M. Wu, C.S. Wang, N.C. MacDonald, and J.E. Bowers, "MEMS-Tunable Vertical-Cavity SOAs", *IEEE J. Quant. Elec.*, vol. 41, no.3, pp.390-407, 2005.

[23] Elaine Wong, Xiaoxue Zhao, C.J. Chang-Hasnain, W. Hofmann, and M.C. Amann, "Optically Injection-Locked 1.55 µm VCSELs as Upstream Transmitters in WDM-PONs", *IEEE Phot. Tech. Lett.*, vol. 18, no. 21, pp. 2371-2373, 2006.

[24] Wen-Shing Tsai, Hai-Han Lu, Sha-Jye Tzeng, Tzu-Shen Chien, Shih-Hung Chen, and Yu-Chieh Chi, "Bidirectional Dense Wavelength-Division Multiplexing Passive Optical Network Based on Injection-Locked Vertical-Cavity Surface-Emitting Lasers and a Data Comparator", *Optical Engineering*, vol. 45, no. 9, 2006.

[25] E. Wong, X. Zhao, C.J. Chang-Hasnain, W. Hofmann, and M.C. Amann, "Rayleigh Backscattering and Extinction Ratio Study of Optically Injection-Locked 1.55 µm VCSELs", *Elec. Lett.*, vol. 43, no.3, pp. 182-183, 2007.

[26] D. Parekh, W. Yang, W. Hofmann, M.C. Amann, and C.J. Chang-Hasnain, "Isolator-Less Optically Injection-Locked 1.55 µm VCSELs for Upstream Transmitters in WDM-PONs", in *Optical Fiber Communication Conference and Exposition (OFC) and National Fiber Optic Engineers Conference (NFOEC)*(Optical Society of America, Washington, DC, 2009) .

[27] G.P. Agrawal and N.K. Dutta, Semiconductor Lasers, *Klewer Academic*, 1993.

[28] A.A. Sawchuk and T.C. Strand, "Digital Optical Computing", *Proc. IEEE*, vol. 72, no. 7, p. 758, 1984.

[29] H. Kawaguchi, Bistabilities and Nonlinearities in Laser Diodes, Artech House, Boston, 1994.

[30] M.J. Adams, “Optical Amplifier Bistability on Reflection”, *Opt. Quant. Electron.*, vol. 19, no. 37, 1987.

[31] N.K. Dutta and Q. Wang, Semiconductor Optical Amplifiers, World Scientific, Hackensack, N.J., 2006.

[32] Q. Lin *et al*, “40 Gb/s Optical Switching and Wavelength Multicasting in a Two-Pump Parametric Device”, *IEEE Phot. Tech. Lett*., vol. 17, no. 11, p. 2376, 2005.

[33] P. Pakdeevanich and M.J. Adams, “Measurements and Modeling of Reflective Bistability in 1.55 µm Laser Diode Amplifiers”, *IEEE. J. Quant. Elec.*, vol. 35, pp. 1894-1903, 1999.

[34] J. Mitchell *et al*, “Optical Bistability in Asymmetric Fabry-Perot Laser Diode Amplifiers”, *Opt. Lett.*, vol. 19, p. 269, 1994.

[35] T. Mori *et al*, “Low-Switching-Energy and High-Repitition-Frequency All-Optical Flip-Flop Operations of a Polarization Bistable Vertical-Cavity Surface-Emitting Laser”, *Appl. Phys. Lett.*, vol. 88, no. 101102, 2006.

[36] Pengyue Wen, Michael Sanchez, M. Gross, and S. Esener, “Optical Bistability in Vertical-Cavity Semiconductor Optical Amplifiers”, *Appl. Optics*, vol. 45, no.25, pp. 6349-6357, 2006.

[37] Haijiang Zhang, C.F. Marki, M. Gross, Pengyue Wen, and S. Esener, “All-Optical Oscillator Based on a Single Bistable Vertical-Cavity Semiconductor Optical Amplifier (VCSOA), *Proc. Conference on Lasers and Electro-Optics (CLEO),* 2008.

[38] M. Sanchez *et al*, “Rate Equations for Modeling Dispersive Nonlinearity in Fabry-Perot Semiconductor Optical Amplifiers”, *Optics Express*, vol. 11, p. 2689, 2003.

[39] Deqiang Song, V. Gauss, Haijang Zhang, M. Gross, Pengyue Wen, and S. Esener, “All-Optical Flip-Flop Based on Vertical Cavity Semiconductor Optical Amplifiers”, *Opt. Lett.*, vol. 32, no. 20, pp.2969-2971, 2007.

[40] Haijiang Zhang, V. Gauss, Pengyue Wen, and S. Esener, “Observation of Wavelength and Multiple Bistabilities in 850 nm Vertical-Cavity Semiconductor Optical Amplifiers (VCSOAs)”, *Optics Express*, vol. 15, no. 18, pp. 11723-11730, 2007.

[41] Pengyue Wen, Michael Sanchez, M. Gross, and S. Esener, "Vertical-Cavity Optical AND Gate", *Optics Comm.*, vol. 219, pp. 383-387, 2003.

[42] S. Esener and Pengyue Wen, "Photonics in Computing: Interconnects and Beyond", presented at Frontiers in Optics, OSA, Rochester, NY, Oct. 2006.

[43] A. Hurtado, A. Gonzalez-Marcos, I.D. Henning, and M.J. Adams, "Optical Bistability and Nonlinear Gain in 1.55 μm VCSOA", *Elec. Lett.*, vol. 42, no. 8, pp. 483-484, 2006.

[44] A. Hurtado, A. Gonzalez-Marcos, and J.A. Martin-Pereda, "Modeling Reflective Bistability in Vertical-Cavity Semiconductor Optical Amplifiers", *IEEE J. Quant. Elec.*, vol. 41, no. 3, pp.376-383, 2005.

[45] S.F. Yu, Analysis and Design of Vertical Cavity Surface Emitting Lasers, John Wiley & Sons, Hoboken, N.J., 2003.

[46] S.F. Yu, "Theoretical Analysis of Polarization Bistability in Vertical Cavity Surface Emitting Semiconductor Lasers", *IEEE J. Light. Tech.*, vol. 15, pp. 1032-1041, 1997.

[47] Qing Gu, W. Hofmann, M.C. Amann, C.L. Chrostowski, "Optically Injection-Locked VCSEL as a Duplex Transmitter/Receiver", *IEEE Phot. Tech. Lett.*, vol. 20, no. 5, pp. 463-465, 2008.

[48] Wei Li Zhang and Siu Fung Yu, "Bistabilities of Birefringent Vertical-Cavity Semiconductor Optical Amplifiers with Antiresonant Reflecting Optical Waveguide", *IEEE J. Quant. Electronics*, vol. 46, no. 1, pp.11-18, 2010.

[49] A. Hurtado, A. Quirce, A. Valle, L. Pesquera, M.J. Adams, "Power and Wavelength Polarization Bistability with Very Wide Hysterisis Cycles in a 1550nm-VCSEL Subject to Orthogonal Optical Injection", *Optics Express*, vol. 17, no. 26, pp.23637-23642, 2009.

[50] Wei Li Zhang and Siu Fung Yu, "Optical Flip-Flop Using Bistable Vertical-Cavity Semiconductor Optical Amplifiers with Anti-Resonant Reflecting Optical Waveguide", *J. Light. Tech.*, vol. 27, no.21, pp.4703-4710, 2009.

[51] A.M. Kaplan, G.P. Agrawal, D.N. Maywar, "All-Optical Flip-Flop Operation of VCSOA", *Elec. Lett.*, vol. 45, no.2, pp.127-128, 2009.

[52] M. Vasileiadis, D. Alexandropoulos, M.J.Adams, H. Simos, D. Syvridis, “Potential of InGaAs/GaAs Quantum Dots for Applications in Vertical Cavity Semiconductor Amplifiers”, *IEEE J. Selec. Top. Quant. Elec.*, vol. 14, no.4, pp.1180-1187, 2008.

[53] A. Hurtado, I.D. Henning, M.J. Adams, “Two-Wavelength Switching with a 1550 nm VCSEL under Single Orthogonal Optical Injection”, *IEEE J. Selec. Top. Quant. Elec.*, vol. 14, no.3, pp. 911-917, 2008.

[54] A. Hurtado, I.D. Henning, M.J. Adams, “Bistability and Nonlinear Gain in 1.55 µm Vertical Cavity Semiconductor Optical Amplifiers: Theory and Experiments”, *Appl. Phys. Lett.*, vol. 91, no. 15, p. 151106.

[55] Deqiang Song, Haijiang Zhang, Pengyue Wen, M. Gross, and S. Esener, “Misalignment Correction for Optical Interconnects Using Vertical Cavity Semiconductor Optical Amplifiers”, *Applied Optics*, vol. 46, no. 22, pp. 5168-5175, 2007.

[56] A. Hurtado, I.D. Henning, and M.J. Adams, “Two-Wavelength Switching with 1.55 µm VCSOA”, *Elec. Lett.*, vol. 43, no. 16, pp. 887-889, 2007.

[57] A. Hurtado, I.D. Henning, and M.J. Adams, “Effects of Parallel and Orthogonal Polarization on Nonlinear Optical Characteristics of a 1550 nm VCSOA”, *Optics Express*, vol. 15, no. 14, pp.9084-9089, 2007.

[58] Haijiang Zhang, Pengyue Wen, and S. Esener, “Cascadable All-Optical Inverter Based on a Nonliner Vertical-Cavity Semiconductor Optical Amplifier”, *Optics Lett.*, vol. 32, no. 13, pp.1884-1886, 2007.

[59] J. Javaloyes and S. Balle, “Influence of Thermal Effects on Cross-Gain Modulation Characteristics in VCSOA”, *IEEE J. Quant. Elec.*, vol. 43, no.1, pp.65-71, 2007.

[60] C. F. Marki, D. Jorgesen, Haijiang Zhang, Pengyue Wen, and S. Esener, “Observation of Counterclockwise, Clockwise, and Butterfly Bistability in 1550 nm VCSOAs”, *Optics Express*, vol. 15, no. 8, pp.4953-4959, 2007.

5. Conclusion

This thesis has been concerned with evolutionary improvements that are possible to the existing infrastructure of passive optical networks. As many of these networks are already deployed and in service it is critical that these improvements be robust, low cost, backwards compatible with existing installations, and offer a significant value proposition to network operators motivating their adoption. In the following sections we will summarize the contributions of this work and comment on their integration into existing network infrastructure in light of these concerns.

5.1 The Future of Optical Communications

Before considering the impact and future role of each of the technologies considered here, it is important to estimate what the requirements of future networks will be. The purpose of optical communications research is to predict what the network of the future will could look like and how to best realize this vision. Currently there are many different forms of information that consumers want to transmit. The legacy infrastructure has been built around transmitting point-to-point audio for telecommunications and broadcasting video, as well as transmitting business data. The advent of the world wide web in the 1990s led to the dramatic increase in demand for data communications that drove the adoption of fiber optic communications. During this period last mile connections have been served by electrical connections, typically digital subscriber line (DSL) technologies that transmit equalized, high density signal constellations over low bandwidth legacy telephone wires.

Very recently an astounding increase in the availability of communications has been realized through mobile technology. With cell phone subscriptions expected to reach 5 billion by the end of 2010 [1], there will soon be as many cell phone subscriptions as there are people. This expansion in communications seen in the last decade is the most dramatic and rapid increase in connectivity ever experienced in history, primarily due to the adoption of mobile phone use in developing countries. In many countries the average person will never have a land based telephone or internet service, but will experience the network completely through a mobile device.

Thus the electrical communications network is being squeezed by photons on both directions. Bandwidth limitations is leading optical systems, which have distance-bandwidth products thousands of times larger than electrical cables, to displace electrical systems farther and farther down from the backbone network. On the other side the desire for mobile connectivity, and the high cost of laying and maintaining physical cables, is pushing wireless communications to displace wired connections at the final connection point. From a physical standpoint this squeezing is inevitable. Electrons interact strongly with each other, making them inherently good at computing, and bad at communications. Photons do not interact with each other except through a medium, making them inherently bad at computing, but good for communications. Hence the network of the future will be optical to the wireless node, with maximum bandwidth and flexibility at each point and minimum installation and maintenance cost throughout.

These end nodes are going to be either network operator maintained towers or user maintained access ‘femtonodes’ [2]. There are difficult technical and economic

challenges that need to be addressed to accommodate the mixing of high-priority, low latency mobile traffic with “best effort” internet protocol (IP) traffic, but it appears that these will be overcome and there will be a confluence of home/building based access nodes and mobile nodes.

With these forces in mind it is now assumed that the key requirement for passive optical networks is that they must be flexible. They will be required to reach a number of different distances and serve a number of different data formats and bandwidth requirements on a single network. In addition to digital baseband data they will be required to serve mobile telephony and mobile real time video connections with very low latency requirements. The WDM-PON is ideally suited to these requirements, particularly with the adaptability afforded by a central light source. Applicability of the methods discussed in this thesis will be addressed below.

5.2 Filtering of Rayleigh Noise in PONs

5.2.1 Contributions

It has been shown from Chapter 2 that proper high pass filtering of Rayleigh noise concentrated around the linewidth of the source laser used can be highly effective, increasing Rayleigh noise immunity by up to 10 dB in certain circumstances. While this filtering is not universally beneficial, it comes at no extra cost in construction of the link. While designing a PON the results of Chapter show conclusively that the value of the receiver coupling capacitor must be treated as a design variable. The parameters that affect the choice of this variable are primarily the source laser linewidth, the datarate, the line coding of the data, and the impact of

Rayleigh noise, determined by the model developed previously. Baseline wander effects, previously poorly understood, are properly accounted for using the rigorous model presented. While this model is significantly more computationally intensive than previous models, modern computers are more than capable of handling these demands. Proper link design can generally be achieved by simply following the rules of thumb derived; significant eye closure will occur beginning with a high pass filter of .001 times the datarate for random data and .01 times the datarate for 8B/10B encoded data. Extension of the generalized Rayleigh noise model to bidirectional links appears to adequately account for the various link parameters, and should serve useful as a design tool.

5.2.2 Suggestions and Future Directions

In light of the future optical link requirements laid out at the beginning of this chapter, high pass filtering in CLS-PONs appears to be a very promising technique. The earliest form of CLS-PON to be deployed will likely be CW downstream and NRZ-OOK upstream links using Ethernet communication standards. Since the Ethernet standard employs 8B/10B encoding for easy clock recovery a high cutoff frequency will appropriate for these links, blocking a great deal of low frequency Rayleigh noise and significantly increasing link margins. As the links expand to bidirectional data transmission the HPF technique should remain relevant. Indeed, as long as bidirectional intensity transmission is employed the strategy of employing low frequency noise blocking will remain relevant.

Similarly the paradigm presented by the Rayleigh noise model should outlive the model itself. The specific implementation presented in this thesis is only relevant

to baseband data modulation, and further work needs to be performed to apply it to subcarrier, OFDM, PolMUX DQPSK, and other data formats that will become dominant as electronic technology begins to catch up to optical datarates. There is no reason that the method of the model should not, however, be applicable to these modulation formats. The basic technique of determining the spectrum of the noise and calculating the overlap with the signal spectrum to determine the signal-Rayleigh beat noise will be applicable to advanced modulation formats. Once this is performed appropriate filtering procedures can be determined.

5.3 Modulation Methods for PONs

5.3.1 Contributions

Transmitter predistortion for ONU modulators is an obvious benefit for PONs so long as sufficient electrical amplification is present, which should generally be the case given the current low cost and high performance of electrical amplifiers. This technique will be particularly applicable to first and second stage PONs where baseband Ethernet is used to transmit data. The addition of equalization taps to the transmission signal generator is very low cost and adaptive equalization control is readily available. PON designers would be wise to use both transmitter and receiver side equalization to compensate for low transmitter modulation bandwidth wherever excess electrical amplification is available.

Four level intensity modulation, conversely, is an unqualified failure. The dramatic and unexpected increase in SNR required to compensate for the signal-ASE and signal-Rayleigh beat noise present on the received signal eliminates any

advantage that may be gained by increased datarates. Four level modulation using bidirectional orthogonal phase modulation of a microwave subcarrier, however, was a significant success. This scheme demonstrated noise immunity improvement of 4 dB over saturated SOAs and 9 dB over linear MZMs and operation of an error free link at 50 km; OOK modulation was incapable of error free transmission at 50 km. This suggests a possible third generation methodology for PONs when bidirectional OOK transmission can no longer meet link requirements. Conversely, OOK modulation using the proper sampling threshold performed surprisingly well considering the appearance of the eye diagrams. The prudent PON designer would be reluctant to sacrifice this technology until the cost of electrical driving components for subcarrier modulation falls sufficiently to justify the upgrade to this technology.

5.3.2 Suggestions and Future Directions

There is little future work to do with equalization besides implementation. With sufficient computing power and sampling more advanced error correction and sequence detection algorithms such as most likely sequence estimation (MLSE) can be implemented, but these will be implemented using mass produced chips and thus this work will not be specific to PONs.

The orthogonal modulation technique holds promise as it does not apply specifically to NRZ modulation, but analog data, wireless data, almost any modulation format can be transmitted in this manner so long as the subcarrier frequency is significantly higher than the datarate. Significant work needs to be done in this area to determine whether this method is applicable to OFDM and other similar modulation formats, as well as determining the optimal filtering scheme to

remove Rayleigh under this technique. Once optimal filtering has been determined, a fair comparison can be made between the orthogonal phase SCM method and other techniques like direct SCM modulation and mixed transmission such as downstream DPSK and upstream OOK or SCM, etc. This concept of using orthogonal phase modulation may prove to be fruitful for a variety of applications however, such as the transmission of downstream and upstream wireless data on a single subcarrier with no processing electronics at the node.

5.4 Applications of VCSELs in PONs

5.4.1 Contributions

Determination of the applicability of VCSELs as CO modulators depends on many primarily economic factors. For this reason any theoretical investigation of the subject will remain largely unsatisfactory. While the topology presented at the beginning of chapter 4 is satisfactory, both the improvement in SBS immunity and the penalty from baseline wander are marginal. The choice of whether to use them ultimately will come down to concerns about reliability and cost, both of which are fabrication problems that have continually plagued 1550 nm VCSELs since their invention.

Optical bistability in 1550 nm VCSOAs however shows great promise. Given the extremely low switching power these devices could feasibly be used for secure network applications. Since this work was completed inverters using these devices have been shown at low powers and high speeds [3], leading to the possibility of higher order logic gates and optical buffering.

5.4.2 Suggestions and Future Directions

To use VCSELs as CO source lasers the major work needs to be performed in VCSEL fabrication. This is an ongoing process, as it has been for the last decade. Recent progress suggests that ongoing work in long wavelength VCSELs is continuing and still shows promise [3]. If significant gains in yield, reliability, and manufacturing cost reduction can be realized the intrinsic potential for these VCSELs is tremendous. These improvements are the kind that would be realized from mass scale adoption of VCSELs, as is presently occurring for VCSELs in short reach applications [4].

Optical logic using VCSOAs has significant potential, but also similar fabrication issues as VCSELs for use as CO sources. The major hurtle is large scale integration, which would be necessary to create an array of gates of the scale to perform logic operations, to reduce the latency of the system to match the modulation bandwidth of the VCSOAs, to improve the reliability of the system, and to make the costs realizable. Integration may involve micro-optic components, but a more likely path would be to use bistability in silicon microcavities with evanescently coupled gain regions as a bistable cavity [5]. These could then be coupled together with all the fabrication advantages provided by silicon and high volume manufacturing.

5.5 References

[1] L. Whitney, "Cell Phone Subscriptions to Hit 5 Billion Globally", *3GSM Blog,* CNET.com, February 16, 2010, http://reviews.cnet.com/8301-13970_7-10454065-78.html, retrieved July 2010.

[2] M. Popov, “Radio-over-fibre and FTTx: Opportunities and Challenges”, *Digest of the LEOS Summer Topical Meeting*, Newport Beach, CA, pp. 49-50, 2009.

[3] M. Muller, W. Hofmann, G. Bohm, and M.C. Amann, “Short-Cavity Long-Wavelength VCSELs with Modulation Bandwidths in Excess of 15 GHz”, *IEEE Phot. Tech. Lett.*, vol. 21, no. 21, pp. 1615-1617, 2009.

[4] Intel Corp., “Light Peak Technology”, available at http://techresearch.intel.com/articles/None/1813.htm, retrieved July 2010.

[5] Di Liang, M. Fiorentino, T. Okumura, Hsu-Hao Chang, D.T. Spencer, *et al*, “Electrically-Pumped Compact Hybrid Silicon Microring Lasers for Optical Interconnects”, *Opt. Exp.*, vol. 17, no 22, pp. 20355-20364, 2009.

I. Review of Line Coding Techniques

Line coding is a technique used to impart desirable qualities onto random data that is to be sent over a communication channel. Desirable qualities include a guarantee of transitions to facilitate clock recovery and DC balancing, whereby the number of ones and zeros are made to be kept as close as equal as possible. The way that these line coding techniques work is to take an incoming random data stream and translate a short string of bits into a longer string of bits. There is an overhead associated with this translation that is equal to the number of extra bits in the translated string divided by the number of bits in the original bitstring. For example the 8B/10B code frequently referenced in this thesis has an overhead of 25%.

Many commonly used electrical line coding techniques, such as four binary three ternary (4B3T) and Manchester coding, are not applicable to on-off keyed optical links because they require three level signaling. This is effective for electrical signaling since the positive and negative voltages have equivalent noise levels, and the zero level has very low noise. For optical links, however, the noise increases significantly with each additional noise level, as seen in Chapter 3.

The most commonly used techniques for optical line coding are 8B/10B, which is used for Ethernet and Fibre Channel, and 64b/66b, which is used for the SONET standard. These are reviewed below.

I.1 8B/10B Encoding

The 8B/10B code was developed at IBM in 1983 [1]. This technique encodes 8 bits into 10 using two sets of bits. The first is 5 bits, which is encoded into 6 bits, and then the last 3 bits are encoded into 4 bits. Because the first group uses 64

possible output bit sequences to encode 32 possible input bit sequences, there are extra bit sequences available for start of string and end of string symbols.

The main features of 8B/10B encoding are that it ensures that there are no more than 5 ones or zeros in a row and that in a string of 20 bits there is a difference between the number of ones and zeros of no more than 2. It also ensures that the running disparity, defined as the difference between the total number of ones and total number of zeros transmitted, also never exceeds two bits either way. For individual code words that are not DC balanced (that have more zeros or ones), the encoder keeps track of the running disparity and selects one of two possible codewords to bring the running disparity as close to zero as possible (see for example codeword D.00). To demonstrate the coding technique the coding tables are reproduced below.

Rules for Running Disparity

Previous RD	Disparity of code word	Disparity chosen	Next RD
	□0	□0	−1
	±2	+2	+1
+1	□0	□0	+1
+1	±2	−2	−1

5B/6B code

input		RD = −1	RD = +1	input		RD = −1	RD = +1
	EDCBA	abcdei			EDCBA	abcdei	
D.00	00000	100111	011000	D.16	10000	011011	100100
D.01	00001	011101	100010	D.17	10001	100011	
D.02	00010	101101	010010	D.18	10010	010011	
D.03	00011	110001		D.19	10011	110010	
D.04	00100	110101	001010	D.20	10100	001011	
D.05	00101	101001		D.21	10101	101010	
D.06	00110	011001		D.22	10110	011010	

D.07	00111	111000	000111	D.23 †	10111	111010	000101
D.08	01000	111001	000110	D.24	11000	110011	001100
D.09	01001	100101		D.25	11001	100110	
D.10	01010	010101		D.26	11010	010110	
D.11	01011	110100		D.27 †	11011	110110	001001
D.12	01100	001101		D.28	11100	001110	
D.13	01101	101100		D.29 †	11101	101110	010001
D.14	01110	011100		D.30 †	11110	011110	100001
D.15	01111	010111	101000	D.31	11111	101011	010100
				K.28	11100	001111	110000

† Same code is used for K.x.7

3b/4b code

input		RD = −1	RD = +1	input		RD = −1	RD = +1
	HGF	fghj			HGF	fghj	
D.x.0	000	1011	0100	K.x.0	000	1011	0100
D.x.1	001	1001		K.x.1 ‡	001	0110	1001
D.x.2	010	0101		K.x.2 ‡	010	1010	0101
D.x.3	011	1100	0011	K.x.3	011	1100	0011
D.x.4	100	1101	0010	K.x.4	100	1101	0010
D.x.5	101	1010		K.x.5 ‡	101	0101	1010
D.x.6	110	0110		K.x.6 ‡	110	1001	0110
D.x.P7 †	111	1110	0001				
D.x.A7 †	111	0111	1000	K.x.7 † ‡	111	0111	1000

† For D.x.7, either the Primary (D.x.P7), or the Alternate (D.x.A7) encoding must be selected in order to avoid a run of five consecutive 0s or 1s when combined with the preceding 5b/6b code. Sequences of five identical bits are used in comma codes for synchronization issues. D.x.A7 is only used for x=17, x=18, and x=20 when RD=−1 and for x=11, x=13, and x=14 when RD=+1. With x=23, x=27, x=29, and x=30, the same code forms the control codes K.x.7. Any other x.A7 code can't be used as it would result in chances for misaligned comma sequences.
‡ The alternate encoding for the K.x.y codes with disparity 0 allow for K.28.1, K.28.5, and K.28.7 to be "comma" codes that contain a bit sequence that can't be found elsewhere in the data stream.

8B/10B encoding significantly restricts the low frequency bandwidth of the encoded signal, as shown in Fig. I.1.

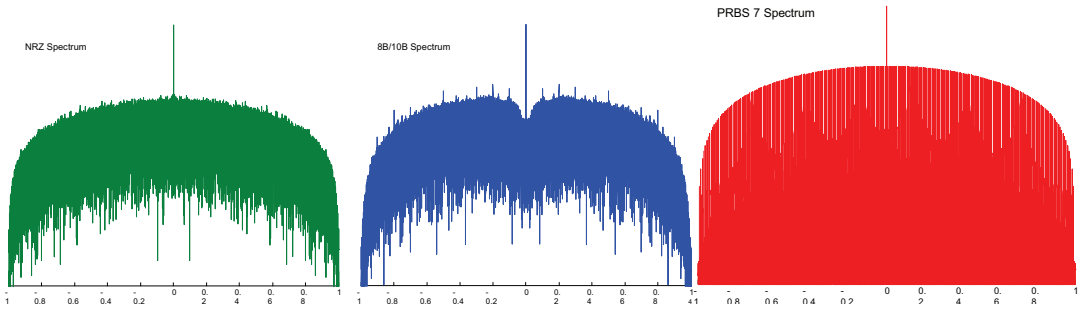

Fig. I.1. Calculated spectrum of noiseless infinite bandwidth, infinite extinction ratio random NRZ data, 8B/10B encoded data, and 2^7-1 PRBS data (PRBS data appears as a solid block on a logarithmic plot because the magnitude at some values is zero)

As can be seen the low frequency data of the 8B/10B encoded data is significantly reduced, below even the 27-1 PRBS data, with a 3 dB rolloff at around 0.07 times the datarate. The encoding also creates additional spikes in the data spectrum due to the preponderance of certain transitions. Note that the PRBS spectrum consists of a series of discrete impulses corresponding to each of the 127 bits in the data pattern. Therefore the low frequency content is zero below 1/127 (.0079) times the datarate, which is why it is used to emulate 8B/10B encoding.

I.2 64b/66b Encoding

While 8B/10B encoding uses a code lookup table, 64b/66b encoding uses an entirely different method for ensuring transitions and DC balance. To ensure DC balance the random data is passed through a transmission encoder, similar to a PRBS generator, that pseudo-randomly scrambles the data [2]. This ensures that an initial data block that has a long string of zeros or ones will be transmitted as a data block

with both DC balance and relatively frequent transitions. However, there is no guarantee that a pathological data sequence will not result in either a data packet with no DC balance or long periods without transitions. The only guarantee provided by 64b/66b encoding is that it will have a transition at least once every 66 bits, since each scrambled 64 bit sequence is transmitted with a two bit pre-amble of either 01 or 10. The benefit of this technique is that it has an overhead of only .3 times the datarate instead of .25 times the datarate, as with 8B/10B. When performing laboratory experiments it is common to use 223-1 PRBS patterns as an approximation to 64b/66b encoded data.

I.3 References

[1] A.X. Widmer and P.A. Franaszek, "A DC-Balanced, Partitioned-Block, 8B/10B Transmission Code", *IBM J. Res. Develop.*, vol. 27, no.5 pp. 440-451, 1983.

[2] Sowmya S. Luckoor, "Introduction to 10 Gigabit 64b/66b (Clause 49)", UNH traning services, 2001, http://www.iol.unh.edu/services/testing/10gec/training/10GbE_Cl49.pdf#search=%2264B%2F66B%20encoding%22, retrieved July 2010.